Acute AMPK activation does not adequately stimulate insulin signaling in skeletal muscle models of Myotonic Dystrophy Type 1

Yaw Ofosu Adjei-Afriyie

Thesis submitted to the University of Ottawa in partial fulfillment of the requirements for the Master of Science degree in Cellular and Molecular Medicine

Department of Cellular and Molecular Medicine

Faculty of Medicine

University of Ottawa

Table of Contents

Acknowledgments

First and foremost, I would like to thank God for watching, protecting and providing for me through this journey. I thank him for placing all the mentors, friends and family in my life to support me every step of the way through my academic journey.

I would like to express my gratitude to my Supervisor, Dr. Hanns Lochmüller and Lab Manager, Dr. Sally Spendiff for all their mentorship, inspiration and support in my research endeavours from the beginning of my undergraduate honours thesis to the end of my Masters research project. Thank you for taking a chance on me and supporting me in all my aspirations and ambitions through the years.

I would like to also thank those of you at CHEO Research Institute. All of those in the Lochmüller Lab who never made it a dull day to show up and do some research. Times of laughter and encouraging morale made every single day worth showing up for. I extend special thanks to Kelly Ho, Daniel O'Neil and Ricardo Carmona-Martinez for helping me in my experimentation for this study. I also thank my thesis advisory committee, Dr. Alex MacKenzie and Dr. Aymeric Ravel-Chapuis for supporting and guiding me through this project.

I would like to thank all the friends I have made along the way. My circle of friends from my hometown, Guelph, that I could always turn to when I needed a break from science. I also remain grateful to the friends that I made in my undergraduate program when I first moved to Ottawa in 2018. I extend thanks to all the friends I made at my church community at Ottawa East SDA and Nepean SDA church. You all always made sure I was always in good company and always kept me accountable to my faith in God.

I would also like to extend a deep thanks to my family. I thank my eldest brother Opoku Adjei-Afriyie always imparting wisdom and encouragement to ensure that I pursued my

ambitions in good health and spirit. I also thank my next eldest brother, Gyamfi Adjei-Afriyie, his wife, Nicole Adjei-Afriyie, and children, Micah and Malachi for always allowing me to come and spend time with them in their Ottawa home. Even though I live so far from my parents and other siblings, you have always reminded me that I have family right here in this city. I would also like to thank my little sister, Aba Hiroko Adjei-Afriyie. You may not realize, but your antics, jokes and crazy stories have always brought joy to my every single day.

Mom and Dad, you have inspired me to be a better person every single day. I thank you, Victoria Adjei-Afriyie and Dr. Francis Adjei-Afriyie for all the sacrifices you have made to give my siblings and I such a wonderful life in Canada. Mom, I draw upon your hard work and compassion to guide my everyday the interactions. Dad, I draw upon your grit and determination for scientific discovery and drew upon that to persevere and deliver the body of work you see here. Words cannot fully express my gratitude for your continual support and inspiration in my life. And to that, I to dedicate this thesis to the both of you.

List of Tables and Figures

1. Introduction

2. Manuscript

3. Extended Discussion

List of Abbreviations

ACC	Acetyl-CoA carboxylase
AICAR	5-aminoimidazole-4-carboxamide ribonucleotide
AMP	Adenosine monophosphate
AMPK	Adenosine monophosphate-activated protein kinase
AS160	Akt substrate of 160 kDa
BIN1	Bridging Integrator 1
BSA	Bovine Serum Albumin
CTL	Control
CELF	CUG-binding protein 1 and elav-like family member 1
ClC-1	Chloride Channel 1
CUGBP1	CUG-Binding Protein 1
DM	Differentiation Media
DM1	Myotonic Dystrophy Type 1
DMEM	Dulbecco's Modified Eagle Medium
DMPK	Dystrophia Myotonica Protein Kinase
EDL	Extensor Digitorum Longus
GAP	GTPase Activating Protein
Gas	Gastrocnemius
GLUT	Glucose Transporters
GLUT4	Glucose Transporter 4
GSV	GLUT4 Storage Vesicle
HRP	Horseradish Peroxidase
HSA-LR	Human Skeletal Actin Long Repeat
INSR	Insulin Receptor Gene
IPA	Ingenuity Pathway Analysis
MBNL1	Muscleblind like-1
mGLUT4	Membrane Bound Glut4
mTORC2	mechanistic target of rapamycin complex 2
MyoVa	Myosin Va
nc	No Change
p	phosphorylated
PBS	Phosphate Buffered Saline
PGC-1α/ PPARGC1A	Peroxisome Proliferator-Activated Receptor Gamma Coactivator Alpha 1
PKB	Protein Kinase B
SEM	Standard Error of the Mean
SIRT1	Sirtuin 1
SLC2	Solute carrier family 2

SLC2A4	Solute carrier family 2 member 4
T2D	Type 2 Diabetes
TBC1D15	Tre-2/Bub2/Cdc16 (TBC) domain family member 15
tGLUT4	Total GLUT4
T-tubule	Transverse Tubule
TUG	Tether, containing a UBX domain for GLUT4
USP25m	Muscle Ubiquitin Specific Peptidase 25
Veh	Vehicle

1. Introduction

1.1 Abstract

Myotonic Dystrophy Type 1 (DM1) is a multisystemic neuromuscular disease characterized by skeletal muscle weakness, muscle atrophy, and myotonia. However, patients often also experience cognitive impairments, gastrointestinal complications, and insulin resistance. Insulin resistance exacerbates muscle weakness and atrophy in DM1, but its pathomechanism has not been adequately described in the context of DM1. The aim of this study is to characterize the molecular mechanisms of insulin resistance in DM1 and how AMPK stimulation can impact insulin signaling. My first aim analyzes proteomic data from sedentary wildtype, sedentary HSA-LR, and exercised HSA-LR mice to detect and predict dysregulated proteins in insulin and exercise molecular pathways. My second aim examines molecular interactions impacting GLUT4 translocation in the HSA-LR mouse model after acute AMPK stimulation. My final aim examines molecular interactions impacting GLUT4 translocation in a DM1 myotube model after insulin and AMPK stimulation. Proteomic analysis predicted that exercise significantly upregulates PGC-1α, a transcription coactivator integral to metabolic regulation. When AMPK, an upstream regulator to PGC-1α, is targeted in HSA-LR mice and DM1 myotubes with AICAR, there is no improvement in the AKT-AS160 insulin signaling axis. Our findings confirm insulin resistance in DM1 and demonstrates an impaired response to acute AMPK stimulation.

1.2 Myotonic Dystrophy Type 1

Myotonic dystrophy 1 (DM1), also known as Steinart's Disease, is a multisystemic neuromuscular disease that afflicts approximately 1 in 8500 people worldwide, making it the most common muscular disease in adults (Chau & Kalsotra, 2015; Yotova et al., 2005). Due to a founder effect, there is a strikingly high prevalence of 1 in 550 individuals with DM1 in the Charlevoix and Saguenay-Lac-Saint-Jean regions of Quebec (Chau & Kalsotra, 2015; Yotova et al., 2005).

In healthy individuals there are approximately 5 to 37 CTG repeats in the 3' untranslated region of the *dystrophia myotonica protein kinase* (*DMPK*) gene, but in DM1 there are at least 50 CTG repeats, leading to the pathophysiology of the disease (Figure 1.1) (Brook, 1992; Caskey et al., 1992). This CTG region can be up to several thousand repeats long, with disease severity correlating with the length of the repeats (Mahadevan et al., 1992; Meola and Cardani, 2015). This repeat length can increase from generation to generation, which is denoted as genetic anticipation (Mahadevan et al., 1992). With the varying length of the repeat region, there arises different severities and classes of DM1. Congenital DM1 is the earliest presenting, and most severe form of the disease (Meola and Cardani, 2015). Juvenile DM1 are patients that present with symptoms in their childhood/teenage years and then adult-onset DM1 reflects the most common cases of DM1 where symptoms do not appear until adulthood. Finally, there is late-onset DM1 which is when the disease is detected in late adulthood, where patients present with mild symptoms (Meola and Cardani, 2015).

When transcribed, these CUG repeats form a stable hairpin loop of RNA which sequesters Muscleblind like-1 (MBNL1), an RNA binding protein, to the nucleus, resulting in its loss of function (Figure 1.1) (Chau & Kalsotra, 2015; Kalsotra et al., 2015). Additionally, CUG-binding

protein 1 (CUGBP1) and Elav-like family member 1 (CELF1), an RNA binding protein that functions antagonistically to MBNL1, are hyperactivated in DM1 skeletal muscle cells and contribute to mis-splicing events in pre-mRNA (Figure 1.1) (Chau & Kalsotra, 2015; Kuyumcu-Martinez et al., 2007; Philips et al., 1998). The mis-splicing of varying pre-mRNA contributes to the multisystemic nature of the disease. Patients can present with myotonia, muscle weakness, atrophy, insulin resistance, cognitive impairments, endocrine dysregulation, gastrointestinal complication, and cardiac conduction issues among other symptoms (Bird, 2019; Meola and Cardani, 2015).

Myotonia, characterized as prolonged muscle contraction, is one of the key symptoms observed in DM1 patients (Mankodi et al., 2002; Charlet-B. et al., 2002) and in day-to-day life it can make fine motor tasks challenging for patients (Heatwole, 2012). Myotonia is attributed to the functional loss of the chloride channel 1 (ClC-1) after its mis-splicing (Mankodi et al., 2002). In healthy individuals, ClC-1 pre-mRNA is spliced to remove exon 7A, but in DM1 there is an aberrant inclusion of exon 7A. ClC-1 is important for maintaining and re-establishing the sarcolemma membrane potential after the hyperpolarization phase of an action potential (Pedersen et al., 2016; Brenes et al., 2023). Without adequate ClC-1, chloride conductance diminishes, impeding the repolarization phase (Mankodi et al., 2002; Pedersen et al., 2016). This delays repolarization and subjects the membrane to hyper-excitability, rendering it difficult for patients to cease muscle contractions (Mankodi et al., 2002; Charlet-B. et al., 2002).

Patients can also experience muscle weakness and fatigue which ultimately impact gait and mobility (Fugier et al., 2011). Muscle weakness can be linked to bridging integrator 1 (BIN1), a membrane protein which aligns the transverse tubule (T-tubule) membrane with the sarcoplasmic

reticulum membrane (Prokic et al., 2020). It helps couple the depolarization of the T-tubule membrane with the calcium release of the sarcoplasmic reticulum which initiates muscle contraction. In DM1, when exon 11 of *BIN1* is aberrantly skipped, sarcolemma depolarization and sarcoplasmic reticulum calcium release become decoupled. This leads to the weakened muscle contractions which patients experience (Fugier et al., 2011).

In addition to muscle weakness, patients can also experience muscle loss, also known as muscle atrophy. Muscle atrophy in DM1 is related to the mis-splicing of insulin receptor gene (*INSR*) (Renna et al., 2019). In DM1, exon 11 of *INSR* is skipped which results in the IR-A fetal isoform of the receptor (Figure 1.2) (Savkur et al., 2001). This isoform has less specificity for insulin and thus dysregulates downstream cellular signaling. As a result, atrogin genes, the genes that direct muscle atrophy, are transcribed (Timchenko, 2013).

Mis-splicing of *INSR*, has also been attributed to metabolic disorders like insulin resistance in DM1 patients (Nieuwenhuis et al., 2019). In DM1 patients, systemic glucose disposal is diminished by 15-25% post-insulin infusion and studies on forearm muscle have shown that patients can have up to 70% decrease in insulin sensitivity (Moxley et al., 1977a, 1984a). Insulin signaling is integral to the energy status of the cell because it governs the intake of glucose to fuel energy demanding processes like cell growth and division. When insulin signalling is impaired in DM1, it can exacerbate coexisting symptoms such as muscle weakness and muscle atrophy (Nieuwenhuis et al., 2019). Thus, there is a need to understand insulin resistance in the context of DM1.

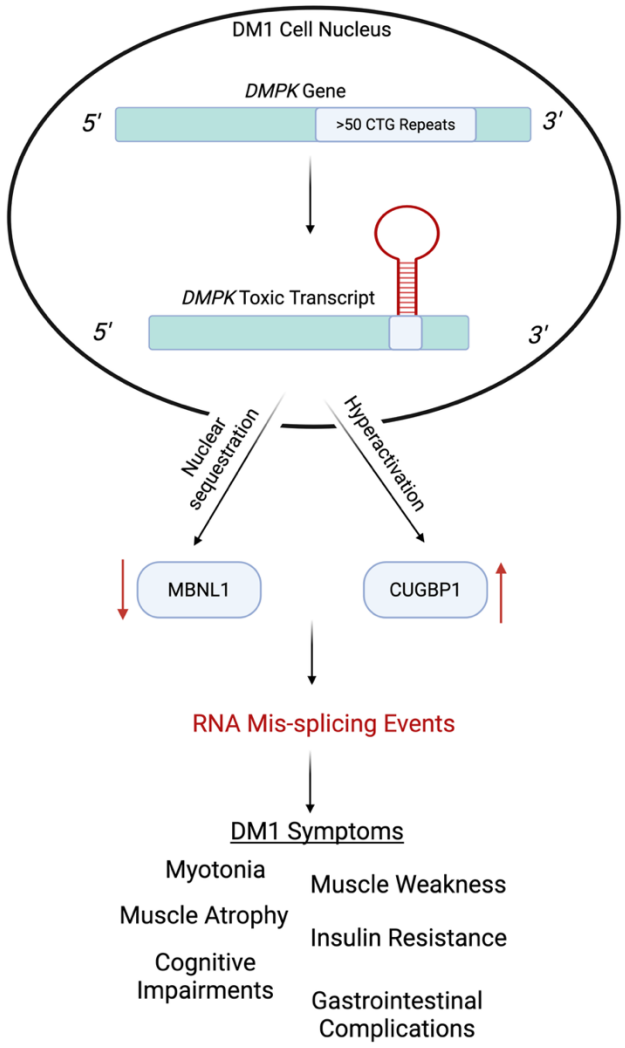

Figure 1.1 Pathomechanism of myotonic dystrophy type 1. When the *dystrophin myotonica protein kinase* (DMPK) gene has greater than 50 CTG repeats in the 3' untranslated region (faint blue) then a toxic transcript forms with a stable hairpin loop. This results in dysregulation of RNA binding proteins via the nuclear sequestration of muscleblind-like 1 (MBNL1) and hyperactivation of CUG binding protein 1 (CUGBP1). Subsequently, RNA mis-splicing events occur which manifests as the multisystemic symptoms that patients experience.

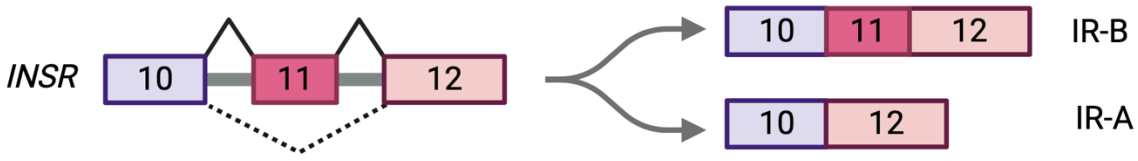

Figure 1.2. *INSR* Splicing. Alternative splicing of the *INSR* mRNA yields the IR-A and IR-B isoforms. IR-A is the predominant isoform of the insulin receptor in fetal tissue and has lower specificity for insulin than IR-B. The typical adult isoform, IR-B, is expressed when exon 11 is retained. In DM1, exon 11 is aberrantly skipped, favouring IR-A isoform expression in patients.

1.3 Models of DM1

Many studies have used cellular models of DM1 to investigate molecular mechanisms and interventions of the disease. Fibroblasts can be obtained from skin biopsies of DM1 patients and then used for in vitro studies (Taneja et al., 1995; Takarada et al., 2015). Fibroblasts are commonly employed to examine RNA foci formation and MBNL1 sequestration and have been used to conduct preliminary screens of candidate pharmacological treatments (Taneja et al., 1995; Takarada et al., 2015). A limitation of fibroblasts is that they do not recapitulate the cell specific protein expression and metabolism of skeletal muscle cell models.

There are also studies that have investigated the use of transfected myoblasts. Murine C2C12 skeletal muscle cells can be transfected with plasmids expressing expanded CTG repeats (Liang et al., 2016). These cells can recapitulate CELF1 upregulation and impaired differentiation, but mis-splicing was not detailed for these myoblasts (Liang et al., 2016). There are also some studies that have taken patient muscle biopsies and then expanded the myoblasts in cell culture

(Pantic et al., 2016; Santoro et al., 2020). These myoblasts can then be differentiated to reproduce the protein interactions and metabolism that the donating patients exhibited (Pantic et al., 2016; Santoro et al., 2020).

Many studies also employ mouse models to understand the systemic and physiological manifestations of DM1. A common mouse model is the transgenic mouse that expresses the human skeletal actin (HSA) with a long repeat (LR) of CTG nucleotides (Mankodi et al., 2002). This HSA-LR mouse model effectively models nuclear transcript accumulation, MBNL1 aggregation, transcript mis-splicing and exhibits myotonia and progressive muscle wasting (Mankodi et al., 2002). While it does exhibit transcript mis-splicing, this mouse model does not recapitulate the insulin receptor mis-splicing (Brockhoff et al., 2017). There is no reported evidence of hyperglycemia or hyperinsulinemia in this model which are common indicators of insulin resistance. Using this model thus allows us to isolate the insulin signaling pathway from the mis-splicing of the receptor, helping to determine if there may be insulin receptor independent changes in the pathway.

1.4 GLUT4

Glucose transporters (GLUTs) are integral membrane proteins expressed by the *solute carrier family 2* (*SLC2)* gene family. There are 14 distinct transporters and they are classed based on their sequence similarity. All GLUT proteins consist of 12 transmembrane segments, a central cytoplasmic linker domain, an N-linked glycosylation site, and the cytoplasmic facing N and C termini (Mueckler and Thorens, 2013). This redundancy likely suggests the metabolic need to

transport different monosaccharides to varying tissues with specialized kinetics (Mueckler and Thorens, 2013).

Among these isoforms, GLUT4 is unique as the primary insulin- and exercise-sensitive transporter. It is sparingly expressed in the brain and heart but highly expressed in adipose and skeletal muscle tissue (McNay and Pearson-Leary, 2020; Watson and Pessin, 2006a). In skeletal muscle tissue, GLUT4 has a higher expression profile in type I slow-twitch oxidative fibres compared to type II fast twitch fibres, consistent with the metabolic demands of the slow-twitch fibres (Daugaard et al., 2000a).

After transcription of the *SLC2A4* gene, GLUT4 is translated and undergoes N-linked glycosylation at Asn57 to ensure proper folding and stability (Zaarour et al., 2012). GLUT4 can be marked by additional post-translational modifications to regulate trafficking and turnover. SUMOylation can stabilize and direct GLUT4 into storage vesicles (GSVs) (Giorgino et al., 2000). Contrarily, GLUT4 O-GlcNAcylation can interfere with GLUT4 trafficking and could be implicated in insulin resistance (Buse et al., 2002).

Six to nine hours after synthesis and modifications, GLUT4 is stored in GSVs and retained in the intracellular compartment until insulin or exercise prompts its translocation to the plasma membrane (Figure 1.3) (Hou et al., 2006). It contains cytosolic targeting motifs in its central loop that directs it into GSVs (Khan et al., 2004). GSVs are retained to the perinuclear space of the cell by tether, containing a UBX domain for GLUT4 (TUG) (Habtemichael et al., 2021). The carboxyl terminal of TUG binds to Golgin-160, of the Golgi matrix and the amino terminus binds to the GSV (Bogan, 2012, 2022). Insulin or exercise stimulation promotes the endolytic cleavage of TUG to liberate the GSVs and permit their transport to the plasma membrane (Bogan, 2012;

Habtemichael et al., 2021). TUG cleavage is facilitated by muscle ubiquitin specific peptidase 25 (USP25m), which acts upon the UBX region of TUG (Habtemichael et al., 2018). GLUT4 translocation and TUG cleavage are highly correlated and provides insight on the insulin sensitivity of a cell (Bogan, 2012).

A unique characteristic of GLUT4 is its insulin- and exercise-dependent methods of translocation to the plasma membrane (Derave et al., 1999; Arias et al., 2007a; White and Kahn, 2021). Insulin and exercise stimulating pathways both converge upon Akt substate of 160 kDa (AS160) to initiate the translocation of GSVs towards the plasma membrane.

1.5 Insulin Signaling Pathway

When food is ingested, the body transitions from a low blood glucose fasted state to a high glucose postprandial state. Insulin is a hormone that regulates the uptake of glucose into muscle, adipose, liver, and brain tissue in this postprandial state (Heni et al., 2015). The beta cells of the pancreas sense high blood glucose and secrete insulin to increase glucose uptake into energy demanding tissues (Chadt and Al-Hasani, 2020).

Insulin signaling is a signalling cascade that contributes to cellular growth, development, and differentiation (Boucher et al., 2014; Renna et al., 2019). The insulin receptor is encoded by the *INSR* gene on chromosome 19p13.2 and is alternatively spliced to yield two isoforms, IR-A and IR-B (Russo et al., 2005). The isoform highly expressed in healthy adults is IR-B. At the molecular level, the insulin receptor autophosphorylates on the intracellular face when it is bound to insulin (Figure 1.3) (Boucher et al., 2014). Once the insulin receptor is phosphorylated, a cascade of signaling events leads to the phosphorylation of protein kinase B (PKB, Akt). Subsequently, Akt phosphorylates AS160, a GTPase activating protein (GAP) domain for Rab

proteins. Rab proteins are physically associated with GSVs and are important for facilitating vesicle mobilization and fusion when bound to GTP (Zerial and McBride, 2001). When the GAP interacts with a Rab, it inhibits the mobilization of GSVs to the plasma membrane. Then when Akt phosphorylates AS160 it inhibits its GAP activity and promotes a greater proportion of active GTP-bound Rabs and increased GSV translocation (Figure 1.3) (Mîinea et al., 2005).

1.6 Insulin Resistance

Insulin resistance is a hallmark symptom of T2D and is thus best characterized in the context of this disease. Findings indicate that insulin resistance in T2D leads to inefficient GLUT4 translocation and inefficient glucose uptake (Jackson et al., 2000; Michael et al., 2001).

AKT is a protein that is integral to the insulin signaling pathway as it signals for the translocation of GLUT4 to the plasma membrane through AS160. In fact, it has been shown that the ablation of AKT can induce insulin resistance in mice (Garofalo et al., 2003; George et al., 2004). In DM1, AKT is not known to be mis-spliced, but it was under-stimulated in DM1 skeletal muscle (Renna et al., 2017). AMPK activity is impaired in T2D (Sriwijitkamol et al., 2007), and is one of the purported targets for insulin resistance treatment (Wang et al., 2019). Downstream of AMPK, PGC-1α is also downregulated and targeted to improve insulin sensitivity (Sriwijitkamol et al., 2007; Wende et al., 2007a; Zhang et al., 2013). Since PGC-1α drives the expression of the *SLC2A4* gene, its downregulation can impact the expression of GLUT4 (Michael et al., 2001). GLUT4 translocation is typically impaired in T2D patients and translates to the diminished glucose uptake of the cell. AS160 activity, which governs GLUT4 translocation, is also found to be diminished in cases of insulin resistance (Karlsson et al., 2005).

Metformin is a common T2D drug that improves insulin sensitivity through increased GLUT4 translocation via AMPK activation and has also been associated with PGC-1α activation (Herman et al., 2022). Clinically, exercise has demonstrated efficacy for increasing insulin sensitivity in T2D whilst improving cardiovascular health, reducing obesity, and improving overall strength (Renna et al., 2019; Whillier, 2020). Evidence demonstrates that increased GLUT4 localization to the PM through exercise or pharmacological means is correlated with improved insulin sensitivity (Herman et al., 2022; Mîinea et al., 2005; Watson and Pessin, 2006b).

1.7 AMPK- PGC-1α Axis and Insulin Signaling Stimulation

Findings indicate that exercise improves insulin sensitivity in Type 2 Diabetes (T2D) patients (Boulé et al., 2005). T2D is characterized by increased hepatic glucose output, insulin resistance and diminished glucose disposal. However, when T2D patients exercise, insulin sensitivity improves and glucose disposal improves (Martin et al., 1995; Rose and Richter, 2005). This observation has prompted investigators to explore the underlying mechanism of exercise stimulated glucose uptake. Exercise stimulated glucose uptake reflects increased blood flow to the muscle, greater transport across the plasma membrane, and enhanced intracellular metabolism of glucose (Rose and Richter, 2005). Evidence supports that all these factors contribute to increased glucose disposal, but mounting data indicates that GLUT4 translocation to the plasma membrane is a considerable contributor to improved glucose uptake (Derave et al., 1999).

Adenosine monophosphate (AMP)-activated protein kinase (AMPK) is an energy sensing molecule in the cell which drives catabolic processes in low energy conditions. Higher AMP concentrations in the cell are found in lower energy conditions which explains why exercise can stimulate AMPK activation (Cantó and Auwerx, 2009a). AMPK is a heterotrimer comprised of 3

subunits: the catalytic α subunit, the beta subunit and the gamma subunit. The α subunit contains the threonine-172 residue which is phosphorylated and activates the kinase in cellular catabolic states (Cantó and Auwerx, 2009a). AMPK can also be stimulated by 5-aminoimidazole-4carboxamide ribonucleotide (AICAR) by mimicking elevated AMP/ATP ratios in the cell (Višnjić et al., 2021). When activated, AMPK stimulates AS160 to initiate GLUT4 translocation to the membrane (Arias et al., 2007a) (Figure 1.3). Increased glucose disposal after exercise lasts 2-3 hours and is insulin independent, but after this period, insulin sensitivity is enhanced for as long as 48 hours (Arias et al., 2007a; Perseghin et al., 1996).

Activated AMPK also stimulates peroxisome proliferator-activated receptor gamma coactivator alpha 1 (PGC-1α). PGC-1α exerts its function by coactivating transcription factors which regulate the expression of genes important for mitochondrial biogenesis, cellular respiration, and glucose flux (Wende et al., 2007b; Cantó and Auwerx, 2009b). Integral to mitochondrial regulation and glucose metabolism, PGC-1α dysregulation in skeletal muscle has been linked to insulin resistance and T2D (Cantó and Auwerx, 2009b).

Increased AMPK stimulation leads to increased PGC-1α expression and activity. And when PGC-1α is increased in expression and activity it leads to elevated GLUT4 expression, increased GLUT4 translocation and improved glucose uptake (Michael et al., 2001; Wende et al., 2007a) (Figure 1.3). For instance, when rats were subjected to a chronic swim training regimen, PGC-1α stability increased and was sustained 5 days post-training cessation (Park et al., 2020). Another study found that PGC-1α was required for AICAR-induced GLUT4 expression in mice (Leick et al., 2010). In cultured myotubes, it was found that activated PGC-1α binds to myocyte enhancement factor 2C (MEF2C) to drive the expression of GLUT4 (Michael et al., 2001). Further work in mice found that induced expression of PGC-1α increased glucose uptake into skeletal

muscle tissue in mice (Wende et al., 2007a). Altogether, previous work has implicated AMPK-PGC-1α stimulation in regulating insulin signaling and glucose uptake (Figure 1.3).

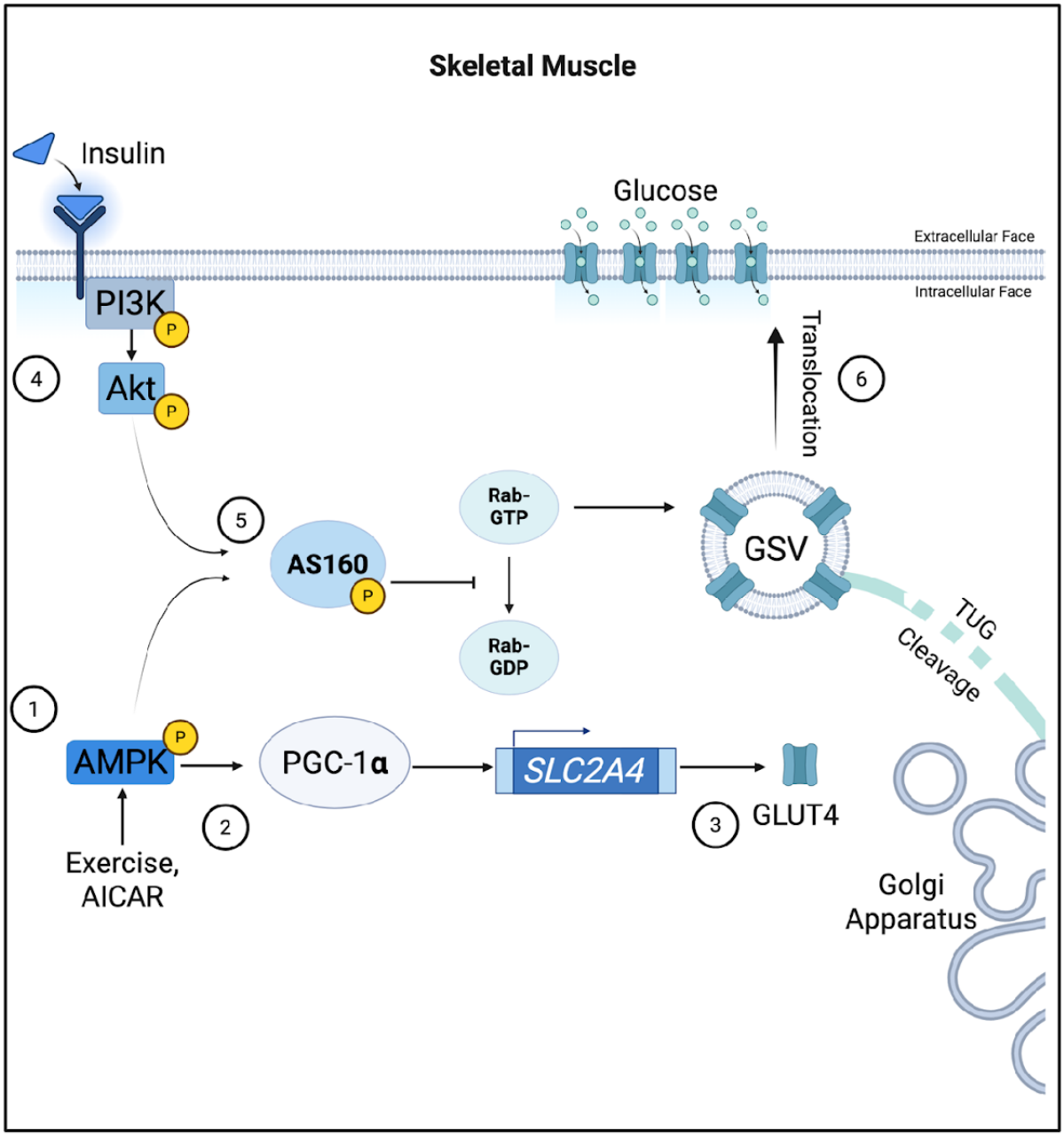

Figure 1.3 Predicted interactions of AMPK-PGC-1α and insulin signaling pathway. Graphical depiction of proposed interactions between insulin signaling and exercise pathways in

skeletal muscle. AMPK stimulation via exercise or AICAR (1) can drive PGC-1α activity and expression (2) to increase expression of GLUT4 (3). Insulin binds to the insulin receptor which activates AKT (4) which leads to AS160 stimulation (5). AS160 stimulation then drives GSV translocation to transport GLUT4 to the plasma membrane (6).

1.8 DM1 and Insulin Resistance

DM1 patients have up to a 4-fold increased risk of developing T2D (Winters, 2021). Furthermore, some patients have hypertriglyceridemia and reduced high density lipoprotein cholesterol levels which are additional hallmarks of insulin resistance (Vujnic et al., 2015). Insulin resistance may contribute to muscle weakness, heart disease and cognitive decline in DM1 (Winters, 2021), thus, understanding insulin resistance in DM1 is important. Clinically, many DM1 patients present with post-prandial hyperinsulinemia, a hallmark of insulin resistance (Moxley et al., 1977b, 1984b). The prevalence of metabolic syndrome has also been estimated at 17% in DM1 patients (Vujnic et al., 2015).

In T2D, insulin resistance is linked to smaller and dysregulated mitochondria (Kelley et al., 2002), which mirrors the impaired mitochondrial dynamics that are observed in DM1 (Gramegna et al., 2018; García-Puga et al., 2020). A study showed that PGC-1α integrates insulin signaling and mitochondrial dynamics and function (Pagel-Langenickel et al., 2010). With PGC-1α downregulation in diseases like T2D or DM1, there can be subsequent mitochondrial dysfunction (Pagel-Langenickel et al., 2010; Gramegna et al., 2018; García-Puga et al., 2022). With mitochondrial dysfunction, DM1 patients will have trouble with oxidative respiration which will contribute to the overall weakness and fatigue that patients experience.

Cardiovascular failure and insulin resistance have also been linked in DM1 (Nieuwenhuis et al., 2019). Insulin resistance has been linked to left-ventricle hypertrophy and arterial stiffness

in DM1. Dysregulated lipid metabolism promotes vascular dysfunction, and if left unchecked, arterial stiffness can progress to carotid atherosclerosis, increasing the risk of cardiovascular disease. Arterial stiffness comes from the dysregulated lipid metabolism linked to insulin resistance (Nieuwenhuis et al., 2019; Boengler et al., 2017). These vascular complications may contribute to the 2-3X increased risk of cardiovascular disease in insulin resistant patients (Kannel et al., 1974; Nieuwenhuis et al., 2019).

Studies indicate that T2D patients can experience cognitive decline (McCrimmon et al., 2012). This is consistent with the associated link of insulin resistance and impaired hippocampal plasticity (Spinelli et al., 2019). DM1 patients can also experience a decline in cognition (Gallais et al., 2017). Namely, patients experience a decline in executive function, visuospatial awareness and naming recall (Peric et al., 2017; Gallais et al., 2017). Interestingly a brain positron emission tomography study found that DM1 patients have glucose hypometabolism in the prefrontal, temporal and pericentral regions of the brain (Peric et al., 2017). These studies contextualize and underscore the role that insulin signaling could play in DM1 cognition.

Interestingly, many of the same molecular targets that are impaired in T2D are dysregulated in DM1. For example, diminished AKT activity has been described in DM1 skeletal muscle (Ozimski et al., 2021; Renna et al., 2017, 2019). However, this conflicts with a different study in HSA-LR mice indicating the AKT activity to be no different from healthy controls (Brockhoff et al., 2017). Further, AMPK activity and PGC-1α expression were found to be downregulated in the HSA-LR skeletal muscle tissue (Ravel-Chapuis et al., 2018), aligning with the pathomechanism observed in T2D. Further, there was a study that found downregulated AS160 activity in DM1 biopsy samples (Renna et al., 2019). However, there are no reports that have investigated AS160 and its response to AMPK stimulation in cellular or animal models of DM1. Thus, there is a

knowledge gap in the insulin signaling pathway within the context of DM1 which necessitates its investigation to detail its pathomechanism and how it may respond to therapeutic interventions. There is clear evidence that insulin resistance can impact other symptoms of DM1 including mitochondrial dynamics, cardiac function and cognition which makes it a very important signaling pathway to investigate.

1.9 DM1 Therapeutic Candidates

Current pharmacological candidates for DM1 serve to target dysregulated proteins in patients to help ameliorate symptoms. For instance, resveratrol, a compound that activates sirtuin 1 (SIRT1) and AMPK, has been studied within the context of DM1. Resveratrol stimulates mitochondrial biogenesis and reduces oxidative stress via the SIRT1-AMPK-PGC-1α pathway (Price et al., 2012; Higashida et al., 2013; Ljubicic et al., 2014). In patient derived myotubes, resveratrol corrected some alternative splicing and calcium signaling (Santoro et al., 2020). Another study in DM1 fibroblasts even found the correction of *INSR* splicing after resveratrol treatment (Takarada et al., 2015). In HSA-LR mice, resveratrol also partially corrected splicing, demonstrating the impact of the compound in vivo (Ravel-Chapuis et al., 2018). However, resveratrol has poor stability and undergoes rapid hepatic metabolism in humans, giving it low bioavailability in patients (Walle, 2011).

Dimethyl biguanide, commonly known as metformin, is one of the most prescribed treatments for T2D (García-Puga et al., 2022). Metformin inhibits the mitochondrial complex I and indirectly elicits the phosphorylation of AMPK. Downstream, this increases glucose uptake into the cell, subsequently lowering blood glucose levels (Duca et al., 2015; Wang et al., 2019). In preclinical models of DM1, metformin was reported to have impacts on the metabolism of cells. Namely, it increased ATP to healthier levels in primary DM1 fibroblasts. It also reduced

splicing defects which restored *INSR* exon 11 splicing errors (García-Puga et al., 2022). In DM1 patients, some mis-splicing was corrected in peripheral blood lymphocytes after treatment with metformin (Laustriat et al., 2015). Clinically, metformin had a significant impact on the 6 minute walk test (6MWT), indicating an improvement in mobility (Gagnon et al., 2018). Though functional improvements were observed, metformin failed to improve myotonia or muscular strength (Bassez et al., 2018).

Despite extensive work that has assessed the use of classical insulin sensitizing treatments in DM1, studies have not detailed the impacts of these treatments on insulin signaling in DM1. Further, while some treatments may work in some patients, it is important to assess the validity of other therapeutic avenues, such as exercise, to account for existing therapeutic non-responders.

1.10 Exercise and DM1

Exercise is effective for managing DM1 disease progression in both mice and humans (Okkersen et al., 2018; Ravel-Chapuis et al., 2018; Manta et al., 2019; Mikhail et al., 2023; Misquitta et al., 2022) Studies found that AMPK signaling and PGC-1α content were downregulated in HSA-LR mice (Ravel-Chapuis et al., 2018). When HSA-LR mice were subjected to exercise, AICAR treatment, or a combination of both, RNA foci counts decreased, some mis-splicing events were corrected, and AMPK signaling improved (Ravel-Chapuis et al., 2018; Misquitta et al., 2022). When HSA-LR mice were subjected to chronic exercise through volitional wheel running there were increases in overall muscle strength and reductions in myopathy and myotonia (Manta et al., 2019). Molecularly, there were reductions in mRNA mis-splicing, increased mitochondrial content, and a reduction in toxic nuclear RNA foci (Manta et al., 2019).

Interestingly, a single bout of exhaustive exercise in HSA-LR mice also improved mitochondrial dynamics through corrected organelle fusion and fission (Mikhail et al., 2023).

In DM1 patients, aerobic exercise has demonstrated marked functional and metabolic improvements. 12 DM1 patients undergoing a 12-week aerobic cycling program (Ørngreen et al., 2005), improved aerobic capacity, measured as VO2 max, by approximately 14%. Additionally, maximal workload increased by 11% and cross-sectional muscle fiber area increased, indicating muscle hypertrophy (Ørngreen et al., 2005).

A study conducted nearly two decades later demonstrated similar findings. There were 11 DM1 patients and they were subjected to a 12-week moderate cycling regimen (Mikhail et al., 2022). After 12 weeks of cycling 3 times per week, patients had improvements in VO2 max, improved 6MWT, and increased total lean mass with corresponding reductions in body fat percentage (Mikhail et al., 2022). Contrary to the findings in the preclinical models, the 12-week regimen did not reduce RNA foci counts and showed no significant changes in mRNA mis-splicing. However, there were reported improvements in mitochondrial dynamics, indicating that the exercise-induced benefits may be in part due to metabolic improvements (Mikhail et al., 2022).

Similarly, resistance training has demonstrated increases in strength, cross sectional muscle area and a shift towards type I muscle fibers (Roussel et al., 2019). One study conducted a 12-week study with lower leg resistance training twice a week to assess strength and mobility benefits in DM1 patients (Roussel et al., 2020). Strength and functional mobility improved during and immediately after the 12-week period, with some mobility benefits being retained for up to 9 months (Roussel et al., 2020). While this study did not explicitly assess metabolic benefits, another group employing a similar exercise regimen of two resistance exercise sessions for a 12-week period observed mitochondrial improvements (Di Leo et al., 2023).

Both preclinical and clinical studies have demonstrated the clear benefit of employing exercise in DM1 patients, but some of the underlying molecular mechanisms that underlie these benefits remain elusive.

1.11 Rationale and Research Objectives

Countless studies have shown that AMPK stimulation either with exercise or pharmacological means, yields systemic improvements in DM1 models and patients. However, the effects of AMPK stimulation on insulin sensitivity and GLUT4 translocation in DM1 skeletal muscle has not been studied in detail. The important role that AMPK and PGC-1α have demonstrated in insulin sensitivity necessitates its investigation within the context of DM1 (Cantó and Auwerx, 2009b; Michael et al., 2001; Wende et al., 2007a).

1.12 Research Aims

i. Implement Qiagen's Ingenuity Pathway Analysis program (IPA) to examine proteomic data from exercised and sedentary HSA-LR DM1 mouse tissue (Manta et al., 2019).
ii. Assess the state of insulin signaling and GLUT4 translocation before and after acute AICAR injections in the HSA-LR mouse model.
iii. Assess the state of insulin signaling and GLUT4 translocation before and after acute insulin and AICAR injections in the human DM1 myotubes.

1.13 Hypothesis

Hypothesis: I hypothesize that acute AMPK stimulation increases PGC-1α expression to rescue aberrant GLUT4 expression and translocation in DM1.

2. Manuscript

Acute AMPK activation does not adequately stimulate insulin signaling in skeletal muscle models of Myotonic Dystrophy Type 1

Ofosu Adjei-Afriyie[1,2,3], Sally Spendiff[2,3], Ricardo Carmona-Martinez[2,3], Alexander Manta[2,4], Andreas Hentschel[5], Kelly Ho[2,3], Daniel O'Neil[2,3], Leanne Dawe [1,3], Andreas Roos[2,3,6,7,8], Vladimir Ljubicic[4], Alexander MacKenzie[1,2,3,7], Aymeric Ravel-Chapuis[1,3,8], Hanns Lochmüller[1,2,3,9,10,11,*]

[1]Department of Cellular and Molecular Medicine, University of Ottawa, 451 Smyth Road, Ottawa, Ontario, Canada, K18 HM5; [2]Children's Hospital of Eastern Ontario Research Institute, 401 Smyth Road, Ottawa, Ontario, Canada, K1H 8L1; [3]The Eric Poulin Centre for Neuromuscular Disease, University of Ottawa, 451 Smyth Road, Ottawa, Ontario, Canada, K18 HM5; [4]Department of Kinesiology, McMaster University, 1280 Main Street West, Hamilton, Ontario, L8S 4K1; [5]Leibniz-Institute for Analytical Science -ISAS- e.V., Otto-Hahn-Strasse 6b, 44227 Dortmund, Germany; [6]Department of Pediatric Neurology, Centre for Neuromuscular Disorders, University Duisburg-Essen, 45147 Essen, Germany; [7]Department of Neurology, Medical Faculty and University Hospital Düsseldorf, Heinrich Heine University, 40225 Düsseldorf, Germany; [8]School of Pharmaceutical Sciences, Univeristy of Ottawa, 451 Smyth Road, Ottawa, Ontario, Canada, K18 HM5; [9]Brain and Mind Research Institute, University of Ottawa, 451 Smyth Road, Ottawa, Ontario, Canada, K18 HM5; [10]Department of Neuropediatrics and Muscle Disorders, Medical Center – University of Freiburg, Faculty of Medicine, Mathildenstr. 1, 79160 Freiburg, Germany; [11]Centro Nacional de Análisis Genómico, Baldiri Reixac 4, 08028 Barcelona, Spain

Present address: Children's Hospital of Eastern Ontario Research Institute, 401 Smyth Road, Ottawa, Ontario, Canada

*To whom correspondence should be addressed: Hanns Lochmüller

Keywords: Myotonic dystrophy type 1 (DM1), exercise, insulin, AMPK, PGC-1α, Akt, AS160, GLUT4

Abstract

Myotonic Dystrophy Type 1 (DM1) is a multisystemic neuromuscular disorder characterized by skeletal muscle weakness, muscle atrophy, myotonia, cognitive impairments, gastrointestinal complications, and insulin resistance. While insulin resistance is well characterized in type 2 diabetes, its pathomechanism in DM1 remains unclear. Our study aims to elucidate the pathomechanism of insulin resistance in DM1 and how the pathway responds to AMPK stimulation. Proteomic analysis from sedentary wildtype and sedentary HSA-LR mice, a common DM1 mouse model, revealed downregulation of the AMPK-PGC-1α axis. Analysis of sedentary HSA-LR mice and exercised HSA-LR mice revealed activation of the AMPK-PGC-1α axis in exercised animals. To investigate this pathway, we treated WT and HSA-LR mice with the AMPK activator AICAR to examine the impact of AMPK stimulation on insulin signaling in DM1. This revealed impaired responses in the insulin pathway activation in the HSA-LR mice. Next, we examined whether these differences extended to a human model by treating control and DM1 myotubes with insulin and/or AICAR. In DM1 myotubes, both treatments produced dampened responses of key insulin signaling intermediates compared to controls. Taken together, these results suggest impaired activation of insulin signaling pathways in DM1 models and confirm the presence of insulin resistance with an impaired response to acute AMPK stimulation.

2.1 Introduction

Myotonic dystrophy 1 (DM1), also known as Steinert's Disease, is a multisystemic neuromuscular disease that affects approximately 1 in 8500 people worldwide, making it the most common adult-onset muscular disease (Chau and Kalsotra, 2015; Yotova et al., 2005). Due to a founder effect, there is a strikingly high prevalence of 1 in 550 affected individuals in the Charlevoix and Saguenay-Lac-Saint-Jean regions of Quebec, Canada (Chau and Kalsotra, 2015; Yotova et al., 2005).

DM1 patients present with a heterogeneous set of clinical symptoms, including myotonia, characterized as prolonged muscle contraction. Other symptoms include progressive muscle weakness, muscle atrophy, and metabolic abnormalities, such as insulin resistance (Nieuwenhuis et al., 2019; Mateus et al., 2021). Insulin signaling is integral to the energy status of the cell, governing the intake of glucose to fuel energy demanding processes like cell growth and division. In DM1, systemic glucose disposal is diminished by 15-25%, with up to a 70% decrease in insulin sensitivity observed in the forearm muscle of DM1 patients (Moxley et al., 1977a, 1984a). When insulin signaling is impaired in DM1, it can exacerbate coexisting symptoms such as muscle weakness and atrophy (Nieuwenhuis et al., 2019). Additionally, it can cause significant impairments to skeletal muscle, cardiac, adipose and brain tissue in DM1 (Nieuwenhuis et al., 2019).

DM1 arises from a CUG-expansion repeat in the 3' untranslated region of the dystrophia myotonica protein kinase (*DMPK*) gene (Brook, 1992; Caskey et al., 1992; Mahadevan et al., 1992). When transcribed, these repeats cause a stable hairpin loop of RNA which sequesters Muscleblind-like 1 (MBNL1), an RNA-binding protein, to the nucleus, resulting in its subsequent loss of function (Chau and Kalsotra, 2015). In parallel, CUG-binding protein 1 and

Elav-like family member 1 (CELF1), an RNA-binding protein that functions antagonistically to MBNL1, is hyperactivated in DM1 skeletal muscle cells and contributes to mis-splicing events in pre-mRNA (Philips et al., 1998; Kuyumcu-Martinez et al., 2007; Chau and Kalsotra, 2015). CELF1 aberrantly excludes exon 11 in the insulin receptor (*INSR*) gene which contributes to insulin resistance in patients (Renna et al., 2017, 2019; Savkur et al., 2001). Insulin resistance in DM1 reflects dysregulation of downstream insulin receptor effectors that govern glucose uptake, cell metabolism and muscle trophism in DM1 (Renna et al., 2017, 2019).

The insulin signaling cascade contributes to cellular growth, development, and differentiation (Boucher et al., 2014; Renna et al., 2019). When the insulin hormone binds to the insulin receptor, the receptor phosphorylates and activates a signaling cascade that causes glucose transporter 4 (GLUT4) translocation to the plasma membrane, which allows the influx of glucose into the cell (Figure 1A) (Zerial and McBride, 2001). Once the insulin receptor is phosphorylated, a cascade of signaling events leads to the phosphorylation of Akt. Subsequently, Akt phosphorylates Akt substrate of 160 kDa (AS160), a GTPase-activating protein (GAP) for Rab proteins (Mîinea et al., 2005). In its native state, when AS160 interacts with Rab proteins, mobilization of GLUT4 storage vesicles (GSV) to the plasma membrane is inhibited. However, when Akt phosphorylates AS160 on threonine-642, it inhibits its GAP activity and promotes a greater proportion of active GTP-bound Rabs and increases GSV translocation to the plasma membrane (Figure 1A) (Mîinea et al., 2005).

Adenosine monophosphate (AMP)-activated kinase (AMPK) is an intracellular energy sensing protein which is phosphorylated at threonine-172 when adenosine monophosphate (AMP) allosterically binds to it. AMPK can also stimulate AS160 phosphorylation to initiate GLUT4 translocation to the plasma membrane (Arias et al., 2007a). Downstream of AMPK,

peroxisome proliferator-activated receptor gamma coactivator 1 alpha (PGC-1α) activates transcription programs for mitochondrial biogenesis, oxidative phosphorylation, and glucose metabolism (Wende et al., 2007b; Cantó and Auwerx, 2009b). Importantly, PGC-1α drives GLUT4 expression and is correlated with improved glucose uptake (Michael et al., 2001; Wende et al., 2007a).

Although exercise confers broad systemic benefits in DM1 models and patients, its effects on insulin sensitivity and GLUT4 translocation in DM1 skeletal muscle remains insufficiently described. Given the important role that AMPK and PGC-1α have in GLUT4 translocation and insulin sensitivity, there is a need for its investigation within the context of DM1 (Cantó and Auwerx, 2009b; a; Michael et al., 2001; Wende et al., 2007a). The human skeletal actin long repeat (HSA-LR) mouse model is a transgenic mouse that models nuclear MBNL aggregation and RNA mis-splicing which translates to myotonia and progressive muscle wasting (Mankodi et al., 2002). Importantly, this model presents with downregulated PGC-1α (Ravel-Chapuis et al., 2018). Although there are no known reports of downregulated PGC-1α in DM1 patients, they do present with dysregulated metabolic dynamics, which could be linked to downregulated PGC-1α (García-Puga et al., 2020, 2022; Mikhail et al., 2022). Thus, we hypothesized that acute activation of the AMPK-PGC-1α axis with an exercise mimetic, 5-aminoimidazole-4-carboxamide ribonucleotide (AICAR), could sensitize the insulin signaling pathway to subsequently improve insulin signaling and GLUT4 translocation in the HSA-LR mouse and a human myotube model of DM1 (Figure 1A).

2.2 Methods

2.2.1 Identification of key molecular pathways

To identify relevant targets within the insulin signaling and exercise pathways in HSA-LR mice, we analyzed proteomic data from tissue of mice that had previously undergone an exercise protocol (Manta et al., 2019). Three to six-month old mice had volitional access to a running wheel for a 7-week period and were sacrificed 24 hours after their last exercise activity. Mass-spectrometry data from quadriceps tissue of 3 sedentary WT mice, 5 sedentary HSA-LR and 5 exercised HSA-LR were entered into Qiagen's Ingenuity Pathway Analysis (IPA, RRID:SCR_008653, Fall 2025 Release) program to predict protein fold changes and interactions. Raw abundance values were normalized and used to calculate the $\log_2$ fold change ($\log_2$FC) to determine the expression change of specific targets. P-values were calculated using unpaired two-way Welch's T-test. These values were entered into IPA for subsequent analyses. Using the Core Analysis feature, IPA was used to analyze the proteomic data set against existing public databases and literature to predict the inhibition or activation of upstream pathways. Degree of activation or inhibition of a target or pathway was predicted with a z-score. Z-scores greater than 2 ($z>2$) indicated activation or upregulation of pathways and targets. Z-scores less than -2 ($z<-2$) indicated inhibition or downregulation of pathways and targets. A p-value of less than 0.05 ($P<0.05$) was used to determine statistical significance.

2.2.2 Ethics Approval

Experiments and procedures performed in this study were approved by the University of Ottawa Animal Care Committee and meet the standards of the Canadian Council on Animal Care and Ontario Animals for Research Act. Mice were housed and cared for by the University of Ottawa Animal Care and Veterinary Service.

2.2.3 Animal husbandry and tissue harvesting

Three to six-month old female human skeletal actin-long repeat (HSA-LR) mice and wild-type (WT) FVB/N mice (RRID:IMSR_JAX:001800) were subjected to an *ad-libitum* diet and regular light/dark cycles. Mice were injected subcutaneously with 500 mg/kg AICAR or 0.9% saline solution as a control and sacrificed by carbon dioxide administration followed by cervical dislocation 30 minutes after injection. Samples were either snap frozen in liquid nitrogen or mounted in optimal cutting temperature (OCT) mounting media and submerged in liquid nitrogen-cooled isopentane. Samples were stored at -80 °C until use.

2.2.4 Immunofluorescence

OCT mounted tissues were cryosectioned at 10 µm onto slides and stored at -80 °C. Slides were removed from the freezer and allowed to defrost at room temperature for 20 minutes, then fixed in 3.7% formaldehyde for 15 minutes at room temperature. Sections were then washed in 1 x phosphate buffered saline (PBS; Sigma Aldrich, Cat. No. D8537) to remove excess formaldehyde and then circled by a hydrophobic pen before blocking and permeabilization (5% bovine serum albumin (BSA), 5% normal goat serum (NGS), 0.1% Triton-X100) for 30 minutes. Tissue sections were incubated with 1:750 rabbit anti-GLUT4 (Abcam, Cat. No. ab33780, RRID:AB_2191441) and 1:1000 mouse anti-Laminin (Sigma Aldrich, Cat. No. L8271,

RRID:AB_477162) in blocking buffer (5% BSA, 5% NGS) overnight at 4 °C in a humidified chamber. The following day, sections were washed 3 x 5 minutes in PBS supplemented with 0.05% tween-20 (PBS-T). Then the sections were incubated in 1:500 goat anti-rabbit AF594 (Thermo Fisher Scientific, Cat. No. A-11012, RRID:AB_2534079) and 1:500 goat anti-mouse AF488 (Thermo Fisher Scientific, Cat. No. RRID:AB_2534088) for 1 hour at room temperature. Afterwards, slides were washed 2 x 5 minutes in PBS-T before adding 0.1 µg/mL Hoechst (Thermo Fisher Scientific, Cat. No. H3570) for 10 minutes at room temperature. Sections were finally washed 2 x 5 minutes in PBS before mounting in Fluoremount-G mounting media (Thermo Fisher Scientific, Cat. No. 00-4958-02). Images were captured on a Zeiss Axio Imager (RRID:SCR_018876) widefield microscope to visualize GLUT4, laminin, and the nucleus in the 594 nm, 488 nm and 350 nm emission wavelengths respectively. Tile images were taken to capture ~200-300 fibers per sample. Images were analyzed on ZEISS Efficient Navigation (version 3.9, RRID:SCR_013672) imaging software.

2.2.5 Cell culture

Immortalized patient and control myoblast cell lines were maintained at 20% confluence to prevent spontaneous differentiation. Cells were grown at 37 °C in 5% CO2, in Promo Cell Skeletal Muscle Growth Medium (Cat. No. C-23060) which was supplemented with 10% fetal bovine serum, 1% penicillin/streptomycin, and 1% L-glutamine. To passage the cells, media was removed, the cells were washed in 1 x PBS and then incubated in trypsin at 37 °C for 5 minutes before the trypsin was quenched with serum-containing growth media. The cells were then spun down at 1000 RPM for 5 minutes, resuspended in growth media and placed into a T75 flask. If cells were directed toward experimentation, they were counted and seeded into a collagen (Gibco Collagen I rat tail, A1048301) coated dish to ensure cell adherence during differentiation. Cells

were grown to 90-100% confluence then switched to differentiation media (DM) (Dulbecco's Modified Eagle Medium (DMEM), 2% horse serum, 1% penicillin/streptomycin, and 1% L-glutamine). The cells were maintained in DM for 4 days before drug treatments.

2.2.6 Cell drug treatments

We used and experimented on DM1 patient-derived myotubes that were obtained as a gift from Dr. Elena Pegoraro's group (Pantic et al., 2016)**.** Information pertaining to the sex, age, and biopsy location is described in Table 1.

Table 2.1 Cell model information. Patient's sex, age, and biopsy site.

Cell Line	**Sex**	**Age**	**Biopsy Site**
Control-1	Male	41	*Vastus Lateralis*
Control-3	Male	36	*Vastus Lateralis*
DM1-1	Female	29	*Biceps Brachii*
DM1-2	Male	19	*Vastus Lateralis*

Myoblasts were plated on 6 well plates and differentiated for 4 days before serum starvation for 4 hours in DMEM. Myotubes were then treated with 2mM AICAR in DMSO for 1 hour followed by 100 nM insulin in HEPES buffer for 30 minutes at 37 °C. Vehicle treatment (Veh) cells were treated with a combination of 2% DMSO control and 1.25 μM HEPES buffer. Cells were treated with either vehicle, AICAR, insulin, or both AICAR and insulin.

2.2.7 Western blot

Skeletal muscle tissues were lysed in RIPA buffer (150 mM NaCl, 50 mM Tris HCl, 1% Triton-X100, 0.1% SDS, 0.5% sodium deoxycholate) supplemented with protease and phosphatase inhibitor (Sigma Aldrich, Cat. No. PPC1010-1ML). The tissue was lysed with 3.2 mm steel beads and placed into the Qiagen Tissue Lyser at 25 Hz for 3 x 90 seconds, with 2 minutes cooling on ice in between cycles. Lysates were then placed on a rotator at 4 °C for 2 hours before being spun down at 12 000 RPM for 20 minutes. Supernatant was collected and lysates were stored at -80 °C. Protein was quantified using a DC assay kit (Bio-Rad, Cat. No. 5000112) alongside a BSA standard that ranged from 0.125 to 2 µg/mL.

Myotubes were lysed in the same RIPA buffer cocktail on ice and scraped off the 6-well plate with a cell scraper. Lysates were vortexed and then placed on a rotator at 4 °C for 30 minutes before being spun down at 12 000 RPM for 20 minutes. Supernatant was collected and lysates were stored and quantified the same way that muscle lysates were.

Samples were prepared with 4X Laemmli buffer (Bio-Rad, Cat. No. 161-0747) and supplemented with 2-mercaptoethanol. Samples were then placed on a heat block at 95 °C for 5 minutes before being run through a 7.5% polyacrylamide stacking and 8% polyacrylamide resolving gel in tris-glycine running buffer (25 mM Tris-Base, 190 mM glycine, 0.1% SDS). The samples were run for 15 minutes at 115 V and then 75 minutes at 125 V. The samples were then transferred to 0.2 µm PVDF (Bio-Rad, Cat. No. 1620177) in a cold tris-glycine transfer buffer (25 mM Tris-Base, 190 mM glycine, 20% ethanol) for 90 minutes at 100 V at 4 °C. Membranes were then blocked in Licor blocking buffer (Licor, Cat. No. 927-60001) for 1 hour at room temperature. Primary antibodies (in Licor blocking buffer, 0.1% Tween), detailed in Supplemental Table 1, were added overnight at 4 °C on a rocker (Supplemental Table 1). The

following day blots were washed in tris buffered saline – tween (TBS-T; 20 mM Tris-HCL, 150 mM NaCl, 0.1% Tween-20) for 3 x 5 minutes before being incubated in the respective secondary antibody for 1 hour at room temperature on a rocker (Supplemental Table 1). Finally, blots were incubated in Clarity Max enhance chemiluminescent substrate (Bio-Rad, Cat. No. 1705062) and bands imaged on the ChemiDoc Imaging System (Bio-Rad, RRID:SCR_019037). Band densitometry was analyzed on Image Lab software (Bio-Rad, RRID:SCR_014210), and all proteins were normalized to vinculin loading protein. Images were analyzed on ZEISS Efficient Navigation (version 3.9, RRID:SCR_013672) imaging software.

2.2.8 Statistical analyses

Statistical comparisons were made once the data sets were assessed for normality with the Shapiro-Wilk test. If datasets failed (p-value<0.05), then they were analyzed with the unpaired one-way Welch's t-test. Otherwise, the tests were conducted with unpaired one-way Student's t-test. Multiple comparisons were analyzed with two-way ANOVA followed by Tukey's post hoc analysis. Statistical significance was determined with a threshold of $p< 0.05$. Grubb's extreme student deviate test was used to determine and exclude outliers. Statistics were performed, and graphs were generated using Prism GraphPad (RRID:SCR_002798) with graphs depicted as mean +/- standard error of the mean (SEM).

2.3 Results

2.3.1 Ingenuity Pathway Analysis tool predicts PGC-1α to be dysregulated in HSA-LR mouse model

There were 882 targets identified in the sedentary HSA-LR mice versus sedentary WT condition and 884 targets identified in the exercised HSA-LR mouse versus sedentary HSA-LR mouse condition (Supplemental Table 2,3). Of the targets, solute carrier family 2 member 4 (SLC2A4), also known as GLUT4, was upregulated in the exercised HSA-LR condition (Table 2.2, Supplemental Table 2,3).

Table 2.2 SLC2A4 expression measures in sedentary and exercised HSA-LR conditions

Condition	Expression Log Ratio	Expression p-value
Sedentary HSA-LR vs sedentary WT	2.82	$6.0x10^{-2}$
Exercised HSA-LR vs sedentary HSA-LR	3.80	$4.0x10^{-2}$

When assessing the predicted Canonical pathways, PI3K-Akt was predicted to be activated in sedentary and exercised conditions (Table 2.3, Supplemental Table 4, 5). Within the pathway, the predicted activated molecules were not PI3K or Akt, but rather targets downstream of these molecules (Supplemental Table 6,7). Of these downstream effectors overlapping with the proteomic dataset, none of them met the thresholds for z-score (>|2|) and p-value (<0.05) (Supplemental Table 6,7).

Table 2.3 PI3K-Akt canonical pathway activation measures in sedentary and exercised HSA-LR conditions.

Condition	Activation z-score	P-value
Sedentary HSA-LR vs sedentary WT	2.67	$1.05x10^{-4}$
Exercised HSA-LR vs sedentary HSA-LR	2.18	$1.08x10^{-4}$

Similarly, the GLUT4 translocation pathway was increased in both conditions. However, within the GLUT4 translocation pathway, GLUT4 was significantly upregulated only in the exercised HSA-LR condition (Table 2.2, 2.4, Supplemental Table 4,5,8,9).

Table 2.4 Translocation of SLC2A4 (GLUT4) canonical pathway activation measures in sedentary and exercised HSA-LR conditions.

Condition	Activation z-score	P-value
Sedentary HSA-LR vs sedentary WT	2.84	$9.05x10^{-9}$
Exercised HSA-LR vs sedentary HSA-LR	2.84	$9.33x10^{-9}$

For the predicted upstream regulators, INSR (insulin receptor) and PPARGC1A (PGC-1α) appeared as relevant targets as both are implicated as glucose metabolism regulators. INSR was predicted to be inhibited in the sedentary HSA-LR mice, but was activated in the exercised HSA-LR mice (Table 2.5, Supplemental table 10, 11). Similarly, PGC-1α was predicted to be inhibited in sedentary HSA-LR mice and was upregulated in exercised HSA-LR mice (Figure 1B – C, Table 6, Supplemental Table 10, 11).

Table 2.5 INSR (insulin receptor) predicted activation measures in sedentary and exercised HSA-LR conditions.

Condition	Activation z-score	P-value
Sedentary HSA-LR vs sedentary WT	-4.27	$2.67x10^{-60}$
Exercised HSA-LR vs sedentary HSA-LR	5.35	$3.56x10^{-60}$

Table 2.6 PPARGC1A (PGC-1α) upstream regulator predicted activation measures in sedentary and exercised HSA-LR conditions.

Condition	Activation z-score	P-value
Sedentary HSA-LR vs sedentary WT	-2.59	$3.75x10^{-48}$
Exercised HSA-LR vs sedentary HSA-LR	6.51	$4.61x10^{-48}$

2.3.2 AMPK-PGC-1α axis has impaired response to AICAR in HSA-LR mice

To determine the specific effect of AMPK stimulation on PGC-1α expression and insulin signaling molecules, mice were subjected to an acute AICAR treatment. They received a subcutaneous injection with 500 mg/kg AICAR or saline. The mice were sacrificed, and tissues were collected 30 minutes after injection to capture the transient action of AMPK. Samples were analyzed with western blotting to assess the abundance and activity levels of proteins involved in the key signaling pathways (Figure 2A, Supplemental Figure 3-6, 9). At baseline, HSA-LR mice expressed lower total AMPK and phosphorylated threonine-172 AMPK (pAMPK) compared to

WT mice, but no difference was observed when pAMPK was normalized to total AMPK (Figure 2B-D). Analysis indicated no significant difference in baseline expression of PGC-1α between HSA-LR and WT groups (Figure 2E). However, there was significantly less GLUT4 in the HSA-LR group compared to the WT group (Figure 2F).

After AICAR stimulation, AMPK activity showed no changes in WT or HSA-LR mice (Supplemental Figure 1A – F). To validate the effect of AICAR, acetyl-CoA carboxylase (ACC) was analyzed for phosphorylation on serine-79 (pACC), a stable readout for AMPK activity (Galic et al., 2018). There was no change in total ACC in either WT or HSA-LR mice (Supplemental Figure 1G – I). However, there was a marked increase in the pACC levels after AICAR treatment, reflecting adequate stimulation of the AMPK signaling pathway (Figure 2G-J).

PGC-1α levels increased in WT mice after AICAR treatment (Figure 2K), but not in HSA-LR mice (Figure 2L). There were also no significant differences in GLUT4 expression after treatment in WT or HSA-LR animals (Figure 2M, N). We then calculated the delta AICAR values for each target for the experimental groups (treatment group values – baseline group values) to compare the normalized response to AICAR treatment. This comparison elucidates the proportional response of the pathway targets. Delta AICAR comparisons for pACC yielded no differences, further validating the proportional activation of AMPK signaling with AICAR in both experimental groups (Figure 2O, P). Delta AICAR comparisons of PGC-1α showed that HSA-LR mice had an impaired response to AICAR treatment (Figure 2Q). Further, delta AICAR comparisons for GLUT4 showed no differences in responses to treatment (Figure 2R). In

summary, we observed that even with proportional AICAR activation of AMPK, we saw that PGC-1α response was impaired in HSA-LR mice (Figure 2S).

2.3.3 Akt-AS160 has impaired response to AICAR in HSA-LR mice

Next, we wanted to determine the impact AICAR had on intrinsic insulin signaling. Thus, we assessed phosphorylated serine-473 Akt (pAkt) and phosphorylated threonine-642 AS160 (pAS160) on western blot (Figure 3A, Supplemental Figure 7-9). No significant differences were detected in baseline pAkt, pAkt/Akt or pAS160 between WT and HSA-LR mice (Figure 3B – D). After AICAR treatment, pAkt and pAkt/Akt showed an increased response in the WT mice, but this was not reflected in the HSA-LR mice (Figure 3E-H). When total Akt was assessed, there were no differences in total expression before or after AICAR treatment (Supplemental Figure 1J – L). Downstream of Akt, pAS160 was measured to determine the signaling capacity for GLUT4 translocation. In WT animals, AICAR stimulation led to a significant increase in pAS160 (Figure 3I). However, there was no such trend found in the HSA-LR mice (Figure 3J).

Again, delta AICAR values were calculated to compare the proportional changes of protein expression after AICAR treatment. The delta AICAR for pAkt revealed that HSA-LR mice had a significantly impaired response to AICAR compared to the WT mice (Figure 3K, L). Similarly, delta AICAR for pAS160 revealed that pAS160 change was significantly lower in HSA-LR mice compared to WT mice (Figure 3M). Despite proportional AMPK stimulation in WT and HSA-LR mice, the insulin signaling pathway was not adequately stimulated in the HSA-LR mice (Figure 3N).

2.3.4 Immunofluorescence indicates trends of increased GLUT4 translocation in WT mice after AICAR stimulation

In gastrocnemius tissue from vehicle- and AICAR-injected WT and HSA-LR mice, GLUT4 translocation was assessed by probing for GLUT4 and laminin. Localization was quantified with the proportion of the total GLUT4 and GLUT4 colocalizing with the laminin-labeled plasma membrane (Figure 4A). The pattern of the GLUT4 staining in the vehicle-treated WT mice was dispersed in the cytosol. Some of the GLUT4 staining was found along the plasma membrane region, denoted by the laminin staining. HSA-LR mice exhibited higher membrane GLUT4 staining after AICAR treatment, but these differences were lost when normalized to total GLUT4 staining (Supplemental Figure 1M – P). WT mice treated with AICAR had trends ($p = 0.0573$) indicating increased GLUT4-Laminin:Total GLUT4, suggesting increased levels of GLUT4 at the plasma membrane (Figure 4B). HSA-LR mice did not show ($p = 0.26$) any shifts in the GLUT4-Laminin:Total GLUT4 after AICAR treatment (Figure 4C). When the delta AICAR was compared there were no differences found, indicating no significant differences in relative GLUT4 translocation (Figure 4D).

2.3.5 AMPK axis is stimulated in human control and DM1 myotubes

Healthy control (CTL) cells and DM1 myotubes were treated with insulin alone, AICAR alone, or AICAR and insulin combined, and then probed for targets to assess the impact that treatment had on the AMPK signaling pathway (Figure 5A, Supplemental Figure 10-13, 16). At baseline, total AMPK was reduced in DM1 myotubes (Figure 5B). However, phosphorylated threonine-172 AMPK (pAMPK) was greater in DM1 myotubes (Figure 5C,D). There was no change in pAMPK after AICAR or insulin treatments (Figure 5E). Given the transient nature of AMPK, ACC, a stable downstream target of AMPK, was also assessed. Phosphorylated serine-79 ACC (pACC) increased with AICAR and combination treatments in CTL and DM1 myotubes (Figure 5F). There were no differences in PGC-1α or GLUT4 expression prior to or after treatments (Figure 5G – H).

Like the analysis in the mice, delta insulin, delta AICAR and delta combination values were calculated to compare the proportional changes of protein expression after treatments. For pACC, there were no significant differences found after insulin, AICAR or combination treatments (Figure 5I-K), further validating the proportional activation of AMPK. In summary, despite AMPK stimulation there were no observed changes in PGC-1α or GLUT4 expression (Figure 5L).

2.3.6 Akt-AS160 signaling is impaired in DM1 myotubes

CTL and DM1 myotubes were treated with vehicle, insulin, AICAR or a combination of both and then analyzed for Akt and AS160 signaling (Figure 6A, Supplemental Figure 2G – J, 14-16). DM1 myotubes had significantly higher pAkt expression than CTL at baseline (Figure 6B).

Unlike CTL myotubes, DM1 pAkt showed no significant response to insulin treatment, but did exhibit an increase with combination treatment (Figure 6C). Similar trends were observed after normalization to total Akt (Figure 6D), with a loss of statistical significance for combination treatment (Figure 6E).

Again, delta insulin, delta AICAR and delta combination values were calculated to compare the proportional changes of protein expression after treatments. DM1 myotubes exhibited an impaired pAkt and pAkt/Akt response to insulin, AICAR, and combination treatments (Figure 6F-K). Altogether, there is consistent indication of impaired Akt signaling in DM1 myotubes (Figure 6L).

AS160 phosphorylation levels were also measured in CTL and DM1 myotubes (Figure 7A). Consistent with pAkt and pAkt/Akt, we found that baseline pAS160 was higher in DM1 myotubes compared to CTL myotubes (Figure 7B). Both CTL and DM1 myotubes exhibit pAS160 increase after combination treatment (Figure 7C). When pAS160 was normalized to total AS160 (pAS160/AS160), similar trends were observed (Figure 7D – E).

Delta insulin, delta AICAR and delta combination values showed a difference in pAS160 responses. There was an impaired DM1 pAS160 response after insulin treatment (Figure 7F). There were also trends ($p = 0.0940$) of impaired pAS160 response after AICAR treatment (Figure 7G). With combination treatment, we again observed a reduced DM1 pAS160 response (Figure 7H). Delta insulin and delta AICAR differences were lost after pAS160 was normalized to total AS160 (pAS160/AS160) (Figure 7I). Even after normalization, we still observed reduced DM1 pAS160/AS160 activation after combination treatment. Overall, we saw a consistent indication of impaired AS160 signaling in the DM1 myotubes (Figure 7L).

2.4 Discussion

2.4.1 Ingenuity Pathway Analysis of sedentary and exercised HSA-LR mice

This study was conducted to understand the insulin signaling pathway and exercise interaction within the context of DM1. Thus, we decided to investigate relevant targets pertaining to insulin and exercise signaling pathways. With IPA, we found some targets that aligned with the relevant pathways in sedentary and exercised HSA-LR mice. We decided to then acutely stimulate AMPK with AICAR in our HSA-LR mice and DM1 myotubes to determine how AMPK- PGC-1α stimulation impacted insulin signaling. Our study, aligned with IPA findings, found that baseline total AMPK was lower in the HSA-LR mouse and in the DM1 myotubes. Additionally, in the HSA-LR mouse, PGC-1α expression did not respond to AICAR treatments as was found in WT mice, suggesting dysregulation of PGC-1α. Further, IPA predicted the insulin receptor to be inhibited in the sedentary HSA-LR mice. Our study found that pAkt signaling, a reporter of proximal insulin signaling, was indeed impaired in the HSA-LR mouse and the DM1 myotubes. After exercise intervention, IPA predicted PGC-1α and insulin receptor to be upregulated. However, in our DM1 models, we observed that acute AMPK stimulation did not improve PGC-1α or Akt levels or activity. Additionally, IPA detected increased GLUT4 expression in the exercised HSA-LR mice, indicating that exercise drives GLUT4 expression. Again, our findings did not align with IPA's, as we saw no clear increase in total GLUT4 after AMPK-PGC-1α stimulation.

The powerful IPA analysis tool helped inform the investigation of targets pertinent to insulin and exercise signaling in DM1. The IPA analysis of the sedentary HSA-LR condition

aligned with a lot of the findings we saw in the baseline expression of our DM1 models. However, when we decided to target the exercise axis, AMPK-PGC-1α, in an acute and targeted manner with AICAR, we saw that neither of the models had significant improvements in insulin resistance markers.

2.4.2 AICAR Treatment in HSA-LR Mouse Model

At baseline, total AMPK levels were lower in HSA-LR mice, however pAMPK was no different from WT. When subjected to AICAR, AMPK phosphorylation did not indicate any significant changes. Due to the transient nature of AMPK signaling, ACC phosphorylation was measured to validate the activity of the AICAR injection. Indeed, pACC increased, suggesting the increased activity of AMPK after AICAR treatment (Taylor et al., 2008).

Baseline expression of PGC-1α showed no differences between WT and HSA-LR. Yet, previous reports indicate a ~43% lower expression of PGC-1α in HSA-LR skeletal muscle tissue (Ravel-Chapuis et al., 2018). Ravel-Chapuis et al. described this downregulation in extensor digitorum longus (EDL) muscle, whereas we analyzed protein content in the gastrocnemius. The HSA transgene is differentially expressed in muscles, with the number of mis-splicing events positively correlated with the expression of the HSA transgene across skeletal muscles (Hicks et al., 2024). It was found that the gastrocnemius had the highest abundance of HSA-LR construct expression which correlated with the highest mis-splicing events compared to the quadriceps and tibialis anterior muscles (Hicks et al., 2024). This research did not explicitly examine HSA construct expression in EDL muscle, but its findings may suggest why we found different results in gastrocnemius tissue.

After AICAR injection, PGC-1α levels did not change in HSA-LR mice, contrasting with the increase observed in WT mice. PGC-1α has a half-life ranging from 0.5-5.5 hours, as it is

subjected to the ubiquitin protease degradation pathway (Trausch-Azar et al., 2010). AMPK drives the expression of PGC-1α and directly phosphorylates the transcription factor; however, AMPK has not been described to directly stabilize PGC-1α (Cantó and Auwerx, 2009a). Rather, p38 MAPK is implicated in phosphorylating PGC-1α and increasing its stability (Puigserver et al., 2001). Both exercise and AICAR have been reported to stimulate p38 activity, implicating the kinase as an intermediary within the AMPK-PGC-1α axis (Gibala et al., 2009; Lemieux et al., 2003). Additionally, activated AMPK upregulates transcription of PPARβ/δ, the receptor for PGC-1β and PGC-1δ, via the myocyte enhancer factor 2A (Koh et al., 2019). Then, PPARβ/δ stabilizes the PGC-1α expression levels in skeletal muscle tissue (Koh et al., 2017). The reduced baseline AMPK expression in HSA-LR mice may suggest that PGC-1α was not optimally regulated. Thus, in the acute treatment period of 30 minutes, we likely see an increased stability of the PGC-1α in WT mice which is reflected as elevated levels in western blotting.

Baseline GLUT4 levels were found to be downregulated in the HSA-LR mice. While this may not be explained by a difference in baseline PGC-1α levels, it could reflect diminished PGC-1α activity. For instance, phosphorylation and acetylation have both been shown to regulate PGC-1α transcriptional activity, which could alter expression levels of *SLC2A4* and the subsequent GLUT4 protein content (Michael et al., 2001; Wende et al., 2007a; Cantó and Auwerx, 2009a). There are no reports of *SLC2A4* mis-splicing in any DM1 models or patients, but mis-splicing could be a feasible explanation for the lower expression levels in HSA-LR tissues.

At baseline, there were no observed differences in pAkt, pAkt/Akt or pAS160 levels, but there were differences in their responses to AICAR. In WT mice, AICAR treatment increased pAkt and pAkt/Akt, similar to previous findings (Dedert et al., 2023). After repleting C2C12s

with nutrient rich media, serine-473 pAkt increased via mTORC2 regulation (Dedert et al., 2023). This effect could explain why we observed an increase in pAkt for WT mice after AICAR treatment. While there is no conclusive literature that directly assesses Akt activity in HSA-LR mice, there is a study that explored GSK-3β, a downstream target inhibited by Akt (Lin et al., 2007). In line with our reports of impaired Akt activity, literature indicates that GSK-3β is upregulated in the HSA-LR mouse model (Jones et al., 2012). We also saw that pAS160 levels remained impaired and blunted even after AICAR injection in HSA-LR mice, which is consistent with the downregulated pAkt. In line with the impaired pAS160 signaling, we saw no significant change in the proportion of GLUT4 at the plasma membrane as evidenced by immunofluorescent staining. This contrasts with the response that we saw in WT mice, which had elevated levels of pAS160 and corresponding trends for increased plasma membrane-bound GLUT4. This is consistent with literature that finds AMPK stimulation, via exercise or AICAR, increases AS160 activity and GLUT4 shuttling (Arias et al., 2007b; Bradley et al., 2014; Wang et al., 2022). We observed that HSA-LR mice, compared to WT mice, consistently demonstrate a diminished response in Akt, PGC-1α, and pAS160. This outcome demonstrates the presence of insulin resistance in the HSA-LR mouse model and its resistance to acute AMPK stimulation.

2.4.3 Insulin and AICAR treatment in DM1 myotube models

Like the HSA-LR model, we saw downregulated expression of total AMPK in DM1 myotubes, however the pAMPK seemed to be upregulated. Given the transient nature of AMPK phosphorylation, we decided to assess pACC as a stable readout of AMPK activity. We found proportionate phosphorylation of ACC after AICAR or combination treatment, indicating stimulation of AMPK. Contrary to what was observed in the HSA-LR skeletal muscle tissue,

PGC-1α and GLUT4 did not show any differences at baseline or after stimulation with insulin or AICAR. This data is consistent with a study that found no differences in PGC-1α content before or after exercise intervention in DM1 patients (Mikhail et al., 2022).

The baseline serine-473 pAkt levels in DM1 myotubes were higher than healthy CTL myotube levels. Consistently, we saw an increased basal level of pAS160 in DM1 myotubes. Yet, following insulin and/or AICAR treatment, the DM1 myotubes had a lower delta response in pAkt, pAkt/Akt and pAS160. When Bertacca et al. subjected human myoblasts to a high concentration of insulin to induce resistance, they hyperactivated the insulin signaling pathway in the myoblasts (Bertacca et al., 2005). This hyperactivated insulin signaling pathway did not reflect higher glucose uptake at baseline and even had a blunted response to subsequent insulin treatment compared to healthy control myoblasts (Bertacca et al., 2005). Their results mimic our findings, where elevated baseline Akt-AS160 signaling in our DM1 myotubes did not have CTL-like responses to insulin and/or AICAR treatment. AS160 phosphorylation leads to GLUT4 translocation, so our data may suggest that GLUT4 translocation and subsequent glucose uptake could be impaired in the human DM1 myotubes.

2.4.4 Possible explanations for insulin resistance in DM1

The data from the HSA-LR mouse model and the DM1 myotube model share some similarities. In both models, we see that there is a proportional and adequate stimulation of pACC indicating the stimulation of AMPK with AICAR. Despite the activation of AMPK in the HSA-LR model, we do not see an increase in PGC-1α protein. We did not see any changes in PGC-1α abundance in the DM1 myotube model, however this was no different than the CTL cells. Further, in both models we saw an impaired response to treatment in Akt phosphorylation.

Consistently, reduced AS160 phosphorylation was observed after AICAR treatment and following insulin treatment in the myotube model. While we see these differences shared across both models, there is no literature describing the mis-splicing of RNA transcripts for AMPK, PGC-1α, Akt, AS160 or GLUT4. *INSR* can be mis-spliced in DM1, but this mechanism cannot account for all our findings since *INSR* is not mis-spliced in the HSA-LR model (Brockhoff et al., 2017). However, there is the prediction that a protein implicated in insulin signaling, Tre-2/Bub2/Cdc16 (TBC) domain family member 15 (TBC1D15), may be dysregulated because of RNA mis-splicing (Nakamori et al., 2013).

TBC1D15 is specifically implicated in the Rab protein interaction with GSVs. Rab GTPase proteins function to transduce signaling to mechanical effectors like myosin and actin to initiate the movement of GSVs (Klip et al., 2014). TBC1D15 then serves as GAP, similar to AS160, for Rab GTPase proteins (Peralta et al., 2010). TBC1D15 is also important for regulating lysosome and mitochondrial morphology (Yamano et al., 2014). Wu et al. knocked TBC1D15 out of different cell lines, including the L6 rate skeletal muscle cell line, and found that GLUT4 content was reduced (Wu et al., 2019). Interestingly, one group predicts that TBC1D15 may be mis-spliced in DM1 (Nakamori et al., 2013), which could possibly explain the post-insulin receptor dysregulations found in our study. This could also provide further context as to why GLUT4 content was reduced in the HSA-LR tissue. Validating TBC1D15 at the RNA and protein levels in future studies would help further explore the dysregulated insulin signaling pathway in DM1.

2.4.5 Significance

Insulin signaling is key to the anabolic processes that occur in the cell to advance cell growth and cell division. Therefore, it is important to investigate insulin resistance in DM1, as it can exacerbate some of the other symptoms implicated in the disorder such as muscle atrophy and weakness (Renna et al., 2019). Studies have assessed the use of classical insulin sensitizing treatments, like metformin, in DM1, however the impacts of these treatments on insulin resistance in DM1 were not extensively explored (Gagnon et al., 2018; García-Puga et al., 2022). Our study sought to provide context on the response of insulin signaling molecules in DM1 following acute AMPK stimulation. In doing so, we were able to explore the responses in two models of DM1 where we confirmed dysregulated insulin signaling, prior to and after AMPK stimulation.

Exercise yields improvements in strength, mobility and metabolism for DM1 patients, but insulin resistance has not been specifically assessed (Okkersen et al., 2018; Roussel et al., 2019, 2020; Di Leo et al., 2023). Metabolic adaptations from exercise are classically linked with improvements in glucose uptake which necessitates the investigation of the insulin signaling pathway. However, other factors such as elevated local blood flow and blood glucose concentration can also contribute to exercised-induced glucose uptake (Martin et al., 1995; Rose and Richter, 2005). This study has demonstrated the downregulated behaviour of insulin signaling molecules in response to AMPK stimulation in DM1 but does not discount the overall validity of exercise for DM1 patients. The design of our study specifically assessed acute AMPK stimulation, which means that DM1 patients could still see insulin signaling benefits with chronic AMPK stimulation.

2.4.6 Limitations

Key to this study was the stimulation of the exercise pathway through the AMPK-PGC-1α axis using acute AICAR treatment. We decided to study this in female HSA-LR mice along with cells derived from patients that were not sex-matched. However, we recognize that DM1 can present in a sex-specific manner, with further sex-specific responses to exercise (Dogan et al., 2016; Ravel-Chapuis et al., 2018). In future studies, it would be ideal to sex-match pre-clinical models to gather a clear scope for sex-specific modifiers.

Due to the transient nature of the AMPK and AS160 phosphorylation, mice were treated for 30 minutes with AICAR, while myotubes were treated with it for 60 minutes (Sriwijitkamol et al., 2007; Funai and Cartee, 2008). It would be insightful to explore time course treatments to investigate the interactions of the proteins after chronic AMPK stimulation. Further, investigations with acute and chronic exercise regimens in the mice could elucidate some of the long term and systemic impacts that exercise has on the insulin signaling pathway.

2.4.7 Conclusions

After employing both a mouse and human myotube model, this study demonstrated that the insulin signaling pathway is impaired in DM1 and is not rescued with acute AMPK stimulation. Namely, we found that acute AMPK activation did not rescue the Akt-AS160 signaling pathway in either of the models, suggesting that GLUT4 translocation is impaired in DM1 prior to and after AMPK stimulation. Further studies could confirm RNA levels of the insulin and exercise pathway proteins to investigate possible spliceopathies. A target of note is TBC1D15, which is involved in GLUT4 stability and translocation and is predicted to be mis-spliced in DM1. Further, time course treatments with AICAR, and long-term exercise studies in mice and humans could further elucidate the interactions of the insulin signaling and exercise

signaling proteins. Altogether, this study provides new insights into the pathomechanisms of insulin resistance in DM1 and furthers the understanding of metabolic behaviour in DM1 patients.

2.5 Manuscript Figures

1.

A.

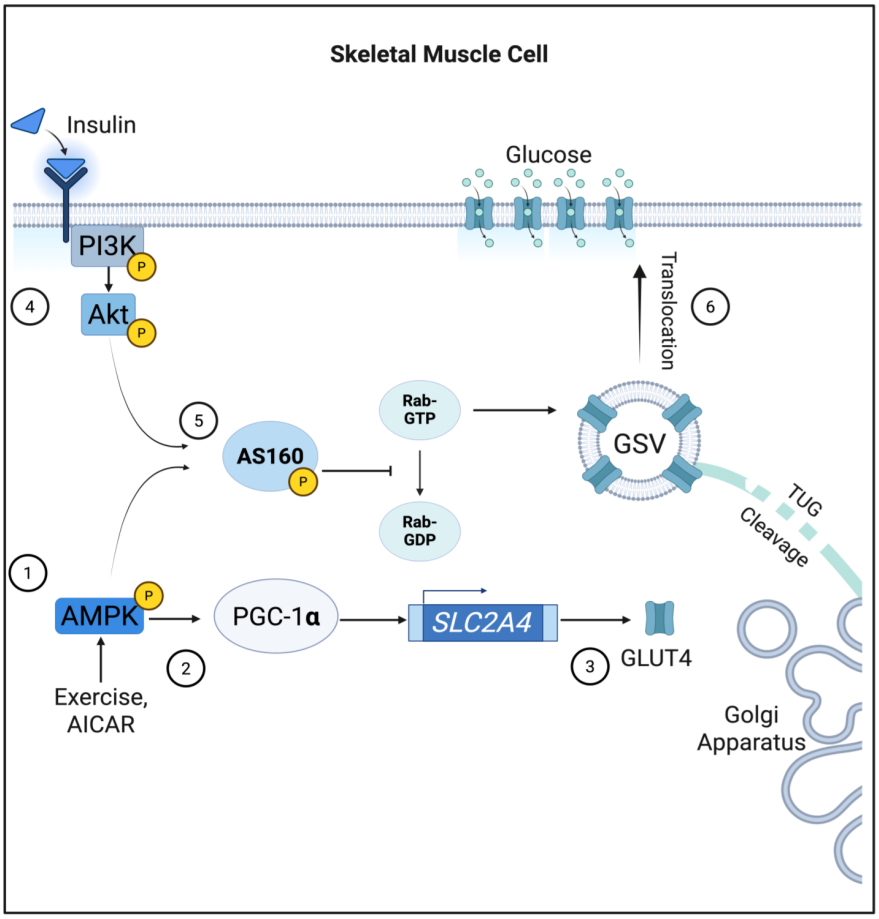

B.

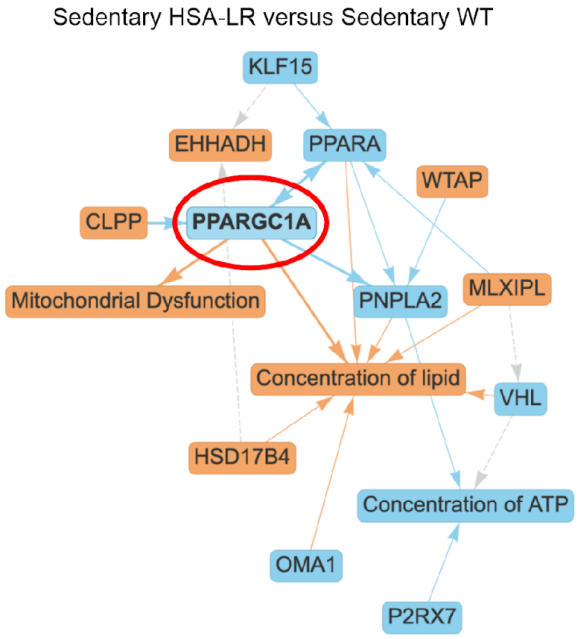
Sedentary HSA-LR versus Sedentary WT
KLF15
EHHADH
PPARA
WTAP
CLPP
PPARGC1A
Mitochondrial Dysfunction
PNPLA2
MLXIPL
Concentration of lipid
VHL
HSD17B4
Concentration of ATP
OMA1
P2RX7

C.

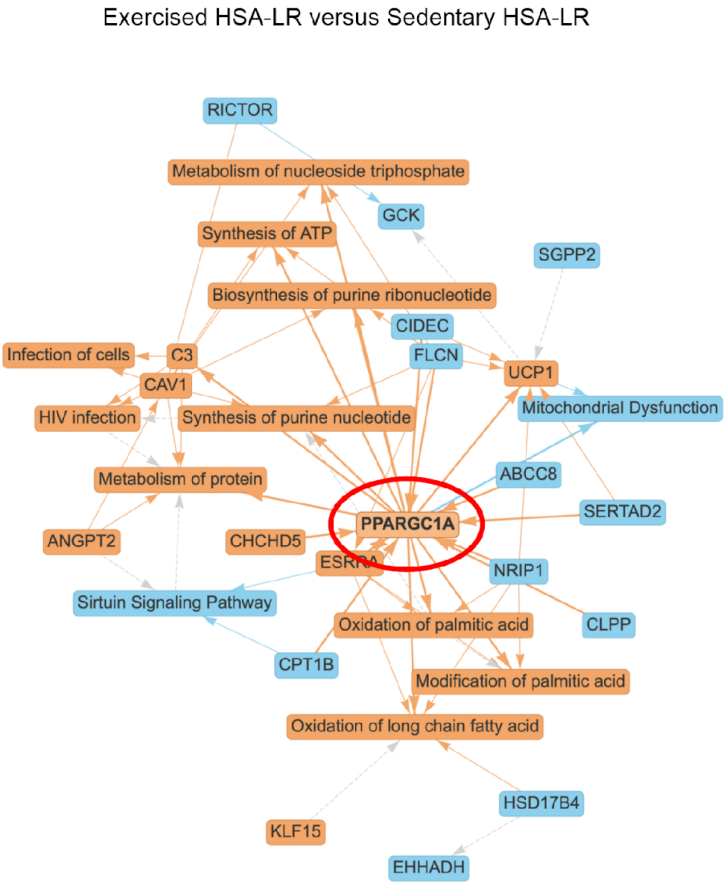
Exercised HSA-LR versus Sedentary HSA-LR
RICTOR
Metabolism of nucleoside triphosphate
GCK
Synthesis of ATP
SGPP2
Biosynthesis of purine ribonucleotide
CIDEC
Infection of cells
C3
FLCN
UCP1
CAV1
HIV infection
Synthesis of purine nucleotide
Mitochondrial Dysfunction
Metabolism of protein
ABCC8
PPARGC1A
SERTAD2
ANGPT2
CHCHD5
ESRRA
NRIP1
Sirtuin Signaling Pathway
Oxidation of palmitic acid
CLPP
CPT1B
Modification of palmitic acid
Oxidation of long chain fatty acid
HSD17B4
KLF15
EHHADH

Figure 1. Predicted interactions of PGC-1α and insulin signaling pathway. A. Graphical depiction of proposed interactions between insulin signaling and exercise pathways in skeletal muscle. Adenosine monophosphate activated protein kinase (AMPK) stimulation via exercise or AICAR (1) can drive peroxisome proliferator-activated receptor gamma coactivator 1 alpha (PGC-1α) activity and expression (2) to increase expression of glucose transporter 4 (GLUT4) (3). Insulin binds to the insulin receptor which activates Akt (4) which leads to Akt substrate of 160 (AS160) stimulation (5). AS160 stimulation then drives GLUT4 storage vesicle (GSV) translocation to transport GLUT4 to the plasma membrane (6). **B.** Predicted inhibition (blue arrow and nodes) of peroxisome proliferator-activated receptor gamma coactivator 1 alpha (PPARGC1A, PGC-1α, red circle) in sedentary human skeletal actin long repeat (HSA-LR) mice vs sedentary wildtype (WT) mice and **C.** Predicted PGC-1α (red circle) activation (orange arrows and nodes) in exercised HSA-LR mice vs sedentary HSA-LR model mice. Panel A. created with Biorender.com.

2.

A.

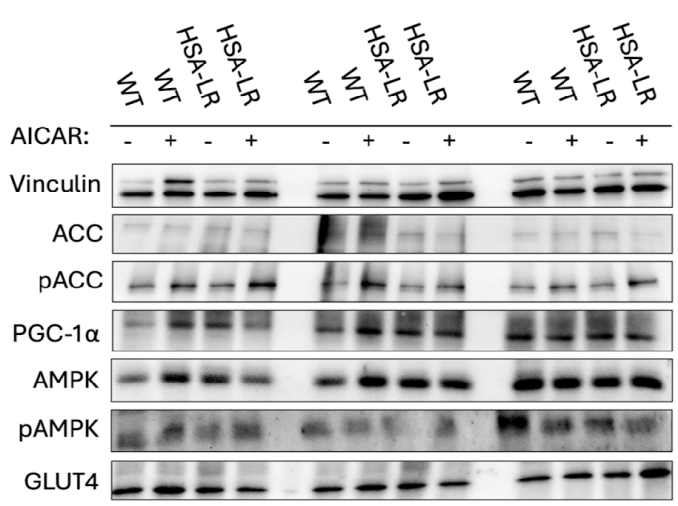
WT
WT
HSA-LR
HSA-LR
AICAR:
- + - +
Vinculin
ACC
pACC
PGC-1α
AMPK
pAMPK
GLUT4

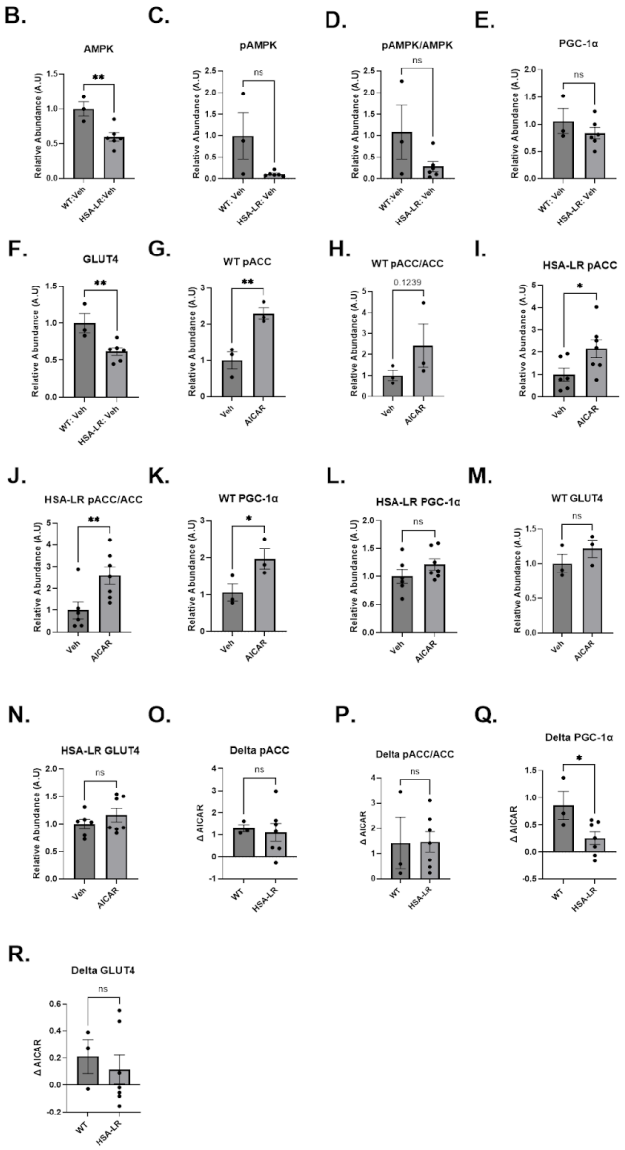
B.
AMPK
C.
pAMPK
D.
pAMPK/AMPK
E.
PGC-1α
F.
GLUT4
G.
WT pACC
H.
WT pACC/ACC
I.
HSA-LR pACC
J.
HSA-LR pACC/ACC
K.
WT PGC-1α
L.
HSA-LR PGC-1α
M.
WT GLUT4
N.
HSA-LR GLUT4
O.
Delta pACC
P.
Delta pACC/ACC
Q.
Delta PGC-1α
R.
Delta GLUT4

S.

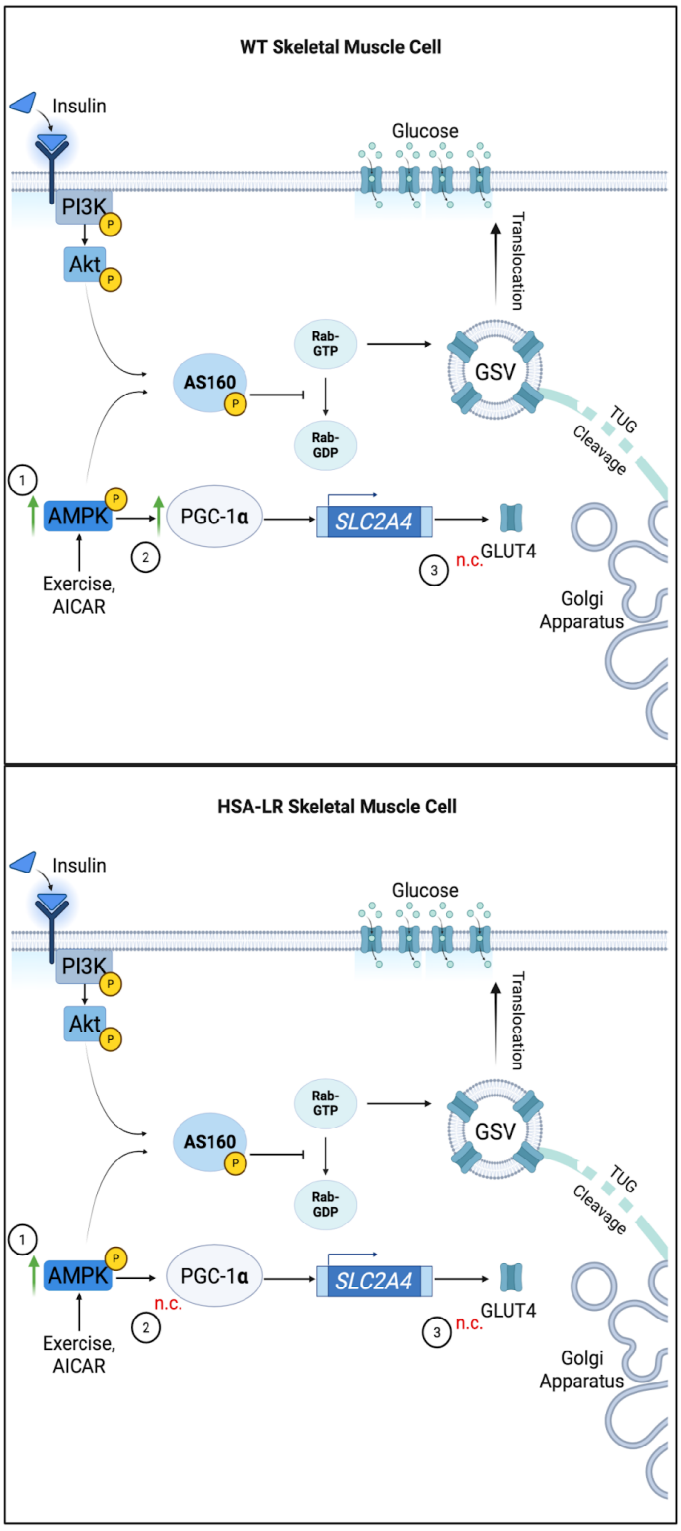
WT Skeletal Muscle Cell
Insulin
Glucose
PI3K
Akt
Translocation
Rab-GTP
AS160
GSV
Rab-GDP
TUG Cleavage
AMPK
PGC-1α
SLC2A4
GLUT4
n.c.
Exercise, AICAR
Golgi Apparatus
HSA-LR Skeletal Muscle Cell
Insulin
Glucose
PI3K
Akt
Translocation
Rab-GTP
AS160
GSV
Rab-GDP
TUG Cleavage
AMPK
PGC-1α
SLC2A4
GLUT4
n.c.
n.c.
Exercise, AICAR
Golgi Apparatus

Figure 2. AMPK-PGC-1α pathway in WT and HSA-LR mice. A. Representative western blots (whole blots found in Supplemental Figure 3-6, 9) of proteins along the exercise signaling pathway in gastrocnemius tissue of wild-type (WT) and human skeletal actin long repeat (HSA-LR) mice injected with saline (-) or 5-aminoimidazole-4-carboxamide ribonucleotide (AICAR, +). **B.** Decreased levels of adenosine monophosphate activated protein kinase (AMPK), **C.** but not threonine-172 phosphorylated AMPK (pAMPK) in HSA-LR mice. No difference when **D.** pAMPK is normalized to total AMPK (pAMPK/AMPK). **E.** Comparison of peroxisome proliferator-activated receptor gamma coactivator 1 alpha (PGC-1α) protein levels shows no significant difference between WT and HSA-LR mice at baseline **F.** Comparison of glucose transporter 4 (GLUT4) protein levels shows higher protein in WT compared to HSA-LR mice at baseline. **G. & H.** Increase of the phosphorylated serine-79 acetyl-CoA carboxylase (pACC) and pACC/ACC in WT mice after AICAR treatment. **I. & J.** Increase of the pACC and pACC/ACC in HSA-LR mice after AICAR treatment. **K.** Increase of the PGC-1α in WT mice after AICAR treatment. **L.** Increase of PGC-1α from HSA-LR mice after AICAR treatment. **M.** No change in GLUT4 levels in WT mice after AICAR treatment. **N.** No change in GLUT4 levels in HSA-LR mice after AICAR treatment **O. & P.** Delta values (treatment values – baseline values) with respect to AICAR treatment for pACC, pACC/ACC shows no differences in the responses to AICAR for WT and HSA-LR mice. **Q.** Delta values with respect to AICAR treatment for PGC-1α indicate a greater response in WT compared to HSA-LR. **R.** Delta values with respect to AICAR treatment for GLUT4 shows no differences between WT and HSA-LR mice**. S.** Graphical depiction of the molecular response to AICAR treatment in WT and HSA-LR mice. Green arrows indicate an increased level of the target after AICAR treatment. Increased signaling of AMPK (1) as reflected in the increased pACC levels (not shown), increased PGC-1α

(2) in WT mice, but no change (red n.c.) in HSA-LR, and GLUT4 (3) reflects no change (n.c.) in either WT or HSA-LR mice. Panel S. created by Biorender.com. N = 3 WT (Veh), 3 WT (AICAR), 6 HSA-LR (Veh), 7 HSA-LR (AICAR) mice. All samples run in technical duplicates. One-tailed unpaired Welch's T-test for panels C, M, N, O, P, R. Remaining panels analyzed with one-tailed unpaired Student's T-test. *$p<0.05$, **$p < 0.005$, ***$p<0.0005$. Graphs are means +/- SEM.

3.

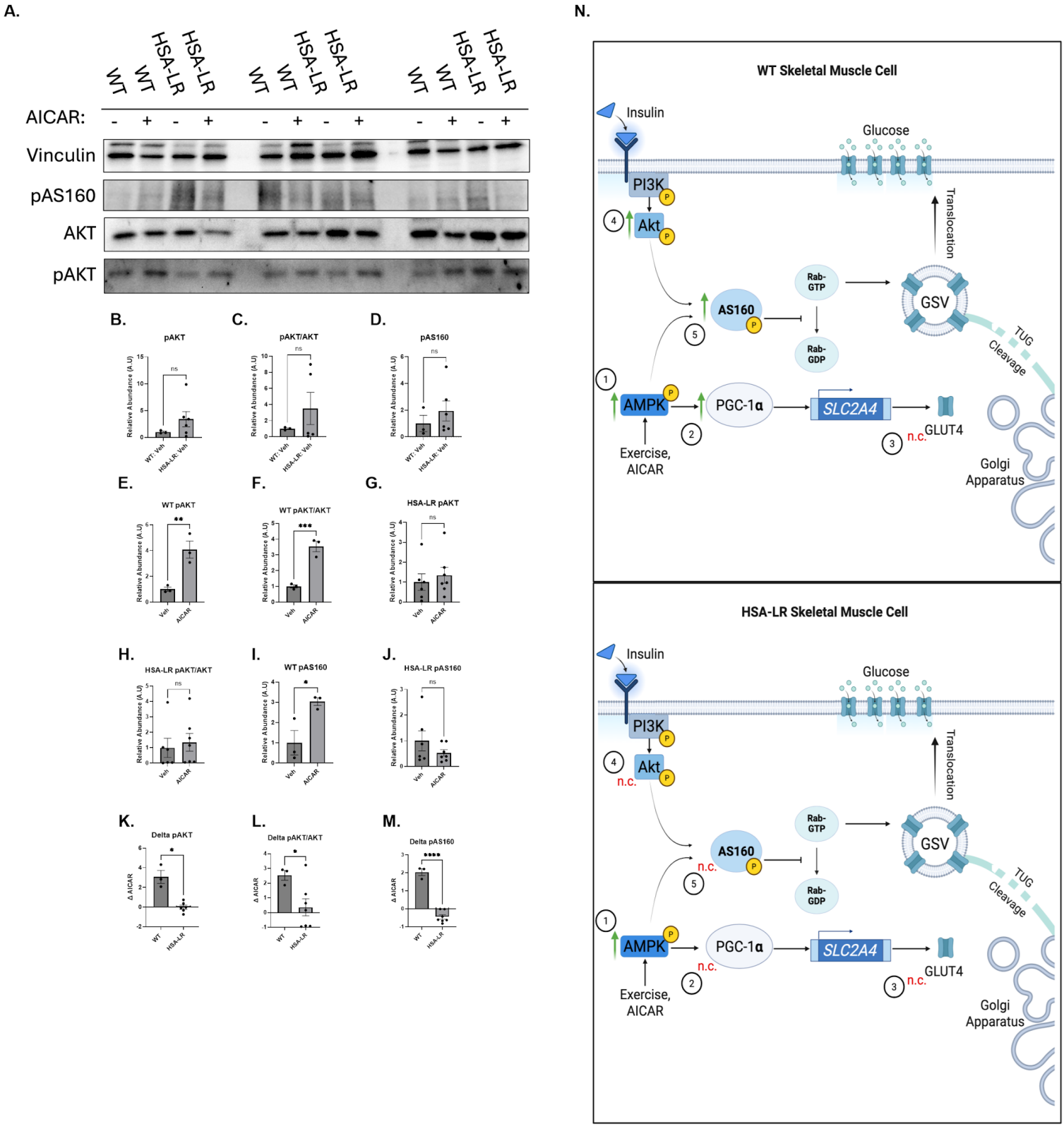
A.
WT
WT
HSA-LR
HSA-LR
AICAR:
Vinculin
pAS160
AKT
pAKT
B.
pAKT
C.
pAKT/AKT
D.
pAS160
E.
WT pAKT
F.
WT pAKT/AKT
G.
HSA-LR pAKT
H.
HSA-LR pAKT/AKT
I.
WT pAS160
J.
HSA-LR pAS160
K.
Delta pAKT
L.
Delta pAKT/AKT
M.
Delta pAS160
Relative Abundance (A.U)
Δ AICAR
Veh
AICAR
WT
HSA-LR
N.
WT Skeletal Muscle Cell
Insulin
Glucose
PI3K
Akt
AS160
Rab-GTP
Rab-GDP
GSV
Translocation
TUG Cleavage
AMPK
PGC-1α
SLC2A4
GLUT4
Exercise, AICAR
Golgi Apparatus
HSA-LR Skeletal Muscle Cell
n.c.

Figure 3. Akt-AS160 pathway in WT and HSA-LR mice. A. Representative western blots (whole blots found in Supplemental Figure 7-9) of proteins along the insulin signaling molecular pathways in gastrocnemius tissue of wild-type (WT) and human skeletal actin long repeat (HSA-LR) mice injected with saline (-) or 5-aminoimidazole-4-carboxamide ribonucleotide (AICAR, +). **B. & C.** Comparison of pAkt and pAkt/Akt protein levels shows no significant difference between WT and HSA-LR mice. **D.** Comparison of phosphorylated threonine-642 Akt substrate of 160 kDA (pAS160) protein levels shows higher total protein in WT compared to HSA-LR mice. **E. & F.** Increase of the pAkt and pAkt/Akt after AICAR treatment in WT mice. **G. & H.** Quantification of the pAkt and pAkt/Akt observed in the HSA-LR mice. **I.** Increase of pAS160 observed in the WT mice after AICAR injection. **J.** Quantification of the pAS160 in HSA-LR mice. **K.-M.** Quantification of the delta values with respect to AICAR treatment for pAkt, pAkt/Akt, pAS160. **N.** Graphical depiction of the response of molecules after treatment with AICAR in WT and HSA-LR mice. Green arrows indicate an increased level of the target after AICAR treatment. (4) indicates the increased phosphorylation of Akt in WT mice with no change (n.c.) observed in HSA-LR mice, reflecting the increased pAS160 (5) in WT mice, but no change (n.c.) in HSA-LR. N = 3 WT (Veh), 3 WT (AICAR), 6 HSA-LR (Veh), 7 HSA-LR (AICAR) mice. Panel N. created by Biorender.com. All samples run in technical duplicates. One-tailed unpaired Welch's T-test for panels B, C, G, H, K, L. Remaining panels analyzed with one-tailed unpaired Student's T-test. *$p<0.05$, **$p < 0.005$, ***$p<0.0005$. Graphs are means +/- SEM.

4.

A.

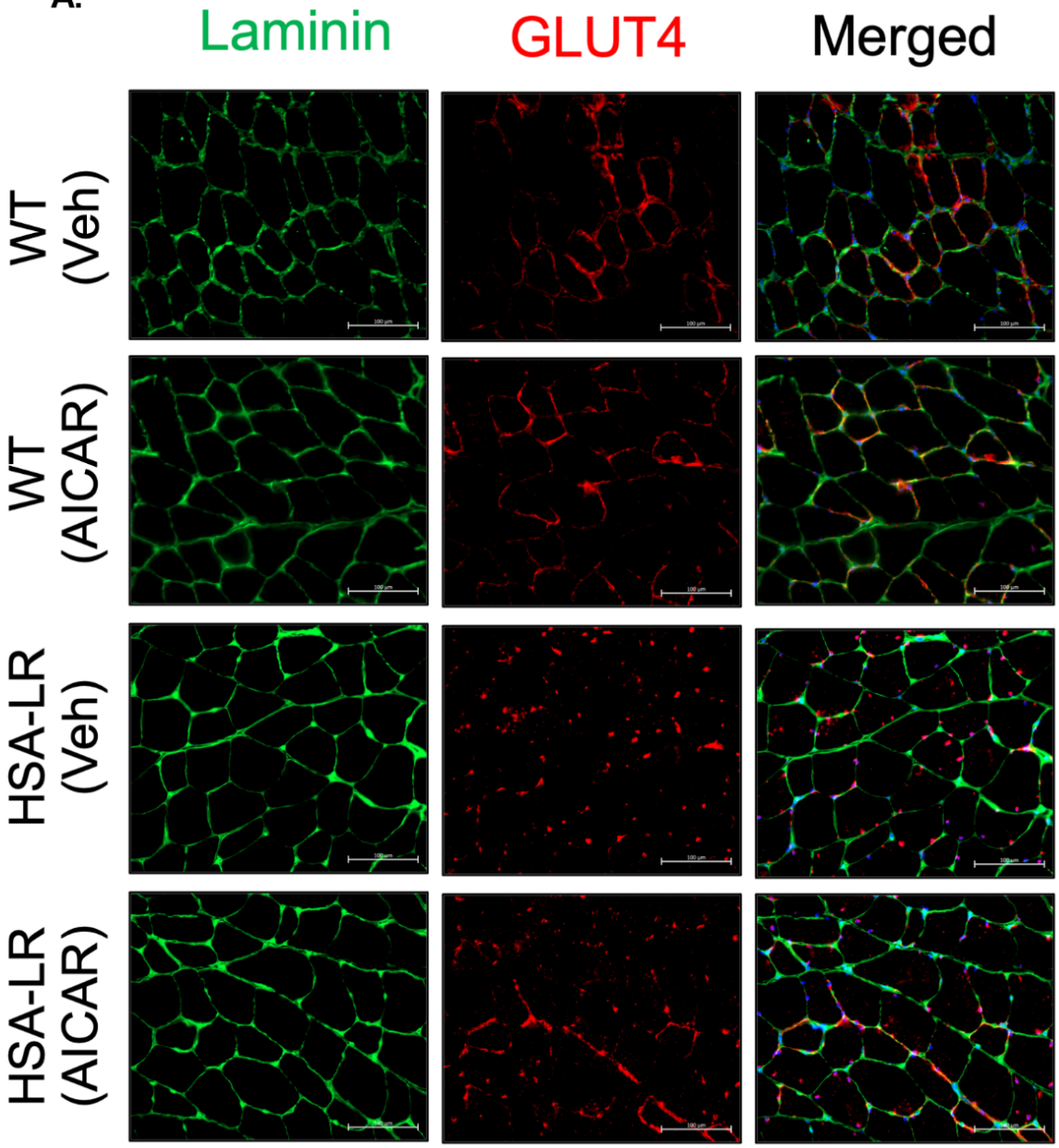
Laminin
GLUT4
Merged
WT (Veh)
WT (AICAR)
HSA-LR (Veh)
HSA-LR (AICAR)

B.

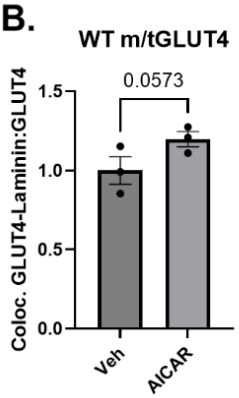
WT m/tGLUT4
0.0573
Coloc. GLUT4-Laminin:GLUT4
1.5
1.0
0.5
0.0
Veh
AICAR

C.

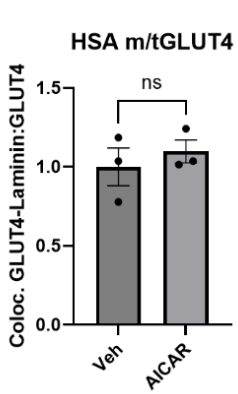
HSA m/tGLUT4
ns
Coloc. GLUT4-Laminin:GLUT4
1.5
1.0
0.5
0.0
Veh
AICAR

D.

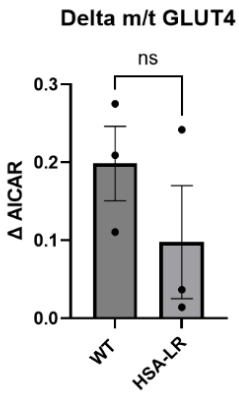
Delta m/t GLUT4
ns
Δ AICAR
0.3
0.2
0.1
0.0
WT
HSA-LR

Figure 4. Immunofluorescence of GLUT4 labelling. **A**. Representative images of immunofluorescent staining of laminin (green), glucose transporter 4 (GLUT4, red) and 4′,6-Diamidino-2-phenylindole (DAPI, blue, merged image) in gastrocnemius sections from saline vehicle (Veh) treated and 5-Aminoimidazole-4-carboxamide ribonucleoside (AICAR) treated mice. **B.** A quantification of the GLUT4-Laminin colocalization (mGLUT4) pixel area relative to the total GLUT4 (tGLUT4) pixel area in WT sections. **C**. A quantification of the GLUT4-Laminin colocalization pixel area relative to the total GLUT4 (tGLUT4) pixel area in HSA-LR sections. **D.** A comparison of the delta responses to AICAR treatment in WT compared to HSA-LR mice. N = 3 WT (Veh), 3 HSA-LR (Veh), 3 WT (AICAR), 3 HSA-LR (AICAR). Experiment conducted in technical duplicates and 200-300 fibres analyzed per section. Scale bar is 100 μm. One-tailed unpaired Student's T-test *$p<0.05$, **$p < 0.005$, ***$p<0.0005$. Graphs are means +/- SEM.

5.

A.

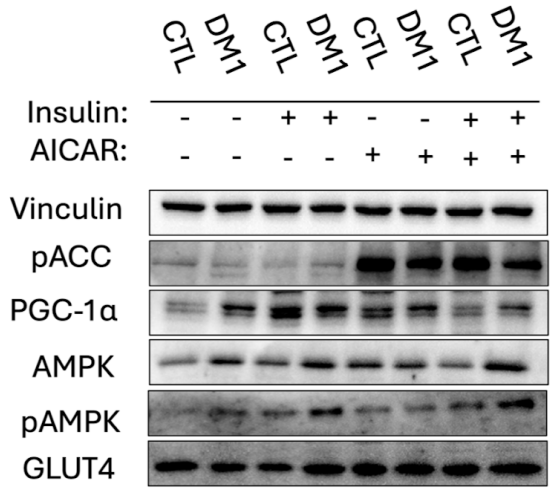

B.

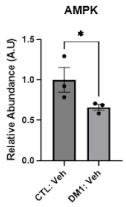

C.

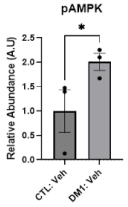

D.

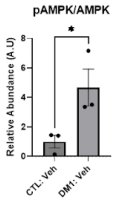

E.

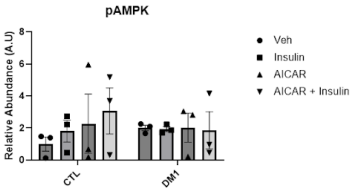

F.

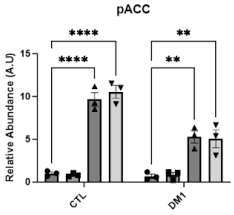

G.

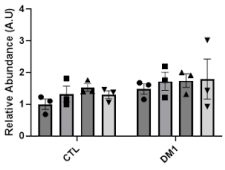

H.

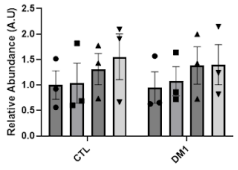

I.

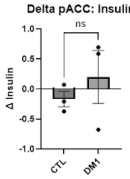

J.

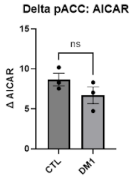

K.

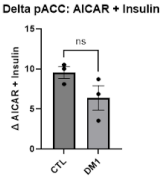

L.

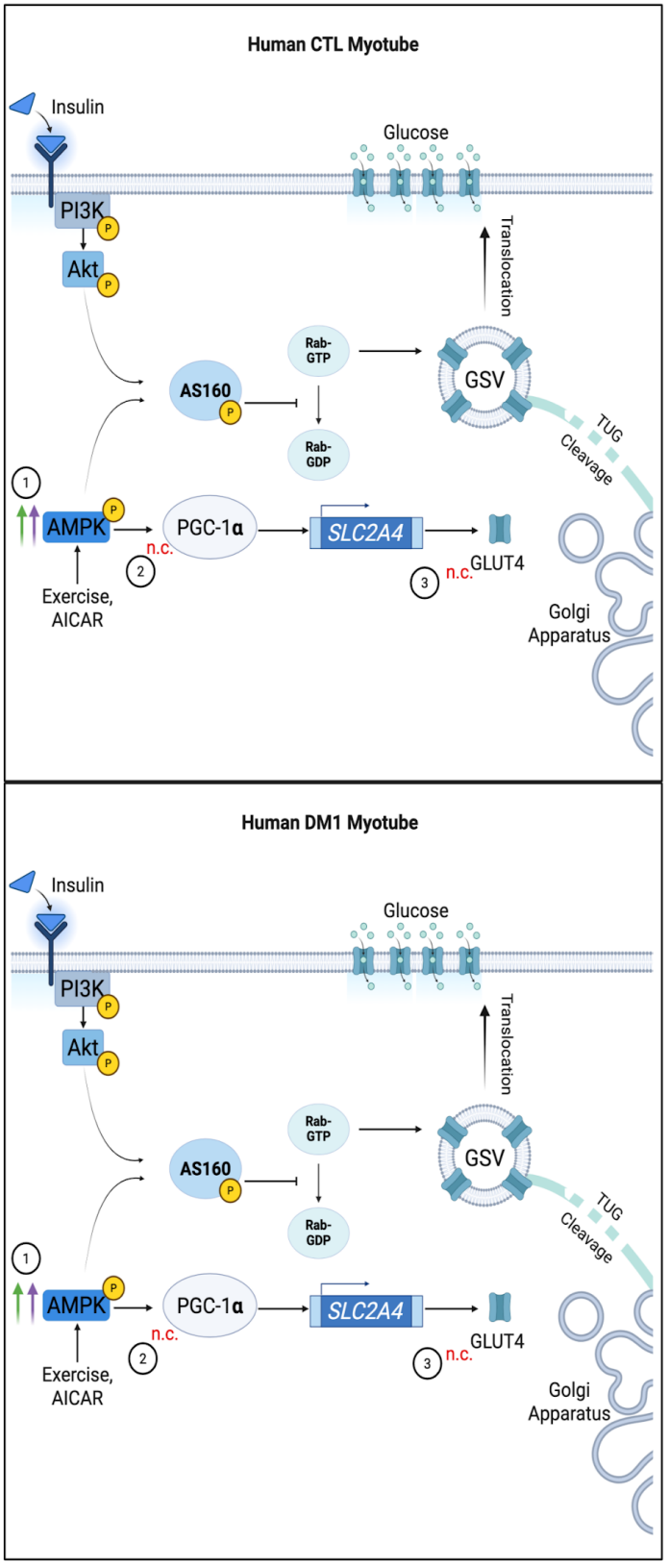

Figure 5. AMPK-PGC-1α pathway in CTL and DM1 myotubes. A. Representative western blots (whole blots found in Supplemental Figure 10-13, 16) of targets along the exercise molecular pathways in human control (CTL) and myotonic dystrophy type 1 (DM1) myotubes mice treated with vehicle (-), insulin, 5-aminoimidazole-4-carboxamide ribonucleotide (AICAR), or a combination of insulin and AICAR. **B.** At baseline, total adenosine monophosphate-activated protein kinase (AMPK) is decreased in human DM1 myotubes. **C.** At baseline, phosphorylated threonine-172 AMPK (pAMPK) is increased in human DM1 myotubes. **D.** At baseline, normalized pAMPK (pAMPK/AMPK) is increased in human DM1 myotubes. **E.** No change for the pAMPK observed in the human CTL and DM1 myotubes after insulin, AICAR or combination treatment. **F.** Increase of the phosphorylated serine-79 acetyl-CoA carboxylase (pACC) observed in the human CTL and DM1 myotubes after AICAR treatment. **G.** No change for the PGC-1α observed in the human CTL and DM1 myotubes after insulin, AICAR or combination treatment. **H.** No change for the glucose transporter 4 (GLUT4) observed in the human CTL and DM1 myotubes after insulin, AICAR or combination treatment. **I.-K.** No change of the delta values with respect to **I.** insulin, **J.** AICAR, or **K.** insulin + AICAR treatment for pACC between CTL and DM1 cell lines. **L.** Graphical depiction of pathway proteins responding to AICAR (green arrow) and/or insulin + AICAR combination (purple arrow) in CTL and DM1 myotubes. (1) Indicates the increased signaling of AMPK levels, (2) reflects no change (n.c.) of PGC-1α and (3) glucose transporter 4 (GLUT4) in DM1 or CTL myotubes. Panel L. created by Biorender.com. N = 2 CTL, 2 DM1. One way ANOVA followed by Tukeys post-hoc test for multiple comparisons E - H., One-tailed unpaired Student's T-test *$p<0.05$, **$p < 0.005$, ***$p<0.0005$. Graphs are means +/- SEM.

6.

A.

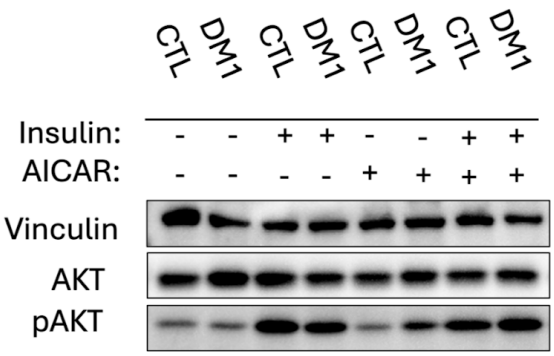

B.

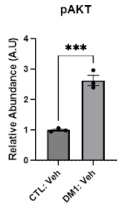

C.

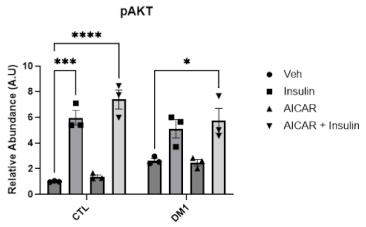

D.

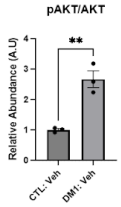

E.

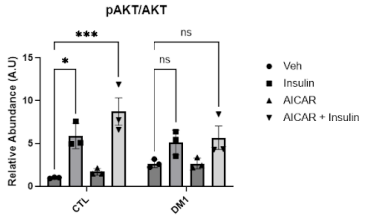

F.

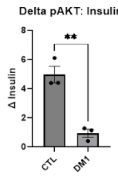

G.

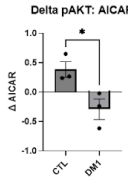

H.

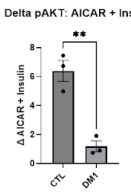

I.

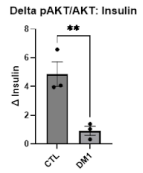

J.

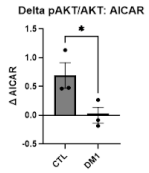

K.

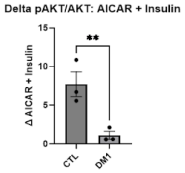

L.

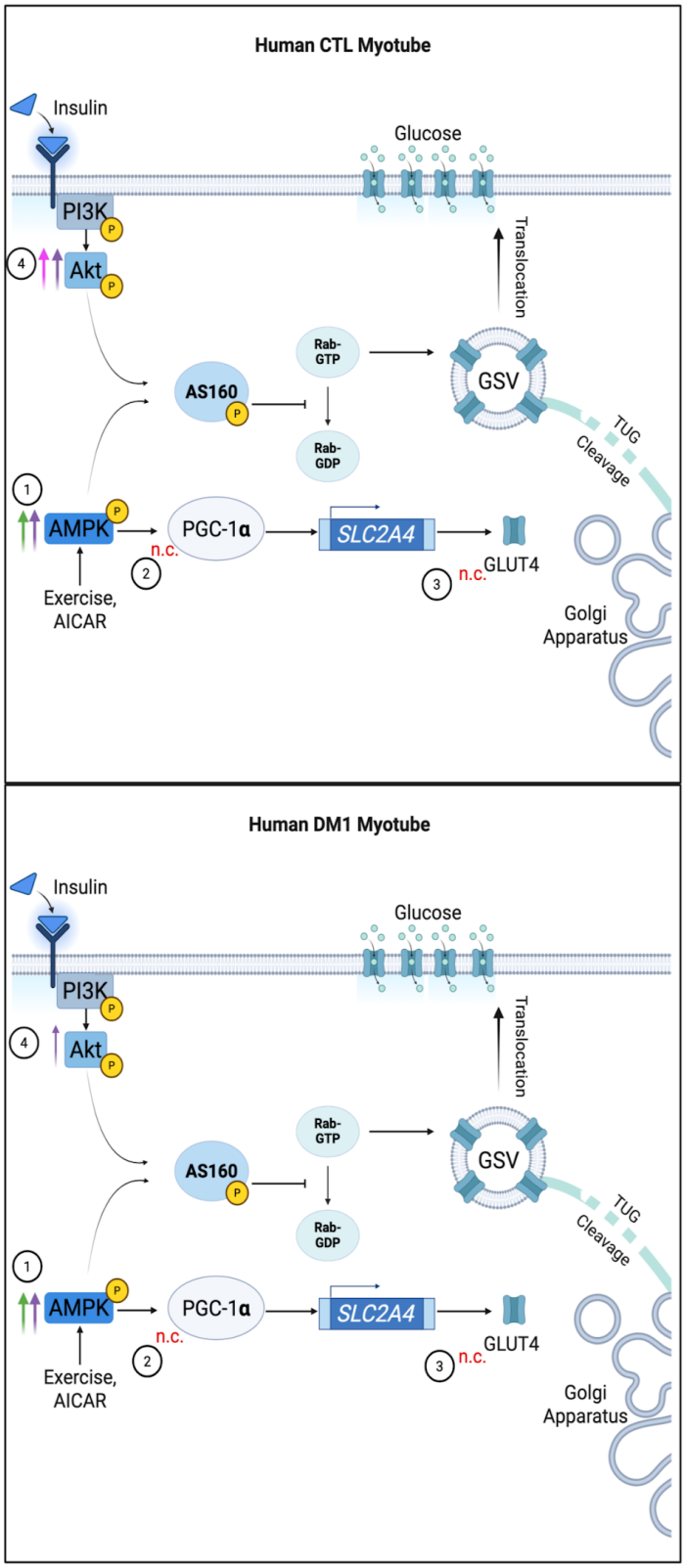

Figure 6. pAkt/Akt signaling in CTL and DM1 myotubes. A. Representative western blots (whole blots found in Supplemental 14,16) of Akt and pAkt in human control (CTL) and myotonic dystrophy type 1 (DM1) myotubes treated with vehicle (-), insulin, 5-Aminoimidazole-4-carboxamide ribonucleoside (AICAR), or a combination of insulin + AICAR. **B.** Increase of the pAkt observed in the human CTL after insulin alone and combination treatment and with an increase only after combination treatment seen in DM1 myotubes. **C.** Increased levels of pAkt in vehicle treated DM1 (DM1:Veh) compared to vehicle treated control (CTL:Veh) myotubes. **D.** Quantification of the pAkt/Akt observed in the human CTL and DM1 myotubes. **E.** Comparison of pAkt/Akt levels shows increased levels in vehicle treated DM1 (DM1:Veh) compared to vehicle treated control (CTL:Veh) myotubes. **F.-H.** Quantification of the delta values with respect to **F.** insulin, **G.** AICAR, or **H.** insulin + AICAR treatment for pAkt reflecting greater delta values in the CTL myotubes. **I.-K.** Greater delta values with respect to **I.** insulin, **J.** AICAR, or **K.** insulin + AICAR treatment for pAkt/Akt in CTL myotubes. **L.** Graphical depiction of the response of molecules after treatment with insulin (pink arrow), AICAR (green arrow) or insulin + AICAR (purple arrow). (4) Reflects increased phosphorylated Akt ratio in CTL myotubes and relatively smaller increase in DM1 myotubes. Panel L. created by Biorender.com. N = 2 CTL, 2 DM1. One way ANOVA followed by Tukeys post-hoc test for multiple comparisons panels C. & E. One-tailed Welch's T-test for panel J. One-tailed unpaired Student's T-test *$p<0.05$, **$p < 0.005$, ***$p<0.0005$. Graphs are means +/- SEM.

7.

A.

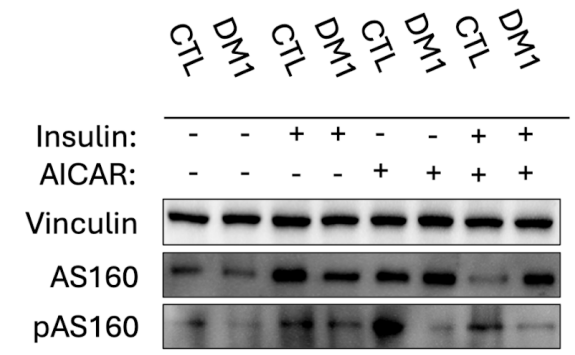

B.

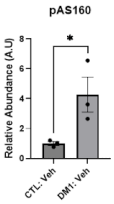

C.

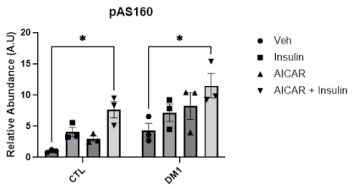

D.

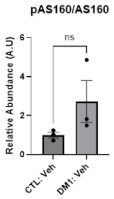

E.

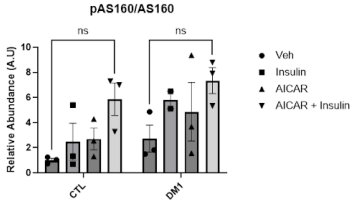

F.

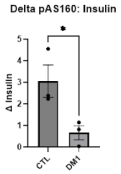

G.

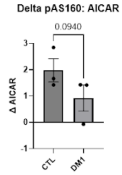

H.

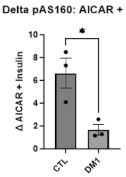

I.

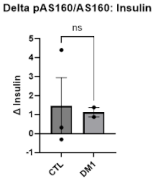

J.

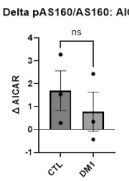

K.

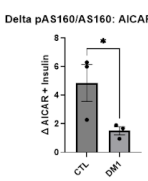

L.

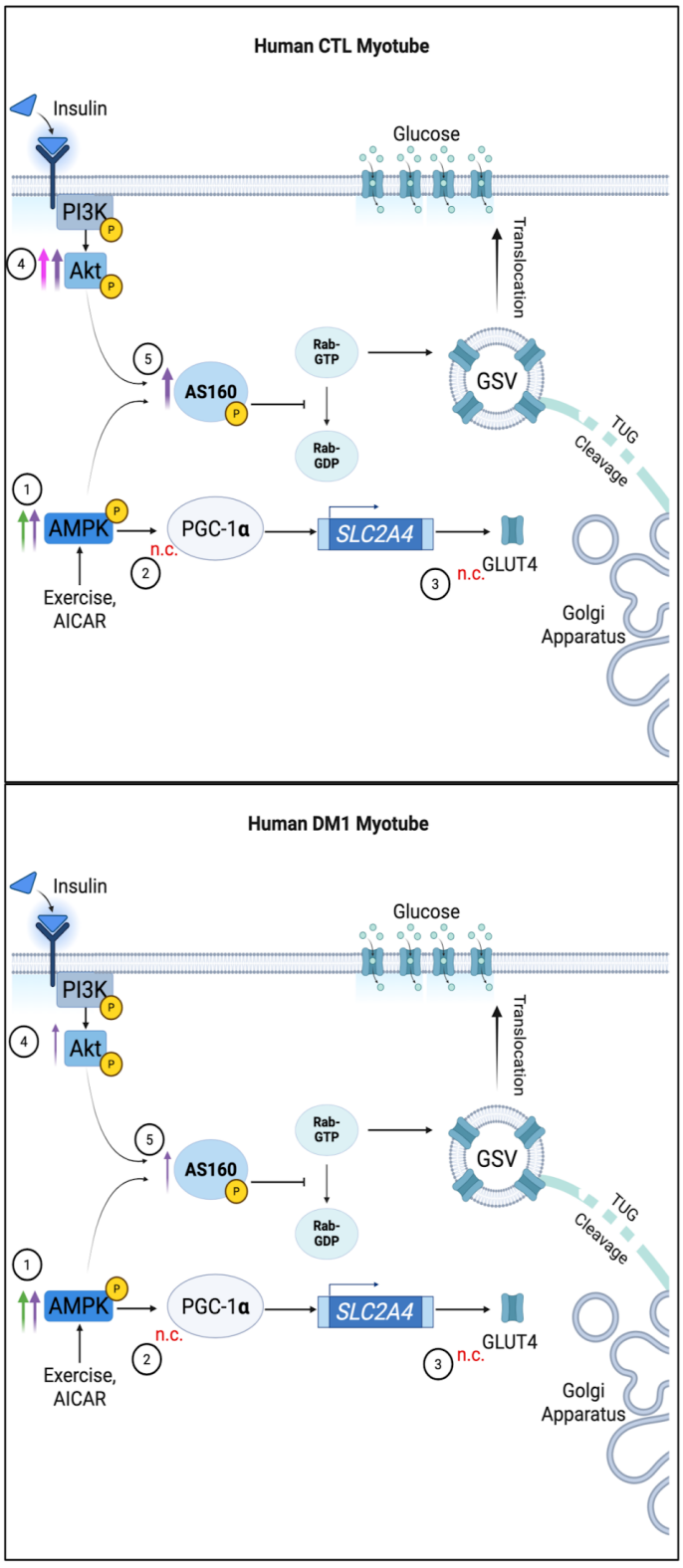

Figure 7. AS160 signaling in CTL and DM1 myotubes. A. Representative western blots (whole blots found in Supplemental 15,16) of the pAS160 and AS160 in human CTL and DM1 myotubes treated with vehicle (-), insulin, 5-aminoimidazole-4-carboxamide ribonucleotide (AICAR), or a combination of insulin and AICAR. **B.** Quantification of the pAS160 observed in the human CTL and DM1 myotubes. **C.** Comparison of pAS160 levels shows increased levels in vehicle treated DM1 (DM1:Veh) compared to vehicle treated control (CTL:Veh) myotubes. **D.** No significant change of the pAS160/AS160 observed in the human CTL and DM1 myotubes after treatments. **E.** Comparison of pAS160/AS160 levels shows no significant difference between vehicle treated DM1 (DM1:Veh) compared to vehicle treated control (CTL:Veh) myotubes. **F.-H.** Greater CLT delta values with respect to **F.** insulin, **G.** AICAR, or **H.** insulin + AICAR treatment for pAS160. **I.-K.** Quantification of the delta values with respect to **I.** insulin, **J.** AICAR, or **K.** insulin + AICAR treatment for pAS160/AS160 with a greater delta value observed in the CTL myotubes. **L.** Graphical depiction of the response of molecules after treatment with insulin (pink arrow), AICAR (green arrow) or insulin + AICAR (purple arrow). (5) reflects increased phosphorylation of AS160 (dashed arrow) in CTL and DM1 myotubes after AICAR and insulin treatment with no change (n.c.) seen in DM1 myotubes. Panel L. created by Biorender.com. N = 2 CTL, 2 DM1. One way ANOVA followed by Tukeys post-hoc test for multiple comparisons C. & E. One-tailed unpaired Student's T-test *$p<0.05$, **$p < 0.005$, ***$p<0.0005$. Graphs are means +/- SEM.

Acknowledgments

We would like to extend thanks to Dr. Elena Pegoraro's group and patient donors for granting us with the patient-derived myoblasts that were implemented in this study.

Contributions

O.A. planned and executed experimentation detailed in the study. He analyzed data, wrote and revised manuscript.

S.S. managed resource allocation, provided guidance and insight for experimentation. Edited and revised manuscript.

R.C. helped with mouse injections and dissections. He also helped prepare cryosections and analysis workflow for immunofluorescent imaging. Also helped edit manuscript.

A.M conducted original exercise study on HSA-LR mice which were used in proteomic analysis. Provided directional insight for study scope and aims.

A.H conducted mass spectrometry analysis on sedentary and exercised HSA-LR mice.

K.H., D.O. helped with mouse injections and dissections. Also helped edit manuscript.

L.D. managed mice in housing facility and assisted with mouse injections and dissections.

A.R., V.L. managed and oversaw sedentary and exercised HSA-LR tissues were processed for mass spectrometry.

A.R.C. was an experimental advisor for the study. Provided HSA-LR mice used in AICAR study. Provided edits and revisions to writing.

A.M. was an experimental advisor for the study. Provided edits and revisions to writing.

H.L. Principal investigator of the project, providing guidance, resources, advice for experimental direction. Helped edits and revisions to writing.

Funding

H.L. receives support from the Canadian Institutes of Health Research (CIHR) for Foundation Grant FDN-167281 (Precision Health for Neuromuscular Diseases), Transnational Team Grant ERT-174211 (ProDGNE) and Network Grant OR2-189333 (NMD4C), from the Canada Foundation for Innovation (CFI-JELF 38412), the Canada Research Chairs program (Canada Research Chair in Neuromuscular Genomics and Health, 950-232279), the European Commission (Grant # 101080249).

A.R.C. receives support from Association Française contre les Myopathies (AFM-Téléthon, 28689).

Conflict of Interest

There are no conflicts of interest to report.

2.6 Manuscript References

Arias, E.B., J. Kim, K. Funai, and G.D. Cartee. 2007a. Prior exercise increases phosphorylation of Akt substrate of 160 kDa (AS160) in rat skeletal muscle. *American Journal of Physiology-Endocrinology and Metabolism*. 292:E1191–E1200. Doi:10.1152/ajpendo.00602.2006.

Arias, E.B., J. Kim, K. Funai, and G.D. Cartee. 2007b. Prior exercise increases phosphorylation of Akt substrate of 160 kDa (AS160) in rat skeletal muscle. *American Journal of Physiology-Endocrinology and Metabolism*. 292:E1191–E1200. Doi:10.1152/ajpendo.00602.2006.

Bertacca, A., A. Ciccarone, P. Cecchetti, B. Vianello, I. Laurenza, M. Maffei, C. Chiellini, S. Del Prato, and L. Benzi. 2005. Continually high insulin levels impair Akt phosphorylation and glucose transport in human myoblasts. *Metabolism*. 54:1687–1693. Doi:10.1016/j.metabol.2005.06.019.

Bradley, H., C.S. Shaw, P.L. Worthington, S.O. Shepherd, M. Cocks, and A.J.M. Wagenmakers. 2014. Quantitative immunofluorescence microscopy of subcellular GLUT4 distribution in human skeletal muscle: Effects of endurance and sprint interval training. *Physiological Reports*. 2:1–16. Doi:10.14814/phy2.12085.

Brockhoff, M., N. Rion, K. Chojnowska, T. Wiktorowicz, C. Eickhorst, B. Erne, S. Frank, C. Angelini, D. Furling, M.A. Rüegg, M. Sinnreich, and P. Castets. 2017. Targeting deregulated AMPK/mTORC1 pathways improves muscle function in myotonic dystrophy type i. *Journal of Clinical Investigation*. 127:549–563. Doi:10.1172/JCI89616.

Brook. 1992. Erratum: Molecular basis of myotonic dystrophy: Expansion of a trinucleotide (CTG) repeat at the 3' end of a transcript encoding a protein kinase family member (Cell 68 (799-808)). *Cell*. 69:385–385. Doi:10.1016/0092-8674(92)90418-C.

Cantó, C., and J. Auwerx. 2009a. PGC-1α, SIRT1 and AMPK, an energy sensing network that controls energy expenditure. *Current Opinion in Lipidology*. 20:98–105. Doi:10.1097/MOL.0b013e328328d0a4.

Cantó, C., and J. Auwerx. 2009b. PGC-1α, SIRT1 and AMPK, an energy sensing network that controls energy expenditure. *Current Opinion in Lipidology*. 20:98–105. Doi:10.1097/MOL.0b013e328328d0a4.

Caskey, C.T., A. Pizzuti, Y.H. Fu, R.G. Fenwick, and D.L. Nelson. 1992. Triplet repeat mutations in human disease. *Science*. 256:784–789. Doi:10.1126/science.1589758.

Chau, A., and A. Kalsotra. 2015. Developmental insights into the pathology of and therapeutic strategies for DM1: Back to the basics. *Developmental Dynamics*. 244:377–390. Doi:10.1002/dvdy.24240.

Dedert, C.J., K.R. Bagdady, and J.S. Fisher. 2023. Prior Treatment with AICAR Causes the Selective Phosphorylation of mTOR Substrates in C2C12 Cells. *CIMB*. 45:8040–8052. Doi:10.3390/cimb45100508.

Dogan, C., M. De Antonio, D. Hamroun, H. Varet, M. Fabbro, F. Rougier, K. Amarof, M.-C. Arne Bes, A.-L. Bedat-Millet, A. Behin, R. Bellance, F. Bouhour, C. Boutte, F. Boyer, E. Campana-Salort, F. Chapon, P. Cintas, C. Desnuelle, R. Deschamps, V. Drouin-Garraud, X. Ferrer, H. Gervais-Bernard, K. Ghorab, P. Laforet, A. Magot, L. Magy, D. Menard, M.-C. Minot, A. Nadaj-Pakleza, S. Pellieux, Y. Pereon, M. Preudhomme, J. Pouget, S. Sacconi, G. Sole, T. Stojkovich, V. Tiffreau, A. Urtizberea, C. Vial, F. Zagnoli, G. Caranhac, C. Bourlier, G. Riviere, A. Geille, R.K. Gherardi, B. Eymard, J. Puymirat, S. Katsahian, and G. Bassez. 2016. Gender as a Modifying Factor Influencing Myotonic Dystrophy Type 1 Phenotype Severity and Mortality: A Nationwide Multiple Databases Cross-Sectional Observational Study. *PloS ONE*. 11:e0148264. Doi:10.1371/journal.pone.0148264.

Funai, K., and G.D. Cartee. 2008. Contraction-stimulated glucose transport in rat skeletal muscle is sustained despite reversal of increased PAS-phosphorylation of AS160 and TBC1D1. *Journal of Applied Physiology*. 105:1788–1795. Doi:10.1152/japplphysiol.90838.2008.

Gagnon, C., C. Heatwole, L.J. Hébert, J.-Y. Hogrel, L. Laberge, M. Leone, G. Meola, L. Richer, V. Sansone, and M. Kierkegaard. 2018. Report of the third outcome measures in myotonic dystrophy type 1 (OMMYD-3) international workshop Paris, France, June 8, 2015. *JND*. 5:523–537. Doi:10.3233/JND-180329.

Galic, S., K. Loh, L. Murray-Segal, G.R. Steinberg, Z.B. Andrews, and B.E. Kemp. 2018. AMPK signaling to acetyl-CoA carboxylase is required for fasting- and cold-induced appetite but not thermogenesis. *eLife*. 7:e32656. Doi:10.7554/eLife.32656.

García-Puga, M., A. Saenz-Antoñanzas, R. Fernández-Torrón, A.L.D. Munain, and A. Matheu. 2020. Myotonic Dystrophy type 1 cells display impaired metabolism and mitochondrial dysfunction that are reversed by metformin. *Aging*. 12:6260–6275. Doi:10.18632/aging.103022.

García-Puga, M., A. Saenz-Antoñanzas, A. Matheu, and A.L. de Munain. 2022. Targeting Myotonic Dystrophy Type 1 with Metformin. *International Journal of Molecular Sciences*. 23:1–14. Doi:10.3390/ijms23052901.

Gibala, M.J., S.L. McGee, A.P. Garnham, K.F. Howlett, R.J. Snow, and M. Hargreaves. 2009. Brief intense interval exercise activates AMPK and p38 MAPK signaling and increases the expression of PGC-1α in human skeletal muscle. *Journal of Applied Physiology*. 106:929–934. Doi:10.1152/japplphysiol.90880.2008.

Hicks, S.M., J.A. Frias, S.K. Mishra, M. Scotti, D.R. Muscato, M.C. Valero, L.M. Adams, J.D. Cleary, M. Nakamori, E. Wang, and J.A. Berglund. 2024. Alternative splicing dysregulation across tissue and therapeutic approaches in a mouse model of myotonic dystrophy type 1. *Molecular Therapy – Nucleic Acids*. 35:102338. Doi:10.1016/j.omtn.2024.102338.

Jones, K., C. Wei, P. Iakova, E. Bugiardini, C. Schneider-Gold, G. Meola, J. Woodgett, J. Killian, N.A. Timchenko, and L.T. Timchenko. 2012. GSK3β mediates muscle pathology in myotonic dystrophy. *J. Clin. Invest.* 122:4461–4472. Doi:10.1172/jci64081.

Klip, A., Y. Sun, T.T. Chiu, and K.P. Foley. 2014. Signal transduction meets vesicle traffic: the software and hardware of GLUT4 translocation. *American Journal of Physiology-Cell Physiology*. 306:C879–C886. Doi:10.1152/ajpcell.00069.2014.

Koh, J.-H., C.R. Hancock, D.-H. Han, J.O. Holloszy, K.S. Nair, and S. Dasari. 2019. AMPK and PPARβ positive feedback loop regulates endurance exercise training-mediated GLUT4 expression in skeletal muscle. *American Journal of Physiology-Endocrinology and Metabolism*. 316:E931–E939. Doi:10.1152/ajpendo.00460.2018.

Koh, J.-H., C.R. Hancock, S. Terada, K. Higashida, J.O. Holloszy, and D.-H. Han. 2017. PPARβ Is Essential for Maintaining Normal Levels of PGC-1α and Mitochondria and for the Increase in Muscle Mitochondria Induced by Exercise. *Cell Metabolism*. 25:1176-1185.e5. doi:10.1016/j.cmet.2017.04.029.

Kuyumcu-Martinez, N.M., G.S. Wang, and T.A. Cooper. 2007. Increased Steady-State Levels of CUGBP1 in Myotonic Dystrophy 1 Are Due to PKC-Mediated Hyperphosphorylation. *Molecular Cell*. 28:68–78. Doi:10.1016/j.molcel.2007.07.027.

Lemieux, K., D. Konrad, A. Klip, and A. Marette. 2003. The AMP-activated protein kinase activator AICAR does not induce GLUT4 translocation to transverse tubules but stimulates glucose uptake and p38 mitogen-activated protein kinases α and β in skeletal muscle. *FASEB j.* 17:1658–1665. Doi:10.1096/fj.02-1125com.

Lin, C.-F., C.-L. Chen, C.-W. Chiang, M.-S. Jan, W.-C. Huang, and Y.-S. Lin. 2007. GSK-3β acts downstream of PP2A and the PI 3-kinase-Akt pathway, and upstream of caspase-2 in ceramide-induced mitochondrial apoptosis. *Journal of Cell Science*. 120:2935–2943. Doi:10.1242/jcs.03473.

Mahadevan, M., C. Tsilfidis, L. Sabourin, G. Shutler, C. Amemiya, G. Jansen, C. Neville, M. Narang, J. Barceló, K. O'Hoy, S. LeBlond, J. Earle-MacDonald, P.J. De Jong, B. Wieringa, and R.G. Korneluk. 1992. Myotonic Dystrophy Mutation: an Unstable CTG Repeat in the 3′ Untranslated region of the Gene. *Science*. 255:1253–1255. Doi:10.1126/science.1546325.

Mankodi, A., M.P. Takahashi, H. Jiang, C.L. Beck, W.J. Bowers, R.T. Moxley, S.C. Cannon, and C.A. Thornton. 2002. Expanded CUG repeats trigger aberrant splicing of ClC-1 chloride channel pre-mRNA and hyperexcitability of skeletal muscle in myotonic dystrophy. *Molecular Cell*. 10:35–44. Doi:10.1016/S1097-2765(02)00563-4.

Manta, A., D.W. Stouth, D. Xhuti, L. Chi, I.A. Rebalka, J.M. Kalmar, T.J. Hawke, and V. Ljubicic. 2019. Chronic exercise mitigates disease mechanisms and improves muscle function in myotonic dystrophy type 1 mice. *Journal of Physiology*. 597:1361–1381. Doi:10.1113/JP277123.

Martin, I.K., A. Katz, and J. Wahren. 1995. Splanchnic and muscle metabolism during exercise in NIDDM patients. *American Journal of Physiology-Endocrinology and Metabolism*. 269:E583–E590. Doi:10.1152/ajpendo.1995.269.3.E583.

Mateus, T., F. Martins, A. Nunes, M.T. Herdeiro, and S. Rebelo. 2021. Metabolic Alterations in Myotonic Dystrophy Type 1 and Their Correlation with Lipin. *IJERPH*. 18:1794. Doi:10.3390/ijerph18041794.

Michael, L.F., Z. Wu, R.B. Cheatham, P. Puigserver, G. Adelmant, J.J. Lehman, D.P. Kelly, and B.M. Spiegelman. 2001. Restoration of insulin-sensitive glucose transporter (GLUT4) gene expression in muscle cells by the transcriptional coactivator PGC-1. *Proceedings of the National Academy of Sciences of the United States of America*. 98:3820–3825. Doi:10.1073/pnas.061035098.

Mîinea, C.P., H. Sano, S. Kane, E. Sano, M. Fukuda, J. Peränen, W.S. Lane, and G.E. Lienhard. 2005. AS160, the Akt substrate regulating GLUT4 translocation, has a functional Rab GTPase-activating protein domain. *Biochemical Journal*. 391:87–93. Doi:10.1042/BJ20050887.

Mikhail, A.I., P.L. Nagy, K. Manta, N. Rouse, A. Manta, S.Y. Ng, M.F. Nagy, P. Smith, J.Q. Lu, J.P. Nederveen, V. Ljubicic, and M.A. Tarnopolsky. 2022. Aerobic exercise elicits clinical adaptations in myotonic dystrophy type 1 patients independently of pathophysiological changes. *Journal of Clinical Investigation*. 132. Doi:10.1172/JCI156125.

Moxley, R.T., A.J. Corbett, K.L. Minaker, and J.W. Rowe. 1984. Whole body insulin resistance in myotonic dystrophy. *Annals of Neurology*. 15:157–162. Doi:10.1002/ana.410150208.

Moxley, R.T., R.C. Griggs, D. Goldblatt, V. Vangelder, B.E. Herr, and R. Thiel. 1977. Decreased Insulin Sensitivity of Forearm Muscle in Myotonic Dystrophy with the technical assistance of. *Clin. Res*. 25:395.

Nakamori, M., K. Sobczak, A. Puwanant, S. Welle, K. Eichinger, S. Pandya, J. Dekdebrun, C.R. Heatwole, M.P. McDermott, T. Chen, M. Cline, R. Tawil, R.J. Osborne, T.M. Wheeler, M.S. Swanson, R.T. Moxley, and C.A. Thornton. 2013. Splicing biomarkers of disease severity in myotonic dystrophy. *Annals of Neurology*. 74:862–872. Doi:10.1002/ana.23992.

Nieuwenhuis, S., K. Okkersen, J. Widomska, P. Blom, P.A.C. ’t Hoen, B. van Engelen, and J.C. Glennon. 2019. Insulin Signaling as a Key Moderator in Myotonic Dystrophy Type 1. *Frontiers in Neurology*. 10:1–17. Doi:10.3389/fneur.2019.01229.

Peralta, E.R., B.C. Martin, and A.L. Edinger. 2010. Differential Effects of TBC1D15 and Mammalian Vps39 on Rab7 Activation State, Lysosomal Morphology, and Growth Factor Dependence. *Journal of Biological Chemistry*. 285:16814–16821. Doi:10.1074/jbc.M110.111633.

Philips, A.V., L.T. Timchenko, and T.A. Cooper. 1998. Disruption of splicing regulated by a CUG-binding protein in myotonic dystrophy. *Science*. 280:737–741. Doi:10.1126/science.280.5364.737.

Puigserver, P., J. Rhee, J. Lin, Z. Wu, J.C. Yoon, C.-Y. Zhang, S. Krauss, V.K. Mootha, B.B. Lowell, and B.M. Spiegelman. 2001. Cytokine Stimulation of Energy Expenditure through p38 MAP Kinase Activation of PPARγ Coactivator-1. *Molecular Cell*. 8:971–982. Doi:10.1016/S1097-2765(01)00390-2.

Ravel-Chapuis, A., A. Al-Rewashdy, G. Bélanger, and B.J. Jasmin. 2018. Pharmacological and physiological activation of AMPK improves the spliceopathy in DM1 mouse muscles. *Human Molecular Genetics*. 27:3361–3376. Doi:10.1093/hmg/ddy245.

Renna, L.V., F. Bosè, E. Brigonzi, B. Fossati, G. Meola, and R. Cardani. 2019. Aberrant insulin receptor expression is associated with insulin resistance and skeletal muscle atrophy in myotonic dystrophies. *PloS ONE*. 14:1–18. Doi:10.1371/journal.pone.0214254.

Renna, L.V., F. Bosè, S. Iachettini, B. Fossati, L. Saraceno, V. Milani, R. Colombo, G. Meola, and R. Cardani. 2017. Receptor and post-receptor abnormalities contribute to insulin resistance in myotonic dystrophy type 1 and type 2 skeletal muscle. *PloS ONE*. 12:1–23. Doi:10.1371/journal.pone.0184987.

Rose, A.J., and E.A. Richter. 2005. Skeletal Muscle Glucose Uptake During Exercise: How is it Regulated? *Physiology*. 20:260–270. Doi:10.1152/physiol.00012.2005.

Roussel, M.P., M. Morin, C. Gagnon, and E. Duchesne. 2019a. Correction: What is known about the effects of exercise or training to reduce skeletal muscle impairments of patients with myotonic dystrophy type 1? A scoping review (BMC Musculoskeletal Disorders (2019) 20 (101) DOI: 10.1186/s12891-019-2458-7). *BMC Musculoskeletal Disorders*. 20:1–14. Doi:10.1186/s12891-019-2643-8.

Roussel, M.-P., M. Morin, C. Gagnon, and E. Duchesne. 2019b. What is known about the effects of exercise or training to reduce skeletal muscle impairments of patients with myotonic dystrophy type 1? A scoping review. *BMC Musculoskelet Disord*. 20:101. Doi:10.1186/s12891-019-2458-7.

Savkur, R.S., A.V. Philips, and T.A. Cooper. 2001. Aberrant regulation of insulin receptor alternative splicing is associated with insulin resistance in myotonic dystrophy. *Nature Genetics*. 29:40–47. Doi:10.1038/ng704.

Sriwijitkamol, A., D.K. Coletta, E. Wajcberg, G.B. Balbontin, S.M. Reyna, J. Barrientes, P.A. Eagan, C.P. Jenkinson, E. Cersosimo, R.A. DeFronzo, K. Sakamoto, and N. Musi. 2007. Effect of Acute Exercise on AMPK Signaling in Skeletal Muscle of Subjects With Type 2 Diabetes. *Diabetes*. 56:836–848. Doi:10.2337/db06-1119.

Taylor, E.B., D. An, H.F. Kramer, H. Yu, N.L. Fujii, K.S.C. Roeckl, N. Bowles, M.F. Hirshman, J. Xie, E.P. Feener, and L.J. Goodyear. 2008. Discovery of TBC1D1 as an Insulin-,

AICAR-, and Contraction-stimulated Signaling Nexus in Mouse Skeletal Muscle. *Journal of Biological Chemistry*. 283:9787–9796. Doi:10.1074/jbc.m708839200.

Trausch-Azar, J., T.C. Leone, D.P. Kelly, and A.L. Schwartz. 2010. Ubiquitin Proteasome-dependent Degradation of the Transcriptional Coactivator PGC-1α via the N-terminal Pathway. *Journal of Biological Chemistry*. 285:40192–40200. Doi:10.1074/jbc.m110.131615.

Wang, H., A. Zheng, E.B. Arias, and G.D. Cartee. 2022. Prior AICAR induces elevated glucose uptake concomitant with greater γ3-AMPK activation and reduced membrane cholesterol in skeletal muscle from 26-month-old rats. *FACETS*. 7:774–791. Doi:10.1139/facets-2021-0166.

Wende, A.R., P.J. Schaeffer, G.J. Parker, C. Zechner, D.H. Han, M.M. Chen, C.R. Hancock, J.J. Lehman, J.M. Huss, D.A. McClain, J.O. Holloszy, and D.P. Kelly. 2007a. A role for the transcriptional coactivator PGC-1α in muscle refueling. *Journal of Biological Chemistry*. 282:36642–36651. Doi:10.1074/jbc.M707006200.

Wende, A.R., P.J. Schaeffer, G.J. Parker, C. Zechner, D.H. Han, M.M. Chen, C.R. Hancock, J.J. Lehman, J.M. Huss, D.A. McClain, J.O. Holloszy, and D.P. Kelly. 2007b. A role for the transcriptional coactivator PGC-1α in muscle refueling. *Journal of Biological Chemistry*. 282:36642–36651. Doi:10.1074/jbc.M707006200.

Wu, J., D. Cheng, L. Liu, Z. Lv, and K. Liu. 2019. TBC1D15 affects glucose uptake by regulating GLUT4 translocation. *Gene*. 683:210–215. Doi:10.1016/j.gene.2018.10.025.

Yamano, K., A.I. Fogel, C. Wang, A.M. Van Der Bliek, and R.J. Youle. 2014. Mitochondrial Rab GAPs govern autophagosome biogenesis during mitophagy. *eLife*. 3:e01612. Doi:10.7554/eLife.01612.

Yotova, V., D. Labuda, E. Zietkiewicz, D. Gehl, A. Lovell, J.F. Lefebvre, S. Bourgeois, É. Lemieux-Blanchard, M. Labuda, H. Vézina, L. Houde, M. Tremblay, B. Toupance, E. Heyer, T.J. Hudson, and C. Laberge. 2005. Anatomy of a founder effect: Myotonic dystrophy in Northeastern Quebec. *Human Genetics*. 117:177–187. doi:10.1007/S00439-005-1298-8/FIGURES/5.

Zerial, M., and H. McBride. 2001. Rab proteins as membrane organizers. *Nature Reviews Molecular Cell Biology*. 2:107–117. doi:10.1038/35052055.

3. Extended Discussion

This study was conducted to understand the insulin signaling pathway and exercise interaction within the context of DM1. Insulin resistance exacerbates muscle weakness, muscle atrophy, and metabolic dysfunction in DM1 patients. We sought to elucidate the pathomechanism of insulin resistance in DM1 and how it might be impacted with acute AMPK intervention. After employing IPA we found that AICAR treatment in HSA-LR and human myotube models of DM1, we found that acute AMPK activation did not adequately stimulate the Akt-AS160 signaling pathway (Figure 3.1).

With IPA, we found targets that aligned with the relevant pathways in sedentary and exercised HSA-LR mice. We decided to then acutely stimulate AMPK in our HSA-LR mice and DM1 myotubes to determine how AMPK- PGC-1α impacted insulin signaling proteins. Our study, aligned with IPA findings, found that at baseline, total AMPK was lower in the HSA-LR mouse and in DM1 myotubes. Additionally, in the HSA-LR mouse, PGC-1α expression did not respond to AICAR treatments as was found in WT mice, suggesting dysregulation of PGC-1α. Further, IPA predicted the insulin receptor to be inhibited in the sedentary HSA-LR mice. Our study found that pAkt signaling, a reporter of proximal insulin signaling, was indeed impaired in the HSA-LR mouse and the DM1 myotubes. After exercise intervention, IPA predicted PGC-1α and the insulin receptor to be upregulated. However, in our DM1 models, we observed that acute AMPK stimulation did not improve PGC-1α or Akt levels or activity. Additionally, IPA detected increased GLUT4 expression in the exercised HSA-LR mice, indicating that exercise drives GLUT4 expression. Again, our findings did not align with IPA's, as we saw no clear increase in total GLUT4 after AMPK-PGC-1α stimulation.

3.1 Possible molecular explanations for insulin resistance in DM1 – Extended

The data from the HSA-LR mouse model and the DM1 myotube model share some similarities. In both models, we see that there is a proportional and adequate stimulation of pACC indicating the stimulation of AMPK in both models with AICAR. However, despite the activation of AMPK in the HSA-LR model we do not see an increase in PGC-1α protein. We did not see any changes in PGC-1α abundance in the DM1 myotube model, however this was no different than the control (CTL) responses. Further, in both models we saw an impaired response to treatment in AKT phosphorylation. Consistently, reduced AS160 phosphorylation was observed after AICAR treatment and following insulin treatment in the myotube model.

While we see these differences shared across both models, there is no literature describing the mis-splicing of RNA transcripts for AMPK, PGC-1α, AKT, AS160 or PGC-1α. *INSR* can be mis-spliced in DM1, but this mechanism cannot account for all our findings, since *INSR* is not mis-spliced in the HSA-LR model (Brockhoff et al., 2017). However, there is the prediction that a protein implicated in insulin signaling, Tre-2/Bub2/Cdc16 (TBC) domain family member 15 (TBC1D15), may be subject to RNA mis-splicing (Nakamori et al., 2013).

TBC1D15

TBC1D15 is specifically implicated in the Rab protein interaction with GSVs. Rab GTPase proteins function to transduce the signaling to mechanical effectors like myosin and actin to initiate the movement of GSVs (Klip et al., 2014). TBC1D15 then serves as a GAP, similar to AS160, for Rab GTPase proteins (Peralta et al., 2010). TBC1D15 is also involved in regulating lysosome and mitochondrial morphology (Yamano et al., 2014). Wu et al. knocked TBC1D15 out of different cell lines, including the L6 rat skeletal muscle cell line, and found that

GLUT4 content was reduced (Wu et al., 2019). One group predicts that TBC1D15 may be mis-spliced in DM1, which could possibly explain the post-insulin receptor dysregulations found in our study (Nakamori et al., 2013). This could provide further context as to why GLUT4 content was reduced in the HSA-LR tissue. Validating TBC1D15 at the RNA and protein levels in future studies would help further explore the dysregulated insulin signaling pathway in DM1.

MyoVA

When Rab proteins are activated they transduce their signal to mechanical effectors such as Myosin Va (MyoVa) (Klip et al., 2014). MyoVa is a motor protein that is implicated in cargo shuttling along actin filaments in skeletal muscle tissue (Sun et al., 2014). The *MYO5A* gene encodes for the protein MyoVa and has numerous splice isoforms that allows the protein to adopt tissue specific functionality. Particularly in skeletal muscle tissue, MyoVa has been implicated in binding to GSVs and moving along actin in response to AS160 phosphorylation to facilitate GLUT4 translocation (Sun et al., 2014). Studies in fibroblasts have characterized *MYO5A* as a target that is spliced by MBNL1 to erroneously exclude exon 33 (Rogalska and Sobczak, 2022). Given the involvement of MyoVa in GLUT4 translocation, this is an avenue of investigation that could also unfold connections to the insulin resistance presenting in DM1.

USP25m

TUG, the protein that tethers GSVs to the intracellular domain, is cleaved by USP25m, which acts upon the UBX region of TUG (Habtemichael et al., 2018). The *USP25* gene is expressed ubiquitously in the body, but is spliced to include exon 19a and 19b to encode a longer isoform specific to muscle and adipose tissue, denoted as *USP25m*. In TA muscles from 33 DM1

patients, exon 19a and 19b was excluded and thus mis-spliced by 12.5% compared to the 8 healthy controls that were assessed (Nakamori et al., 2013). They predict that this exclusion could dysregulate deubiquination and would thereby increase proteolysis of proteins in the skeletal muscle tissue. However, this exclusion of 19a and 19b could also alter the function of USP25m in the insulin signaling pathway. When USP25m was knocked down in adipose cells, TUG cleavage and subsequent GLUT4 translocation was impaired (Habtemichael et al., 2018). This demonstrates that if its function is altered by mis-splicing in DM1, then it could impact TUG cleavage thereby dysregulating the translocation of GLUT4 to the plasma membrane.

3.2 Significance – Extended

Insulin signaling is integral in the anabolic processes that drive cell growth and cell division. Therefore, it is important to investigate insulin resistance in DM1, as it can exacerbate some of the other symptoms implicated in the disorder such as muscle atrophy and weakness (Renna et al., 2019). Studies have assessed the use of classical insulin sensitizing treatments in DM1, like metformin, however the impacts of these treatments on insulin resistance in DM1 have not been extensively explored (Gagnon et al., 2018; García-Puga et al., 2022). Our study sought to provide context on the response for insulin molecules in DM1 after AMPK stimulation. In doing so, we were able to explore the responses of the molecules in two models of DM1 where we confirmed dysregulated insulin signaling prior to, and after acute AMPK stimulation. Our data indicates the possibility that proximal AKT insulin signaling is impaired. This could limit the synergistic effect that AMPK stimulation could have on AS160, affecting downstream GLUT4 translocation.

AICAR is not a regulated substance that can be prescribed to patients and is primarily used in studies to isolate the effects of AMPK stimulation on downstream molecular interactions. Thus,

AICAR serves as a proxy for exercise interventions in pre-clinical models and can provide insight for how exercise may affect the insulin signaling pathway. Similar to exercise, AICAR stimulates AMPK signaling, but it does not mimic the exact same systemic benefits that exercise provides patients (Cantó and Auwerx, 2009a). Therefore, our data provides insight on how AMPK stimulation from resistance training or aerobic exercise could interact with the insulin signaling pathway in DM1.

Resistance training, where the muscle is subjected to a sustained load, has been studied in DM1 patients. These studies reliably showed improvements in muscle mass, strength, mobility, and mitochondrial improvements, but provided little details on insulin signaling improvements (Roussel et al., 2020; Di Leo et al., 2023). In a T2D resistance training study, patients were subjected to a 6-week single-leg training regimen which increased functional strength in the trained leg. Additionally, they also found improvements in glucose uptake along with increased protein content for the insulin receptor, AKT and GLUT4 (Holten et al.).

Similar to the resistance training studies in DM1 patients, there was little information pertaining to insulin signaling in patients after aerobic exercise studies (Roussel et al., 2019; Mikhail et al., 2022). There were strength, mobility, and mitochondrial improvements that were detailed, although specific insulin signaling markers were not assessed. However, in a similar T2D study, exercise intervention lowered HbA1c levels, a marker of hyperglycemia (Sigal et al., 2007). This is consistent with another study that found increased GLUT4 translocation to the plasma membrane after an acute cycling bout in T2D patients (Kennedy et al., 1999). Another demonstrated that aerobic training regimen yields improvements in GLUT4 content in skeletal muscle tissues for T2D patients (O'Gorman et al., 2006). GLUT4 has a relatively higher abundance in Type 1 oxidative fibers (Daugaard et al., 2000b), so the selective Type I oxidative fiber atrophy

in DM1 (Vihola et al., 2003) could suggest overall lower GLUT4 content in DM1 patients. A chronic AMPK stimulation study in HSA-LR mice saw an oxidative fiber type shift (Ravel-Chapuis et al., 2018), suggesting that perhaps chronic AMPK stimulation could subsequently increase Type I fibers and GLUT4 content DM1 patients.

Our findings provide molecular insight into the metabolic response that DM1 patients could have after an acute exercise bout. With AMPK stimulation through exercise, DM1 patients may have improved strength, muscle mass, and mobility as seen in previous DM1 exercise studies (Roussel et al., 2019). With chronic exercise regimens, patients may even have increased insulin signaling as seen in T2D patients (Holten et al.; O'Gorman et al., 2006). Metabolic adaptations from exercise are classically linked with improvements in glucose uptake which prompted the investigation of the insulin signaling pathway in DM1. In pre-clinical models, this study has demonstrated the impaired response of insulin signaling molecules prior to and after acute AMPK stimulation in DM1, but it does not discount the overall validity of exercise for DM1 patients. Given the acute nature of our treatment, it is still necessary to investigate if higher intensity or chronic AMPK stimulation can elicit greater insulin signaling benefits.

3.3 Limitations – Extended

Key to this study was the stimulation of the exercise pathway through the AMPK-PGC-1α axis through acute AICAR treatment. We decided to conduct this study in female HSA-LR mice and patient-derived myotubes. However, we recognize that DM1 can present in a sex-specific manner, with further sex-specific responses to exercise (Dogan et al., 2016; Ravel-Chapuis et al., 2018).

Sex can influence metabolic dynamics which impacts insulin activity. Women typically exhibit lower cardiometabolic risk than men, and the decline in circulating estrogen after menopause can narrow this gap (Carr, 2003). Estrogen provides a protective effect against insulin resistance and thus contributes to the lower prevalence of insulin resistance and TD2 in females (Mauvais-Jarvis, 2015). Estrogen can bind to alpha and beta estrogen receptors on the nucleus to exert expression changes for genes, including the gene for PGC-1a (Klinge, 2008). DM1-related hypogonadism has not been extensively studied in females, but there are cases of female DM1 patients presenting with hypogonadism which could contribute to low estradiol levels (Damon et al., 2024). If estradiol levels are lower in female HSA-LR mice, then this protective effect could also potentially be lost. To fully contextualize any potential sex differences, male mice should also be assessed in parallel to female mice. Metabolic responses to exercise are also sex specific (Venables and Jeukendrup, 2008). Men and women will have improved glucose uptake after training, but several human studies report that women have higher baseline insulin sensitivity and distinct post-exercise glucose uptake compared with men (Beaudry et al., 2022). So, in future studies it would be ideal to conduct further studies in sex-matched pre-clinical models to gather a clear scope for the sex-specific modifiers that may contribute to the results of the study.

Due to the transient nature of the AMPK and AS160 phosphorylation, mice were treated for 30 minutes with AICAR, while myotubes were treated with it for 60 minutes (Sriwijitkamol et al., 2007; Funai and Cartee, 2008). It would be insightful to explore time course treatments to investigate the interactions of the proteins after extended AMPK stimulation. Further, investigations with acute and chronic exercise regimens in the mice could elucidate some of the long term and systemic benefits that exercise has on the insulin signaling pathway.

3.4 Conclusion

After employing both a mouse and human myotube model, this study demonstrated that the insulin signaling pathway is impaired in DM1 and is not rescued with acute AMPK stimulation. Namely, we found that acute AMPK activation did not rescue the Akt-AS160 signaling pathway in either of the models, suggesting that GLUT4 translocation is impaired in DM1 and does not respond to acute AMPK stimulation. We contextualize our findings in the clinical sense to highlight the significance of understanding exercise interactions with insulin signaling in DM1. Further, we acknowledge that in future work, investigating sex-differences, assessing chronic AICAR treatment and exploring exercise regimens in pre-clinical models would be insightful for further elucidating these pathways. Altogether, this study provides new insights into the pathomechanisms of insulin resistance in DM1 and furthers the understanding of metabolic behaviour in DM1 patients.

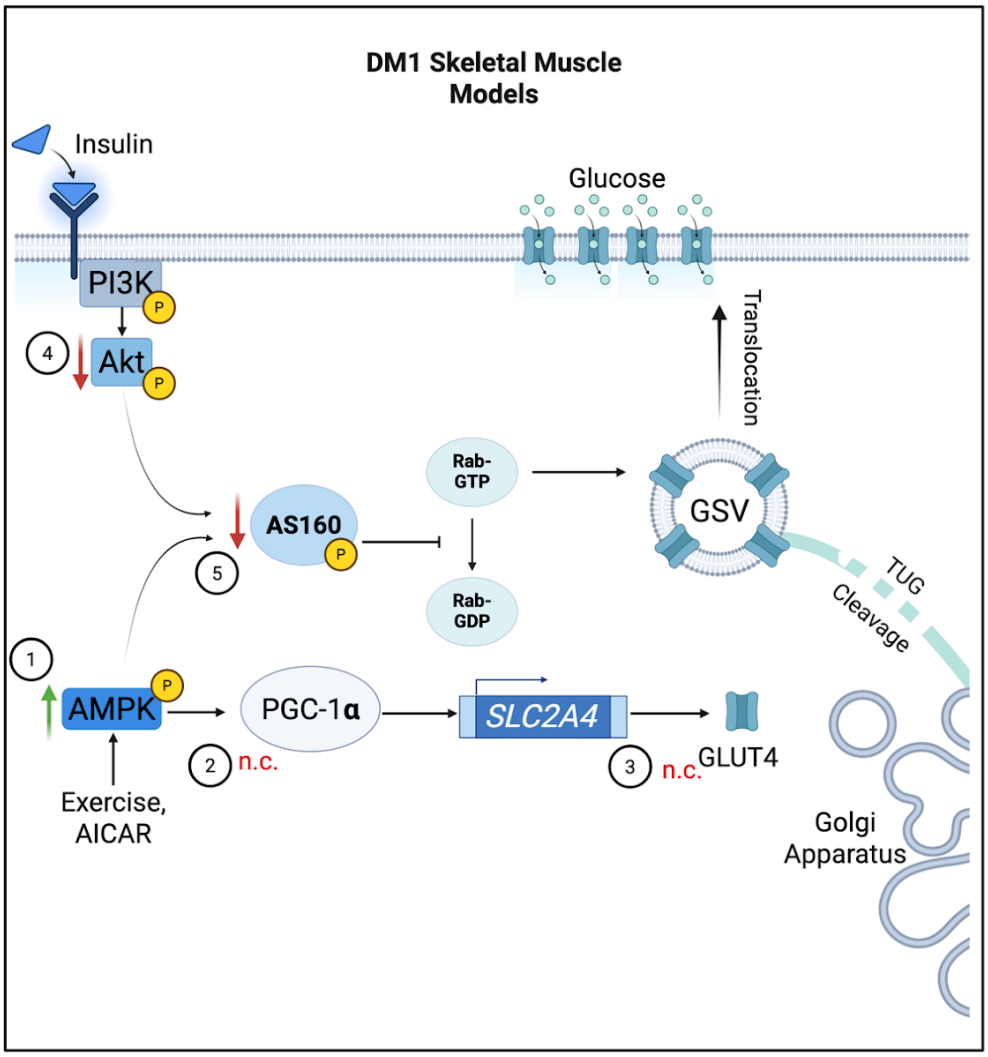

Figure 3.1. Summary of Findings When adenosine monophosphate activated protein kinase (AMPK) was stimulated with AICAR, (1) peroxisome proliferator-activated receptor gamma coactivator 1 alpha (PGC-1α) expression (2) and glucose transporter 4 (GLUT4) expression (3) showed no change (red n.c.) in HSA-LR and human myotube models of DM1 (2,3). Akt and Akt substrate of kDa 160 (AS160) activity was impaired in response to AICAR treatment in both DM1skeletal muscle models (4,5).

4. References

Arias, E.B., J. Kim, K. Funai, and G.D. Cartee. 2007. Prior exercise increases phosphorylation of Akt substrate of 160 kDa (AS160) in rat skeletal muscle. *American Journal of Physiology-Endocrinology and Metabolism*. 292:E1191–E1200. doi:10.1152/ajpendo.00602.2006.

Bassez, G., E. Audureau, J.-Y. Hogrel, R. Arrouasse, S. Baghdoyan, H. Bhugaloo, M.-L. Gourlay-Chu, P. Le Corvoisier, and M. Peschanski. 2018. Improved mobility with metformin in patients with myotonic dystrophy type 1: a randomized controlled trial. *Brain*. 141:2855–2865. doi:10.1093/brain/awy231.

Beaudry, K.M., J.C. Surdi, A. Mari, and M.C. Devries. 2022. Exercise mode influences post-exercise glucose sensitivity and insulin clearance in young, healthy males and females in a sex-dependent manner: A randomized control trial. *Physiological Reports*. 10. doi:10.14814/phy2.15354.

Bird, T.D. 2019. Myotonic Dystrophy Type 1 Summary Genetic counseling Suggestive Findings. *GeneReviews®*. 1–27.

Bogan, J.S. 2012. Regulation of glucose transporter translocation in health and diabetes. *Annual Review of Biochemistry*. 81:507–532. doi:10.1146/annurev-biochem-060109-094246.

Bogan, J.S. 2022. Ubiquitin-like processing of TUG proteins as a mechanism to regulate glucose uptake and energy metabolism in fat and muscle. *Frontiers in Endocrinology*. 13:1–18. doi:10.3389/fendo.2022.1019405.

Boucher, J., A. Kleinridders, and C.R. Kahn. 2014. Insulin Receptor Signaling in Normal. *Cold Spring Harb Perspect Biol 2014*. 6:a009191–a009191.

Boulé, N.G., S.J. Weisnagel, T.A. Lakka, A. Tremblay, R.N. Bergman, T. Rankinen, A.S. Leon, J.S. Skinner, J.H. Wilmore, D.C. Rao, and C. Bouchard. 2005. Effects of Exercise Training on Glucose Homeostasis. *Diabetes Care*. 28:108–114. doi:10.2337/diacare.28.1.108.

Brenes, O., M. Pusch, and F. Morales. 2023. ClC-1 Chloride Channel: Inputs on the Structure–Function Relationship of Myotonia Congenita-Causing Mutations. *Biomedicines*. 11:2622. doi:10.3390/biomedicines11102622.

Brockhoff, M., N. Rion, K. Chojnowska, T. Wiktorowicz, C. Eickhorst, B. Erne, S. Frank, C. Angelini, D. Furling, M.A. Rüegg, M. Sinnreich, and P. Castets. 2017. Targeting deregulated AMPK/mTORC1 pathways improves muscle function in myotonic dystrophy type i. *Journal of Clinical Investigation*. 127:549–563. doi:10.1172/JCI89616.

Buse, M.G., K.A. Robinson, B.A. Marshall, R.C. Hresko, and M.M. Mueckler. 2002. Enhanced *O* -GlcNAc protein modification is associated with insulin resistance in GLUT1-

overexpressing muscles. *American Journal of Physiology-Endocrinology and Metabolism*. 283:E241–E250. doi:10.1152/ajpendo.00060.2002.

Cantó, C., and J. Auwerx. 2009a. PGC-1α, SIRT1 and AMPK, an energy sensing network that controls energy expenditure. *Current Opinion in Lipidology*. 20:98–105. doi:10.1097/MOL.0b013e328328d0a4.

Carr, M.C. 2003. The Emergence of the Metabolic Syndrome with Menopause. *The Journal of Clinical Endocrinology & Metabolism*. 88:2404–2411. doi:10.1210/jc.2003-030242.

Chadt, A., and H. Al-Hasani. 2020. Glucose transporters in adipose tissue, liver, and skeletal muscle in metabolic health and disease. *Pflugers Arch - Eur J Physiol*. 472:1273–1298. doi:10.1007/s00424-020-02417-x.

Charlet-B., N., R.S. Savkur, G. Singh, A.V. Philips, E.A. Grice, and T.A. Cooper. 2002. Loss of the Muscle-Specific Chloride Channel in Type 1 Myotonic Dystrophy Due to Misregulated Alternative Splicing. *Molecular Cell*. 10:45–53. doi:10.1016/S1097-2765(02)00572-5.

Damon, J., C. Chase, and T. Higashimoto. 2024. Primary amenorrhea in myotonic dystrophy type 1: Initial presentation versus incidental finding on whole genome sequencing. *American J of Med Genetics Pt A*. 194:e63650. doi:10.1002/ajmg.a.63650.

Daugaard, J.R., J.N. Nielsen, S. Kristiansen, J.L. Andersen, M. Hargreaves, and E.A. Richter. 2000a. Fiber type-specific expression of GLUT4 in human skeletal muscle: Influence of exercise training. *Diabetes*. 49:1092–1095. doi:10.2337/diabetes.49.7.1092.

Daugaard, J.R., J.N. Nielsen, S. Kristiansen, J.L. Andersen, M. Hargreaves, and E.A. Richter. 2000b. Fiber type-specific expression of GLUT4 in human skeletal muscle: Influence of exercise training. *Diabetes*. 49:1092–1095. doi:10.2337/diabetes.49.7.1092.

Derave, W., S. Lund, G.D. Holman, J. Wojtaszewski, O. Pedersen, and E.A. Richter. 1999. Contraction-stimulated muscle glucose transport and GLUT-4 surface content are dependent on glycogen content. *American Journal of Physiology-Endocrinology and Metabolism*. 277:E1103–E1110. doi:10.1152/ajpendo.1999.277.6.E1103.

Di Leo, V., C. Lawless, M.-P. Roussel, T.B. Gomes, G.S. Gorman, O.M. Russell, H.A.L. Tuppen, E. Duchesne, and A.E. Vincent. 2023. Resistance Exercise Training Rescues Mitochondrial Dysfunction in Skeletal Muscle of Patients with Myotonic Dystrophy Type 1. *Journal of Neuromuscular Diseases*. 10:1111–1126. doi:10.3233/JND-230099.

Dogan, C., M. De Antonio, D. Hamroun, H. Varet, M. Fabbro, F. Rougier, K. Amarof, M.-C. Arne Bes, A.-L. Bedat-Millet, A. Behin, R. Bellance, F. Bouhour, C. Boutte, F. Boyer, E. Campana-Salort, F. Chapon, P. Cintas, C. Desnuelle, R. Deschamps, V. Drouin-Garraud, X. Ferrer, H. Gervais-Bernard, K. Ghorab, P. Laforet, A. Magot, L. Magy, D. Menard, M.-C. Minot, A. Nadaj-Pakleza, S. Pellieux, Y. Pereon, M. Preudhomme, J. Pouget, S. Sacconi, G. Sole, T. Stojkovich, V. Tiffreau, A. Urtizberea, C. Vial, F. Zagnoli, G. Caranhac, C. Bourlier, G. Riviere, A. Geille, R.K. Gherardi, B. Eymard, J. Puymirat, S.

Katsahian, and G. Bassez. 2016. Gender as a Modifying Factor Influencing Myotonic Dystrophy Type 1 Phenotype Severity and Mortality: A Nationwide Multiple Databases Cross-Sectional Observational Study. *PLoS ONE*. 11:e0148264. doi:10.1371/journal.pone.0148264.

Duca, F.A., C.D. Côté, B.A. Rasmussen, M. Zadeh-Tahmasebi, G.A. Rutter, B.M. Filippi, and T.K.T. Lam. 2015. Metformin activates a duodenal Ampk–dependent pathway to lower hepatic glucose production in rats. *Nat Med*. 21:506–511. doi:10.1038/nm.3787.

Fugier, C., A.F. Klein, C. Hammer, S. Vassilopoulos, Y. Ivarsson, A. Toussaint, V. Tosch, A. Vignaud, A. Ferry, N. Messaddeq, Y. Kokunai, R. Tsuburaya, P. De La Grange, D. Dembele, V. Francois, G. Precigout, C. Boulade-Ladame, M.-C. Hummel, A.L. De Munain, N. Sergeant, A. Laquerrière, C. Thibault, F. Deryckere, D. Auboeuf, L. Garcia, P. Zimmermann, B. Udd, B. Schoser, M.P. Takahashi, I. Nishino, G. Bassez, J. Laporte, D. Furling, and N. Charlet-Berguerand. 2011. Misregulated alternative splicing of BIN1 is associated with T tubule alterations and muscle weakness in myotonic dystrophy. *Nat Med*. 17:720–725. doi:10.1038/nm.2374.

Funai, K., and G.D. Cartee. 2008. Contraction-stimulated glucose transport in rat skeletal muscle is sustained despite reversal of increased PAS-phosphorylation of AS160 and TBC1D1. *Journal of Applied Physiology*. 105:1788–1795. doi:10.1152/japplphysiol.90838.2008.

Gagnon, C., C. Heatwole, L.J. Hébert, J.-Y. Hogrel, L. Laberge, M. Leone, G. Meola, L. Richer, V. Sansone, and M. Kierkegaard. 2018. Report of the third outcome measures in myotonic dystrophy type 1 (OMMYD-3) international workshop Paris, France, June 8, 2015. *JND*. 5:523–537. doi:10.3233/JND-180329.

Gallais, B., C. Gagnon, J. Mathieu, and L. Richer. 2017. Cognitive decline over time in adults with myotonic dystrophy type 1: A 9-year longitudinal study. *Neuromuscular Disorders*. 27:61–72. doi:10.1016/j.nmd.2016.10.003.

García-Puga, M., A. Saenz-Antoñanzas, R. Fernández-Torrón, A.L.D. Munain, and A. Matheu. 2020. Myotonic Dystrophy type 1 cells display impaired metabolism and mitochondrial dysfunction that are reversed by metformin. *Aging*. 12:6260–6275. doi:10.18632/aging.103022.

García-Puga, M., A. Saenz-Antoñanzas, A. Matheu, and A.L. de Munain. 2022. Targeting Myotonic Dystrophy Type 1 with Metformin. *International Journal of Molecular Sciences*. 23:1–14. doi:10.3390/ijms23052901.

Garofalo, R.S., S.J. Orena, K. Rafidi, A.J. Torchia, J.L. Stock, A.L. Hildebrandt, T. Coskran, S.C. Black, D.J. Brees, J.R. Wicks, J.D. McNeish, and K.G. Coleman. 2003. Severe diabetes, age-dependent loss of adipose tissue, and mild growth deficiency in mice lacking Akt2/PKBβ. *J. Clin. Invest.* 112:197–208. doi:10.1172/JCI16885.

George, S., J.J. Rochford, C. Wolfrum, S.L. Gray, S. Schinner, J.C. Wilson, M.A. Soos, P.R. Murgatroyd, R.M. Williams, C.L. Acerini, D.B. Dunger, D. Barford, A.M. Umpleby, N.J. Wareham, H.A. Davies, A.J. Schafer, M. Stoffel, S. O'Rahilly, and I. Barroso. 2004. A

Family with Severe Insulin Resistance and Diabetes Due to a Mutation in *AKT2*. *Science*. 304:1325–1328. doi:10.1126/science.1096706.

Giorgino, F., O. De Robertis, L. Laviola, C. Montrone, S. Perrini, K.C. McCowen, and R.J. Smith. 2000. The sentrin-conjugating enzyme mUbc9 interacts with GLUT4 and GLUT1 glucose transporters and regulates transporter levels in skeletal muscle cells. *Proc. Natl. Acad. Sci. U.S.A.* 97:1125–1130. doi:10.1073/pnas.97.3.1125.

Gramegna, L.L., M.P. Giannoccaro, D.N. Manners, C. Testa, S. Zanigni, S. Evangelisti, C. Bianchini, F. Oppi, R. Poda, P. Avoni, R. Lodi, R. Liguori, and C. Tonon. 2018. Mitochondrial dysfunction in myotonic dystrophy type 1. *Neuromuscular Disorders*. 28:144–149. doi:10.1016/j.nmd.2017.10.007.

Habtemichael, E.N., D.T. Li, A. Alcázar-Román, X.O. Westergaard, M. Li, M.C. Petersen, H. Li, S.G. DeVries, E. Li, O. Julca-Zevallos, J.S. Wolenski, and J.S. Bogan. 2018. Usp25m protease regulates ubiquitin-like processing of TUG proteins to control GLUT4 glucose transporter translocation in adipocytes. *Journal of Biological Chemistry*. 293:10466–10486. doi:10.1074/jbc.RA118.003021.

Habtemichael, E.N., D.T. Li, J.P. Camporez, X.O. Westergaard, C.I. Sales, X. Liu, F. López-giráldez, S.G. Devries, H. Li, D.M. Ruiz, K.Y. Wang, B.S. Sayal, S.G. Zapata, P. Dann, S.N. Brown, S. Hirabara, D.F. Vatner, L. Goedeke, W. Philbrick, G.I. Shulman, and J.S. Bogan. 2021. Links Energy Expenditure With Glucose Uptake. *Nature Metabolism*. 3:378–393. doi:10.1038/s42255-021-00359-x.Insulin-stimulated.

Heatwole, C. 2012. Patient-reported impact of symptoms in myotonic dystrophy type 1 (PRISM-1). *Neurology*. 79. doi:https://doi.org/10.1212/WNL.0b013e318260cbe6.

Heni, M., S. Kullmann, H. Preissl, A. Fritsche, and H.U. Häring. 2015. Impaired insulin action in the human brain: causes and metabolic consequences. *Nature Reviews Endocrinology*. 11:701–712. doi:10.1038/NRENDO.2015.173.

Herman, R., N.A. Kravos, M. Jensterle, A. Janež, and V. Dolžan. 2022. Metformin and Insulin Resistance: A Review of the Underlying Mechanisms behind Changes in GLUT4-Mediated Glucose Transport. *International Journal of Molecular Sciences*. 23. doi:10.3390/ijms23031264.

Higashida, K., S.H. Kim, S.R. Jung, M. Asaka, J.O. Holloszy, and D.-H. Han. 2013. Effects of Resveratrol and SIRT1 on PGC-1α Activity and Mitochondrial Biogenesis: A Reevaluation. *PLoS Biol*. 11:e1001603. doi:10.1371/journal.pbio.1001603.

Holten, M.K., M. Zacho, M. Gaster, C. Juel, J.F.P. Wojtaszewski, and F. Dela. Strength Training Increases Insulin-Mediated Glucose Uptake, GLUT4 Content, and Insulin Signaling in Skeletal Muscle in Patients With Type 2 Diabetes.

Hou, J.C., N. Suzuki, J.E. Pessin, and R.T. Watson. 2006. A Specific Dileucine Motif Is Required for the GGA-dependent Entry of Newly Synthesized Insulin-responsive

Aminopeptidase into the Insulin-responsive Compartment. *Journal of Biological Chemistry*. 281:33457–33466. doi:10.1074/jbc.M601583200.

Kannel, W.B., M. Hjortland, and W.P. Castelli. 1974. Role of diabetes in congestive heart failure: The Framingham study. *The American Journal of Cardiology*. 34:29–34. doi:10.1016/0002-9149(74)90089-7.

Karlsson, H.K.R., J.R. Zierath, S. Kane, A. Krook, G.E. Lienhard, and H. Wallberg-Henriksson. 2005. Insulin-Stimulated Phosphorylation of the Akt Substrate AS160 Is Impaired in Skeletal Muscle of Type 2 Diabetic Subjects.

Kelley, D.E., J. He, E.V. Menshikova, and V.B. Ritov. 2002. Dysfunction of Mitochondria in Human Skeletal Muscle in Type 2 Diabetes. *Diabetes*. 51:2944–2950. doi:10.2337/diabetes.51.10.2944.

Kennedy, J.W., M.F. Hirshman, E.V. Gervino, J.V. Ocel, R.A. Forse, S.J. Hoenig, D. Aronson, L.J. Goodyear, and E.S. Horton. 1999. Acute exercise induces GLUT4 translocation in skeletal muscle of normal human subjects and subjects with type 2 diabetes. *Diabetes*. 48:1192–1197. doi:10.2337/diabetes.48.5.1192.

Khan, A.H., E. Capilla, J.C. Hou, R.T. Watson, J.R. Smith, and J.E. Pessin. 2004. Entry of Newly Synthesized GLUT4 into the Insulin-responsive Storage Compartment Is Dependent upon Both the Amino Terminus and the Large Cytoplasmic Loop. *Journal of Biological Chemistry*. 279:37505–37511. doi:10.1074/jbc.M405694200.

Klinge, C.M. 2008. Estrogenic control of mitochondrial function and biogenesis. *J of Cellular Biochemistry*. 105:1342–1351. doi:10.1002/jcb.21936.

Klip, A., Y. Sun, T.T. Chiu, and K.P. Foley. 2014. Signal transduction meets vesicle traffic: the software and hardware of GLUT4 translocation. *American Journal of Physiology-Cell Physiology*. 306:C879–C886. doi:10.1152/ajpcell.00069.2014.

Laustriat, D., J. Gide, L. Barrault, E. Chautard, C. Benoit, D. Auboeuf, A. Boland, C. Battail, F. Artiguenave, J.-F. Deleuze, P. Bénit, P. Rustin, S. Franc, G. Charpentier, D. Furling, G. Bassez, X. Nissan, C. Martinat, M. Peschanski, and S. Baghdoyan. 2015. In Vitro and In Vivo Modulation of Alternative Splicing by the Biguanide Metformin. *Molecular Therapy - Nucleic Acids*. 4:e262. doi:10.1038/mtna.2015.35.

Leick, L., J. Fentz, R.S. Biensø, J.G. Knudsen, J. Jeppesen, B. Kiens, J.F.P. Wojtaszewski, and H. Pilegaard. 2010. PGC-1α is required for AICAR-induced expression of GLUT4 and mitochondrial proteins in mouse skeletal muscle. *American Journal of Physiology-Endocrinology and Metabolism*. 299:E456–E465. doi:10.1152/ajpendo.00648.2009.

Liang, R., W. Dong, X. Shen, X. Peng, A.G. Aceves, and Y. Liu. 2016. Modeling Myotonic Dystrophy 1 in C2C12 Myoblast Cells. *JoVE*. 54078. doi:10.3791/54078.

Ljubicic, V., M. Burt, J.A. Lunde, and B.J. Jasmin. 2014. Resveratrol induces expression of the slow, oxidative phenotype in *mdx* mouse muscle together with enhanced activity of the

SIRT1-PGC-1α axis. *American Journal of Physiology-Cell Physiology*. 307:C66–C82. doi:10.1152/ajpcell.00357.2013.

Mahadevan, M., C. Tsilfidis, L. Sabourin, G. Shutler, C. Amemiya, G. Jansen, C. Neville, M. Narang, J. Barceló, K. O'Hoy, S. LeBlond, J. Earle-MacDonald, P.J. De Jong, B. Wieringa, and R.G. Korneluk. 1992. Myotonic Dystrophy Mutation: an Unstable CTG Repeat in the 3′ Untranslated region of the Gene. *Science*. 255:1253–1255. doi:10.1126/science.1546325.

Mankodi, A., M.P. Takahashi, H. Jiang, C.L. Beck, W.J. Bowers, R.T. Moxley, S.C. Cannon, and C.A. Thornton. 2002. Expanded CUG repeats trigger aberrant splicing of ClC-1 chloride channel pre-mRNA and hyperexcitability of skeletal muscle in myotonic dystrophy. *Molecular Cell*. 10:35–44. doi:10.1016/S1097-2765(02)00563-4.

Manta, A., D.W. Stouth, D. Xhuti, L. Chi, I.A. Rebalka, J.M. Kalmar, T.J. Hawke, and V. Ljubicic. 2019. Chronic exercise mitigates disease mechanisms and improves muscle function in myotonic dystrophy type 1 mice. *Journal of Physiology*. 597:1361–1381. doi:10.1113/JP277123.

Martin, I.K., A. Katz, and J. Wahren. 1995. Splanchnic and muscle metabolism during exercise in NIDDM patients. *American Journal of Physiology-Endocrinology and Metabolism*. 269:E583–E590. doi:10.1152/ajpendo.1995.269.3.E583.

Mauvais-Jarvis, F. 2015. Sex differences in metabolic homeostasis, diabetes, and obesity. *Biol Sex Differ*. 6:14. doi:10.1186/s13293-015-0033-y.

McCrimmon, R.J., C.M. Ryan, and B.M. Frier. 2012. Diabetes and cognitive dysfunction. *The Lancet*. 379:2291–2299. doi:10.1016/S0140-6736(12)60360-2.

McNay, E.C., and J. Pearson-Leary. 2020. GluT4: A central player in hippocampal memory and brain insulin resistance. *Experimental Neurology*. 323:1–22. doi:10.1016/j.expneurol.2019.113076.

Meola, G., and R. Cardani. 2015. Myotonic dystrophies: An update on clinical aspects, genetic, pathology, and molecular pathomechanisms. *Biochimica et Biophysica Acta (BBA) - Molecular Basis of Disease*. 1852:594–606. doi:10.1016/j.bbadis.2014.05.019.

Michael, L.F., Z. Wu, R.B. Cheatham, P. Puigserver, G. Adelmant, J.J. Lehman, D.P. Kelly, and B.M. Spiegelman. 2001. Restoration of insulin-sensitive glucose transporter (GLUT4) gene expression in muscle cells by the transcriptional coactivator PGC-1. *Proceedings of the National Academy of Sciences of the United States of America*. 98:3820–3825. doi:10.1073/pnas.061035098.

Mîinea, C.P., H. Sano, S. Kane, E. Sano, M. Fukuda, J. Peränen, W.S. Lane, and G.E. Lienhard. 2005. AS160, the Akt substrate regulating GLUT4 translocation, has a functional Rab GTPase-activating protein domain. *Biochemical Journal*. 391:87–93. doi:10.1042/BJ20050887.

Mikhail, A.I., A. Manta, S.Y. Ng, A.K. Osborne, S.R. Mattina, M.R. Mackie, and V. Ljubicic. 2023. A single dose of exercise stimulates skeletal muscle mitochondrial plasticity in myotonic dystrophy type 1. *Acta Physiologica*. 237:e13943. doi:10.1111/apha.13943.

Mikhail, A.I., P.L. Nagy, K. Manta, N. Rouse, A. Manta, S.Y. Ng, M.F. Nagy, P. Smith, J.Q. Lu, J.P. Nederveen, V. Ljubicic, and M.A. Tarnopolsky. 2022. Aerobic exercise elicits clinical adaptations in myotonic dystrophy type 1 patients independently of pathophysiological changes. *Journal of Clinical Investigation*. 132. doi:10.1172/JCI156125.

Misquitta, N.S., A. Ravel-Chapuis, and B.J. Jasmin. 2022. Combinatorial treatment with exercise and AICAR potentiates the rescue of myotonic dystrophy type 1 mouse muscles in a sex-specific manner. *Human Molecular Genetics*. 00:1–16. doi:10.1093/hmg/ddac222.

Moxley, R.T., A.J. Corbett, K.L. Minaker, and J.W. Rowe. 1984a. Whole body insulin resistance in myotonic dystrophy. *Annals of Neurology*. 15:157–162. doi:10.1002/ana.410150208.

Moxley, R.T., A.J. Corbett, K.L. Minaker, and J.W. Rowe. 1984b. Whole body insulin resistance in myotonic dystrophy. *Annals of Neurology*. 15:157–162. doi:10.1002/ana.410150208.

Moxley, R.T., R.C. Griggs, D. Goldblatt, V. Vangelder, B.E. Herr, and R. Thiel. 1977a. Decreased Insulin Sensitivity of Forearm Muscle in Myotonic Dystrophy with the technical assistance of. *Clin. Res*. 25:395.

Moxley, R.T., R.C. Griggs, D. Goldblatt, V. Vangelder, B.E. Herr, and R. Thiel. 1977b. Decreased Insulin Sensitivity of Forearm Muscle in Myotonic Dystrophy with the technical assistance of. *Clin. Res*. 25:395–395.

Mueckler, M., and B. Thorens. 2013. The SLC2 (GLUT) family of membrane transporters. *Molecular Aspects of Medicine*. 34:121–138. doi:10.1016/j.mam.2012.07.001.

Nakamori, M., K. Sobczak, A. Puwanant, S. Welle, K. Eichinger, S. Pandya, J. Dekdebrun, C.R. Heatwole, M.P. McDermott, T. Chen, M. Cline, R. Tawil, R.J. Osborne, T.M. Wheeler, M.S. Swanson, R.T. Moxley, and C.A. Thornton. 2013. Splicing biomarkers of disease severity in myotonic dystrophy. *Annals of Neurology*. 74:862–872. doi:10.1002/ana.23992.

Nieuwenhuis, S., K. Okkersen, J. Widomska, P. Blom, P.A.C. 't Hoen, B. van Engelen, and J.C. Glennon. 2019. Insulin Signaling as a Key Moderator in Myotonic Dystrophy Type 1. *Frontiers in Neurology*. 10:1–17. doi:10.3389/fneur.2019.01229.

O'Gorman, D.J., H.K.R. Karlsson, S. McQuaid, O. Yousif, Y. Rahman, D. Gasparro, S. Glund, A.V. Chibalin, J.R. Zierath, and J.J. Nolan. 2006. Exercise training increases insulin-stimulated glucose disposal and GLUT4 (SLC2A4) protein content in patients with type 2 diabetes. *Diabetologia*. 49:2983–2992. doi:10.1007/s00125-006-0457-3.

Okkersen, K., C. Jimenez-Moreno, S. Wenninger, F. Daidj, J. Glennon, S. Cumming, R. Littleford, D.G. Monckton, H. Lochmüller, M. Catt, C.G. Faber, A. Hapca, P.T. Donnan,

G. Gorman, G. Bassez, B. Schoser, H. Knoop, S. Treweek, B.G.M. Van Engelen, M. Kierkegaard, K. Okkersen, C. Jimenez-Moreno, S. Wenninger, F. Daidj, J. Glennon, S. Cumming, R. Littleford, D. Monckton, H. Lochmüller, M. Catt, C. Faber, A. Hapca, P. Donnan, G. Gorman, G. Bassez, B. Schoser, H. Knoop, S. Treweek, B. Van Engelen, D. Maas, S. Nikolaus, Y. Cornelissen, M. Van Nimwegen, E. Klerks, S. Bouman, L. Heskamp, A. Heerschap, R. Rahmadi, P. Groot, T. Heskes, K. Kapusta, S. Abghari, A. Aschrafi, G. Poelmans, J. Raaphorst, M. Trenell, S. Van Laar, L. Wood, S. Cassidy, J. Newman, S. Charman, R. Steffaneti, L. Taylor, A. Brownrigg, S. Day, A. Atalaya, F. Hogarth, A. Schüller, K. Stahl, H. Künzel, M. Wolf, A. Jelinek, B. Lignier, F. Couppey, S. Delmas, J.-F. Deux, K. Hankiewicz, C. Dogan, L. Minier, P. Chevalier, A. Hamadouche, B. Adam, M. Hannah, E. McKenzie, P. Rauchhaus, V. Van Hees, S. Catt, A. Schwalber, I. Merkies, and J. Dittrich. 2018. Cognitive behavioural therapy with optional graded exercise therapy in patients with severe fatigue with myotonic dystrophy type 1: a multicentre, single-blind, randomised trial. *The Lancet Neurology*. 17:671–680. doi:10.1016/S1474-4422(18)30203-5.

Ørngreen, M.C., D.B. Olsen, and J. Vissing. 2005. Aerobic training in patients with myotonic dystrophy type 1. *Annals of Neurology*. 57:754–757. doi:10.1002/ana.20460.

Ozimski, L.L., M. Sabater-Arcis, A. Bargiela, and R. Artero. 2021. The hallmarks of myotonic dystrophy type 1 muscle dysfunction. *Biological Reviews*. 96:716–730. doi:10.1111/brv.12674.

Pagel-Langenickel, I., J. Bao, L. Pang, and M.N. Sack. 2010. The Role of Mitochondria in the Pathophysiology of Skeletal Muscle Insulin Resistance. *Endocrine Reviews*. 31:25–51. doi:10.1210/er.2009-0003.

Pantic, B., D. Borgia, S. Giunco, A. Malena, T. Kiyono, S. Salvatori, A. De Rossi, E. Giardina, F. Sangiuolo, E. Pegoraro, L. Vergani, and A. Botta. 2016. Reliable and versatile immortal muscle cell models from healthy and myotonic dystrophy type 1 primary human myoblasts. *Experimental Cell Research*. 342:39–51. doi:10.1016/j.yexcr.2016.02.013.

Park, J.-S., J.O. Holloszy, K. Kim, and J.-H. Koh. 2020. Exercise Training-Induced PPARβ Increases PGC-1α Protein Stability and Improves Insulin-Induced Glucose Uptake in Rodent Muscles. *Nutrients*. 12:652. doi:10.3390/nu12030652.

Pedersen, T.H., A. Riisager, F.V. De Paoli, T.-Y. Chen, and O.B. Nielsen. 2016. Role of physiological ClC-1 Cl− ion channel regulation for the excitability and function of working skeletal muscle. *Journal of General Physiology*. 147:291–308. doi:10.1085/jgp.201611582.

Peralta, E.R., B.C. Martin, and A.L. Edinger. 2010. Differential Effects of TBC1D15 and Mammalian Vps39 on Rab7 Activation State, Lysosomal Morphology, and Growth Factor Dependence. *Journal of Biological Chemistry*. 285:16814–16821. doi:10.1074/jbc.M110.111633.

Peric, S., L. Brajkovic, B. Belanovic, V. Ilic, B. Salak-Djokic, I. Basta, and V. Rakocevic Stojanovic. 2017. Brain positron emission tomography in patients with myotonic dystrophy type 1 and type 2. *Journal of the Neurological Sciences*. 378:187–192. doi:10.1016/j.jns.2017.05.013.

Perseghin, G., T.B. Price, K.F. Petersen, M. Roden, G.W. Cline, K. Gerow, D.L. Rothman, and G.I. Shulman. 1996. Increased Glucose Transport–Phosphorylation and Muscle Glycogen Synthesis after Exercise Training in Insulin-Resistant Subjects. *N Engl J Med*. 335:1357–1362. doi:10.1056/NEJM199610313351804.

Price, N.L., A.P. Gomes, A.J.Y. Ling, F.V. Duarte, A. Martin-Montalvo, B.J. North, B. Agarwal, L. Ye, G. Ramadori, J.S. Teodoro, B.P. Hubbard, A.T. Varela, J.G. Davis, B. Varamini, A. Hafner, R. Moaddel, A.P. Rolo, R. Coppari, C.M. Palmeira, R. de Cabo, J.A. Baur, and D.A. Sinclair. 2012. SIRT1 Is Required for AMPK Activation and the Beneficial Effects of Resveratrol on Mitochondrial Function. *Cell Metabolism*. 15:675–690. doi:10.1016/j.cmet.2012.04.003.

Prokic, I., B.S. Cowling, C. Kutchukian, C. Kretz, H. Tasfaout, V. Gache, J. Hergueux, O. Wendling, A. Ferry, A. Toussaint, C. Gavriilidis, V. Nattarayan, C. Koch, J. Lainé, R. Combe, L. Tiret, V. Jacquemond, F. Pilot-Storck, and J. Laporte. 2020. Differential physiological roles for BIN1 isoforms in skeletal muscle development, function and regeneration. *Disease Models & Mechanisms*. 13:dmm044354. doi:10.1242/dmm.044354.

Ravel-Chapuis, A., A. Al-Rewashdy, G. Bélanger, and B.J. Jasmin. 2018. Pharmacological and physiological activation of AMPK improves the spliceopathy in DM1 mouse muscles. *Human Molecular Genetics*. 27:3361–3376. doi:10.1093/hmg/ddy245.

Renna, L.V., F. Bosè, E. Brigonzi, B. Fossati, G. Meola, and R. Cardani. 2019. Aberrant insulin receptor expression is associated with insulin resistance and skeletal muscle atrophy in myotonic dystrophies. *PLoS ONE*. 14:1–18. doi:10.1371/journal.pone.0214254.

Renna, L.V., F. Bosè, S. Iachettini, B. Fossati, L. Saraceno, V. Milani, R. Colombo, G. Meola, and R. Cardani. 2017. Receptor and post-receptor abnormalities contribute to insulin resistance in myotonic dystrophy type 1 and type 2 skeletal muscle. *PLoS ONE*. 12:1–23. doi:10.1371/journal.pone.0184987.

Rogalska, Z., and K. Sobczak. 2022. Sustainable recovery of MBNL activity in autoregulatory feedback loop in myotonic dystrophy. *Molecular Therapy - Nucleic Acids*. 30:438–448. doi:10.1016/j.omtn.2022.10.023.

Rose, A.J., and E.A. Richter. 2005. Skeletal Muscle Glucose Uptake During Exercise: How is it Regulated? *Physiology*. 20:260–270. doi:10.1152/physiol.00012.2005.

Roussel, M.P., L.J. Hébert, and E. Duchesne. 2020. Strength-training effectively alleviates skeletal muscle impairments in myotonic dystrophy type 1. *Neuromuscular Disorders*. 30:283–293. doi:10.1016/j.nmd.2020.02.015.

Roussel, M.-P., M. Morin, C. Gagnon, and E. Duchesne. 2019. What is known about the effects of exercise or training to reduce skeletal muscle impairments of patients with myotonic dystrophy type 1? A scoping review. *BMC Musculoskelet Disord*. 20:101. doi:10.1186/s12891-019-2458-7.

Russo, V.C., P.D. Gluckman, E.L. Feldman, and G.A. Werther. 2005. The Insulin-Like Growth Factor System and Its Pleiotropic Functions in Brain. *Endocrine Reviews*. 26:916–943. doi:10.1210/er.2004-0024.

Santoro, M., R. Piacentini, A. Perna, E. Pisano, A. Severino, A. Modoni, C. Grassi, and G. Silvestri. 2020. Resveratrol corrects aberrant splicing of RYR1 pre-mRNA and Ca^{2+} signal in myotonic dystrophy type 1 myotubes. *Neural Regen Res*. 15:1757. doi:10.4103/1673-5374.276336.

Savkur, R.S., A.V. Philips, and T.A. Cooper. 2001. Aberrant regulation of insulin receptor alternative splicing is associated with insulin resistance in myotonic dystrophy. *Nature Genetics*. 29:40–47. doi:10.1038/ng704.

Sigal, R.J., G.P. Kenny, N.G. Boulé, G.A. Wells, D. Prud'homme, M. Fortier, R.D. Reid, H. Tulloch, D. Coyle, P. Phillips, A. Jennings, and J. Jaffey. 2007. Effects of Aerobic Training, Resistance Training, or Both on Glycemic Control in Type 2 Diabetes: A Randomized Trial. *Ann Intern Med*. 147:357–369. doi:10.7326/0003-4819-147-6-200709180-00005.

Spinelli, M., S. Fusco, and C. Grassi. 2019. Brain Insulin Resistance and Hippocampal Plasticity: Mechanisms and Biomarkers of Cognitive Decline. *Front. Neurosci.* 13:788. doi:10.3389/fnins.2019.00788.

Sriwijitkamol, A., D.K. Coletta, E. Wajcberg, G.B. Balbontin, S.M. Reyna, J. Barrientes, P.A. Eagan, C.P. Jenkinson, E. Cersosimo, R.A. DeFronzo, K. Sakamoto, and N. Musi. 2007. Effect of Acute Exercise on AMPK Signaling in Skeletal Muscle of Subjects With Type 2 Diabetes. *Diabetes*. 56:836–848. doi:10.2337/db06-1119.

Sun, Y., T.T. Chiu, K.P. Foley, P.J. Bilan, and A. Klip. 2014. Myosin Va mediates Rab8A-regulated GLUT4 vesicle exocytosis in insulin-stimulated muscle cells. *MBoC*. 25:1159–1170. doi:10.1091/mbc.e13-08-0493.

Takarada, T., A. Nishida, A. Takeuchi, T. Lee, Y. Takeshima, and M. Matsuo. 2015. Resveratrol enhances splicing of insulin receptor exon 11 in myotonic dystrophy type 1 fibroblasts. *Brain and Development*. 37:661–668. doi:10.1016/j.braindev.2014.11.001.

Taneja, K.L., M. McCurrach, M. Schalling, D. Housman, and R.H. Singer. 1995. Foci of trinucleotide repeat transcripts in nuclei of myotonic dystrophy cells and tissues. *The Journal of cell biology*. 128:995–1002. doi:10.1083/jcb.128.6.995.

Timchenko, L. 2013. Molecular mechanisms of muscle atrophy in myotonic dystrophies. *The International Journal of Biochemistry & Cell Biology*. 45:2280–2287. doi:10.1016/j.biocel.2013.06.010.

Venables, M.C., and A.E. Jeukendrup. 2008. Endurance Training and Obesity: Effect on Substrate Metabolism and Insulin Sensitivity. *Medicine & Science in Sports & Exercise*. 40:495–502. doi:10.1249/MSS.0b013e31815f256f.

Vihola, A., G. Bassez, G. Meola, S. Zhang, H. Haapasalo, A. Paetau, E. Mancinelli, A. Rouche, J.Y. Hogrel, P. Laforêt, T. Maisonobe, J.F. Pellissier, R. Krahe, B. Eymard, and B. Udd. 2003. Histopathological differences of myotonic dystrophy type 1 (DM1) and PROMM/DM2. *Neurology*. 60:1854–1857. doi:10.1212/01.wnl.0000065898.61358.09.

Višnjić, D., H. Lalić, V. Dembitz, B. Tomić, and T. Smoljo. 2021. Aicar, a widely used ampk activator with important ampk-independent effects: A systematic review. *Cells*. 10. doi:10.3390/cells10051095.

Vujnic, M., S. Peric, S. Popovic, N. Raseta, V. Ralic, V. Dobricic, I. Novakovic, and V. Rakocevic-Stojanovic. 2015. Metabolic syndrome in patients with myotonic dystrophy type 1. *Muscle and Nerve*. 52:273–277. doi:10.1002/mus.24540.

Walle, T. 2011. Bioavailability of resveratrol. *Annals of the New York Academy of Sciences*. 1215:9–15. doi:10.1111/j.1749-6632.2010.05842.x.

Wang, Y., H. An, T. Liu, C. Qin, H. Sesaki, S. Guo, S. Radovick, M. Hussain, A. Maheshwari, F.E. Wondisford, B. O'Rourke, and L. He. 2019. Metformin Improves Mitochondrial Respiratory Activity through Activation of AMPK. *Cell Reports*. 29:1511-1523.e5. doi:10.1016/j.celrep.2019.09.070.

Watson, R.T., and J.E. Pessin. 2006a. Bridging the GAP between insulin signaling and GLUT4 translocation. *Trends in Biochemical Sciences*. 31:215–222. doi:10.1016/j.tibs.2006.02.007.

Wende, A.R., P.J. Schaeffer, G.J. Parker, C. Zechner, D.H. Han, M.M. Chen, C.R. Hancock, J.J. Lehman, J.M. Huss, D.A. McClain, J.O. Holloszy, and D.P. Kelly. 2007a. A role for the transcriptional coactivator PGC-1α in muscle refueling. *Journal of Biological Chemistry*. 282:36642–36651. doi:10.1074/jbc.M707006200.

Whillier, S. 2020. Exercise and Insulin Resistance. *Advances in Experimental Medicine and Biology*. 1228:137–150. doi:10.1007/978-981-15-1792-1_9.

White, M.F., and C.R. Kahn. 2021. Insulin action at a molecular level – 100 years of progress. *Molecular Metabolism*. 52:101304–101304. doi:10.1016/j.molmet.2021.101304.

Winters, S.J. 2021. Endocrine Dysfunction in Patients With Myotonic Dystrophy. *The Journal of Clinical Endocrinology & Metabolism*. 106:2819–2827. doi:10.1210/clinem/dgab430.

Wu, J., D. Cheng, L. Liu, Z. Lv, and K. Liu. 2019. TBC1D15 affects glucose uptake by regulating GLUT4 translocation. *Gene*. 683:210–215. doi:10.1016/j.gene.2018.10.025.

Yamano, K., A.I. Fogel, C. Wang, A.M. Van Der Bliek, and R.J. Youle. 2014. Mitochondrial Rab GAPs govern autophagosome biogenesis during mitophagy. *eLife*. 3:e01612. doi:10.7554/eLife.01612.

Zaarour, N., M. Berenguer, Y. Le Marchand-Brustel, and R. Govers. 2012. Deciphering the role of GLUT4 N-glycosylation in adipocyte and muscle cell models. *Biochemical Journal*. 445:265–273. doi:10.1042/BJ20120232.

Zerial, M., and H. McBride. 2001. Rab proteins as membrane organizers. *Nature Reviews Molecular Cell Biology*. 2:107–117. doi:10.1038/35052055.

Zhang, L.N., H.Y. Zhou, Y.Y. Fu, Y.Y. Li, F. Wu, M. Gu, L.Y. Wu, C.M. Xia, T.C. Dong, J.Y. Li, J.K. Shen, and J. Li. 2013. Novel small-molecule PGC-1α transcriptional regulator with beneficial effects on diabetic db/db mice. *Diabetes*. 62:1297–1307. doi:10.2337/db12-0703.

5. Appendix

Supplemental Figures and Tables

1.

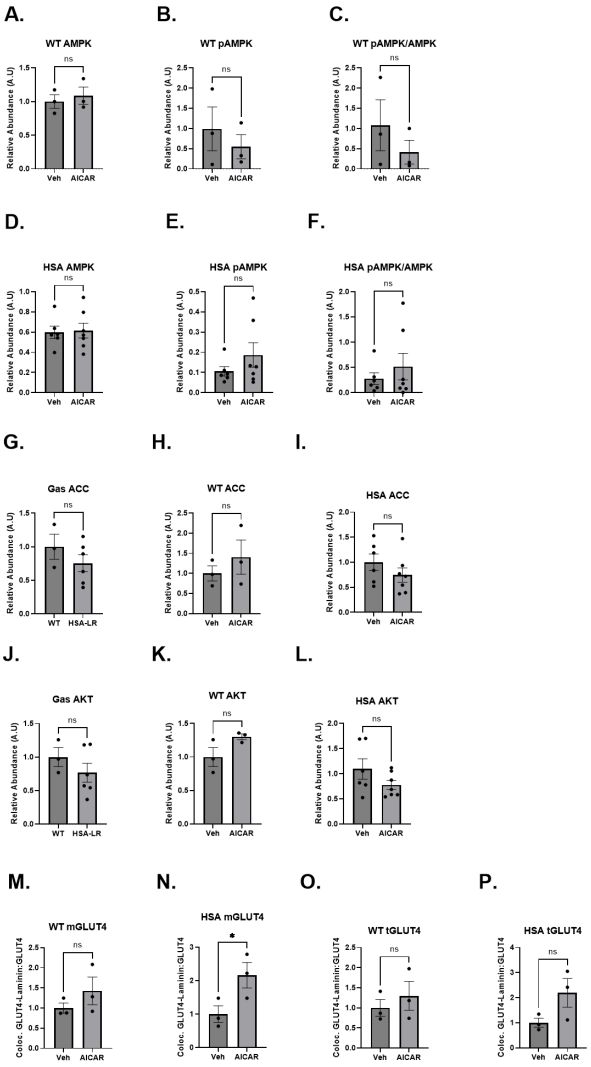

Supplemental Figure 1. Mouse Western blot and IF Quantifications. A.-C. WT comparison of A) total AMPK, B) pAMPK, and C) pAMPK/AMPK before and after AICAR treatment. D.-F. HSA-LR comparison of D) total AMPK, E) pAMPK, and F) pAMPK/AMPK before and after AICAR treatment. G.-I. Total ACC comparison at G) baseline, after AICAR treatment in H) WT and I) HSA-LR mice. J.-L. Total AKT comparison at J) baseline, after AICAR in K) WT and L) HSA-LR mice. M.-P. membrane bound GLUT4 (mGLUT4) response after AICAR treatment in M) WT and N) HSA-LR and total GLUT4 (tGLUT4) response after AICAR treatment in O) WT and P) HSA-LR mice.

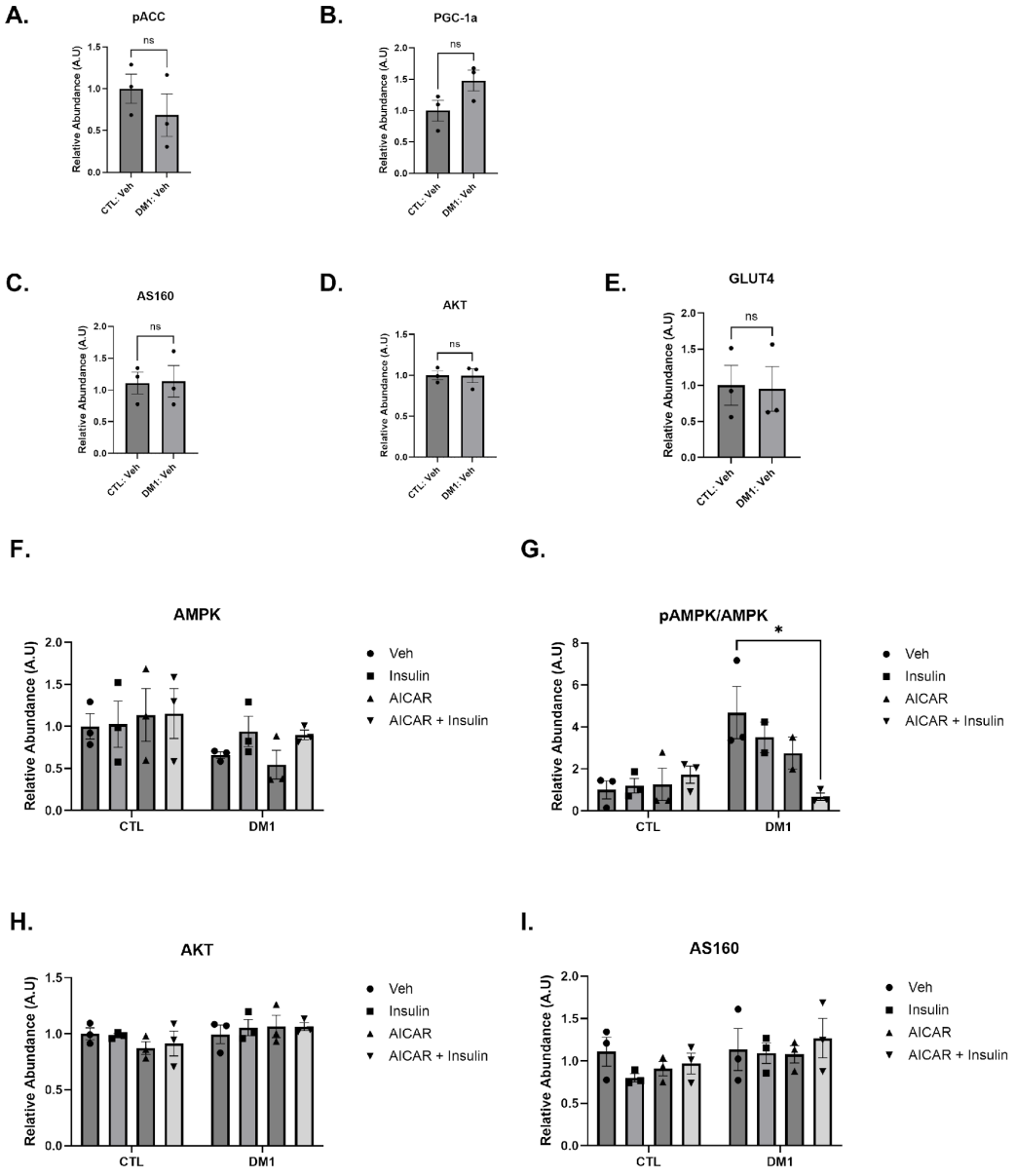

Supplemental Figure 2. Myotube Western blot Quantifications. A.-E. No difference in baseline A. pACC, B. PGC-1a, C. AS160, D. AKT, or E. GLUT4 in control (CTL) or myotonic dystrophy type 1 (DM1) myotubes.
F. No change in total adenosine monophosphate activated protein kinase (AMPK) levels after insulin, AICAR or combination treatment in CTL or DM1 myotubes. G. Decreased pAMPK/AMPK detected after combination treatment in DM1 myotubes. H., I. No difference detected in total H) AKT or I) AS160 levels across treatment groups or conditions in in CTL or DM1 myotubes.

WT-V (1)
WT-A(1)
HSA-V(1)
HSA-A(1)
WT-V(2)
WT-A(2)
HSA-V(2)
HSA-A(2)
WT-V(3)
WT-A(3)
HSA-V(3)
HSA-A(3)
HSA-A(4)
pAMPK
75
63
48
35
64.0
63.7
WT-V (1)
WT-A(1)
HSA-V(4)
HSA-A(5)
WT-V(2)
WT-A(2)
HSA-V(5)
HSA-A(6)
WT-V(3)
WT-A(3)
HSA-V(6)
HSA-A(7)
64.4
64.7
AMPK
63.8
63.9
*

Supplemental Figure 3. Uncropped total and phosphorylated (Threonine 172) AMPK mouse western blots for Figure 2A. Expected banding at 62 kDa. Western blot banding found above ~64 kDa (Pink lines). Red asterisks indicates the blot used for representative blot. “WT” represents wildtype mice and “HSA” represents human skeletal actin long repeat mice. “V” represents vehicle treatment and “A” represents AICAR treatment.

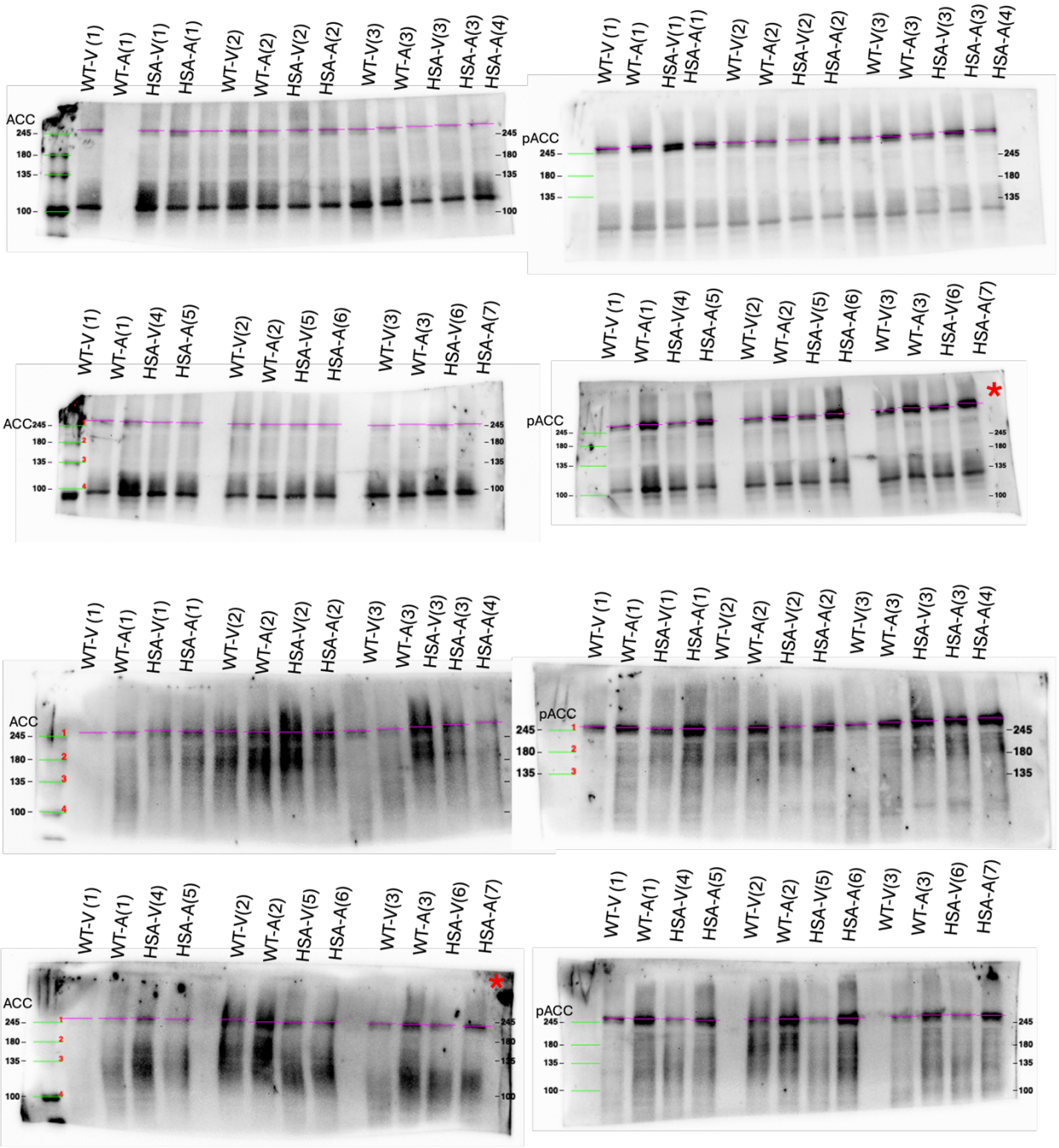

Supplemental Figure 4. Uncropped total and phosphorylated (Serine 79) ACC mouse western blots for Figure 2A. Expected banding at 280 kDa. Western blot banding found above ~245 kDa (Pink lines). Red asterisks indicates the blot used for representative blot. “WT” represents

wildtype mice and “HSA” represents human skeletal actin long repeat mice. “V” represents vehicle treatment and “A” represents AICAR treatment.

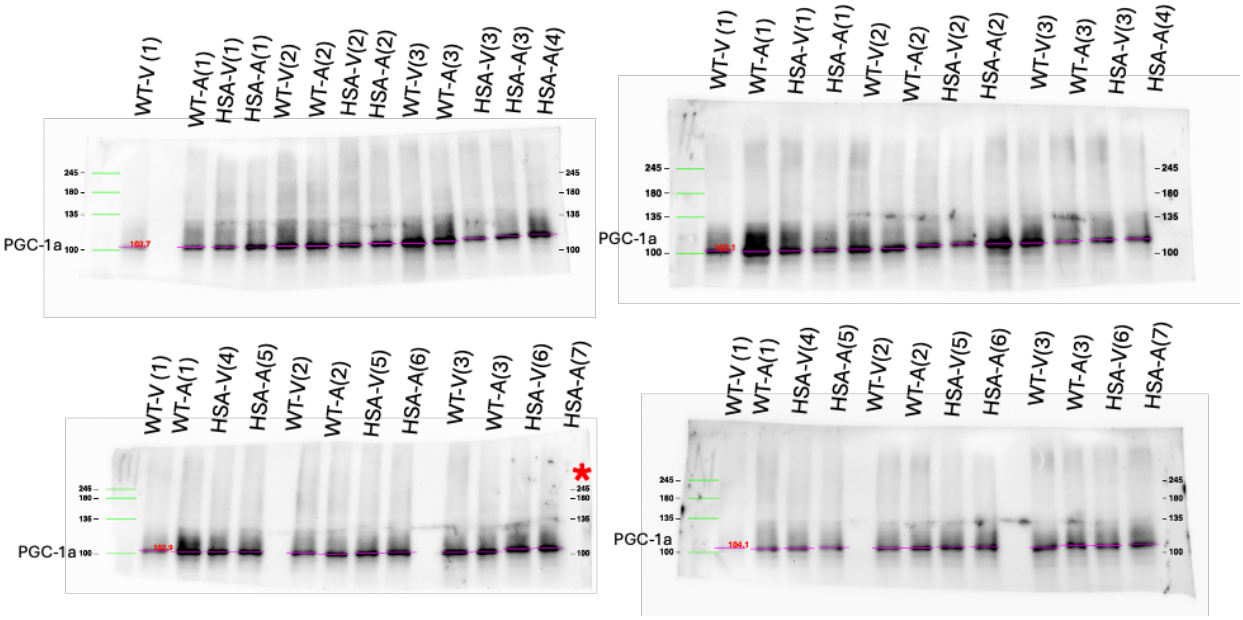

Supplemental Figure 5. Uncropped total PGC-1a mouse western blots used for Figure 2A. Expected banding between 90-100 kDa. Western blot banding found at ~100-105 kDa (Pink lines). Red asterisks indicates the blot used for representative blot. “WT” represents wildtype mice and “HSA” represents human skeletal actin long repeat mice. “V” represents vehicle treatment and “A” represents AICAR treatment.

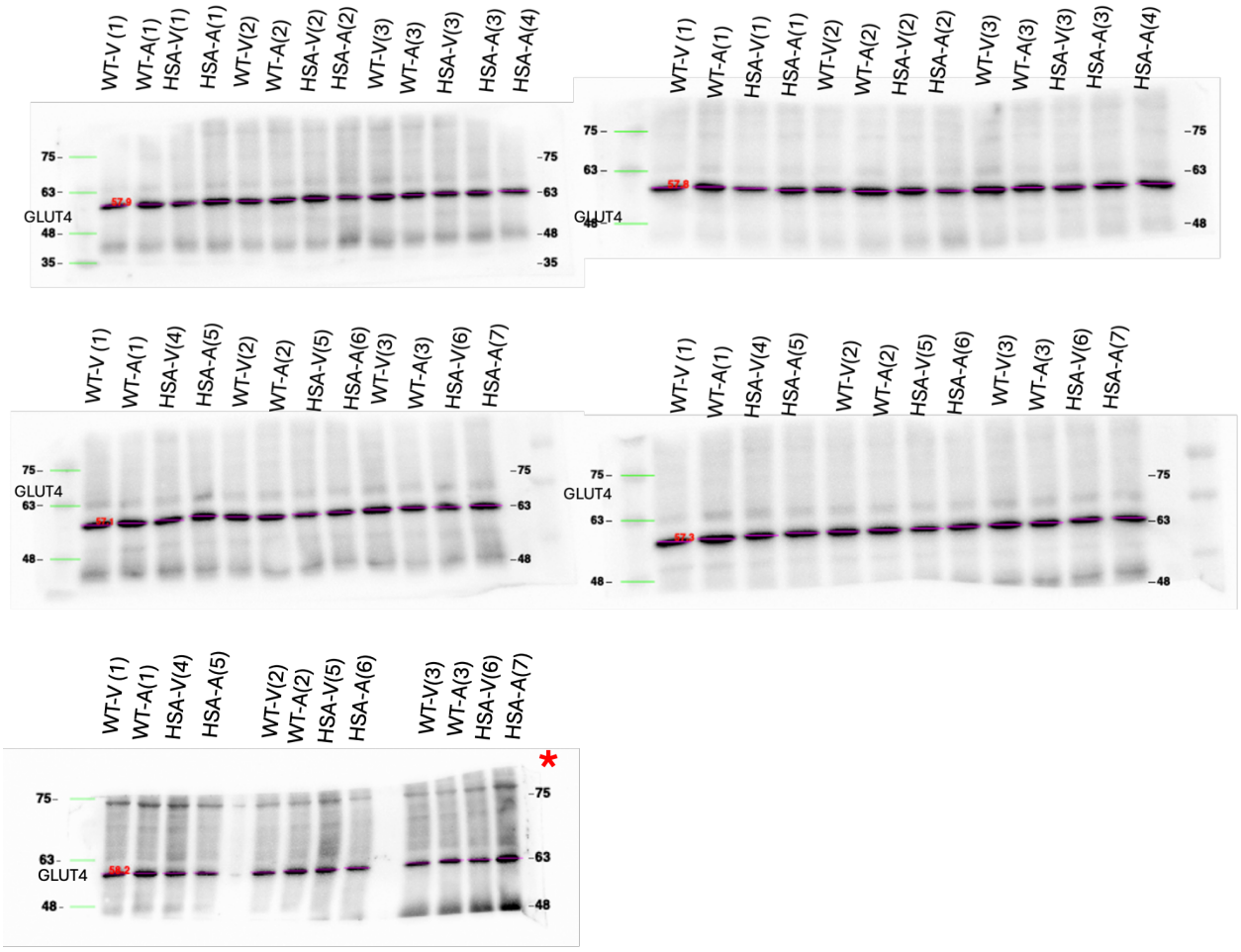

Supplemental Figure 6. Uncropped total GLUT4 mouse western blots used for Figure 2A. Expected banding between ~50-55kDa. Western blot banding found at ~55-60 kDa (Pink lines). Red asterisks indicates the blot used for representative blot. “WT” represents wildtype mice and “HSA” represents human skeletal actin long repeat mice. “V” represents vehicle treatment and “A” represents AICAR treatment.

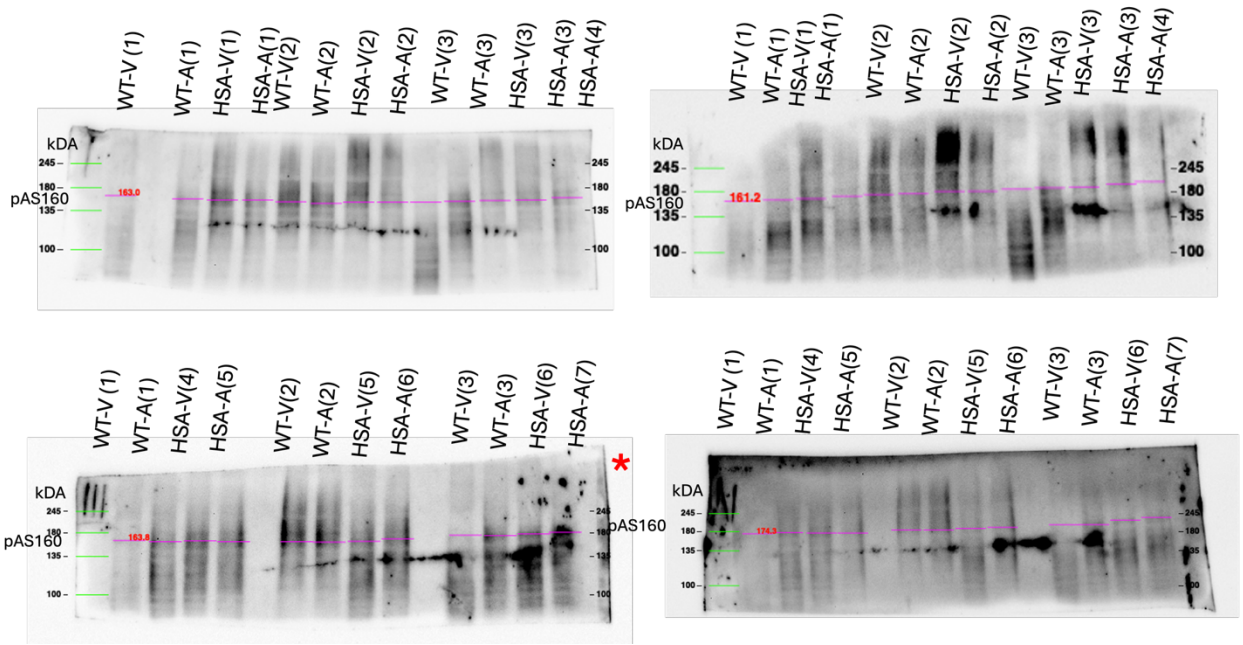

Supplemental Figure 7. Uncropped phosphorylated (Threonine 642) AS160 blots used for Figure 3A. Expected banding at 160 kDa. Western blot banding found between ~160-175 kDa (Pink lines). Red asterisks indicate the blot used for representative blot. "WT" represents wildtype mice and "HSA" represents human skeletal actin long repeat mice. "V" represents vehicle treatment and "A" represents AICAR treatment.

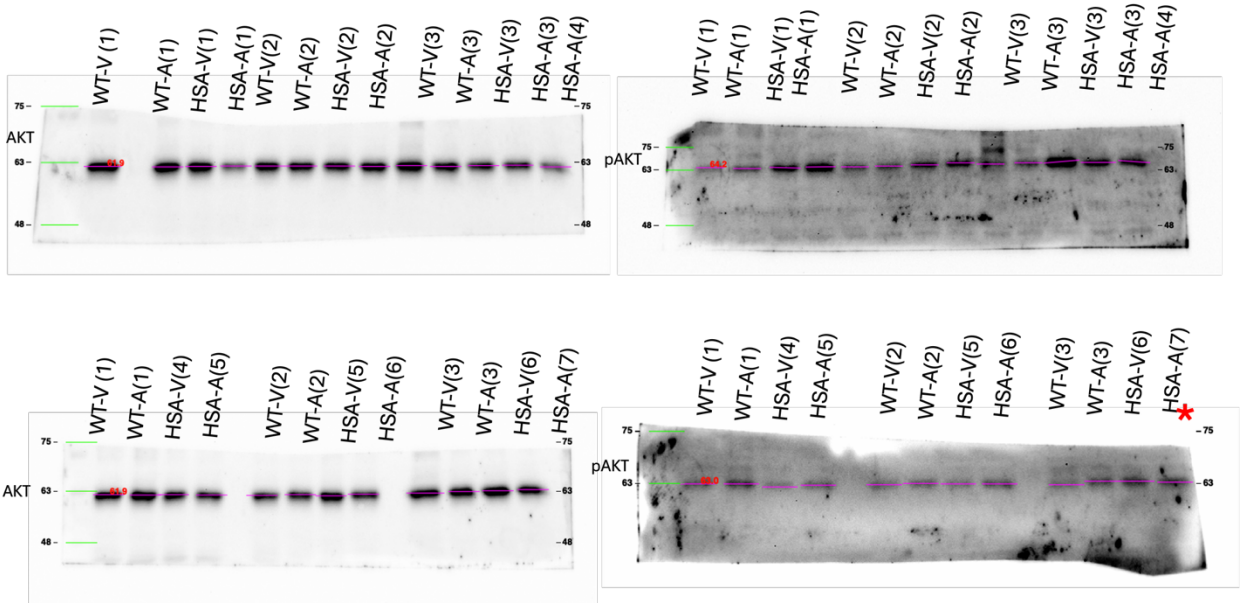

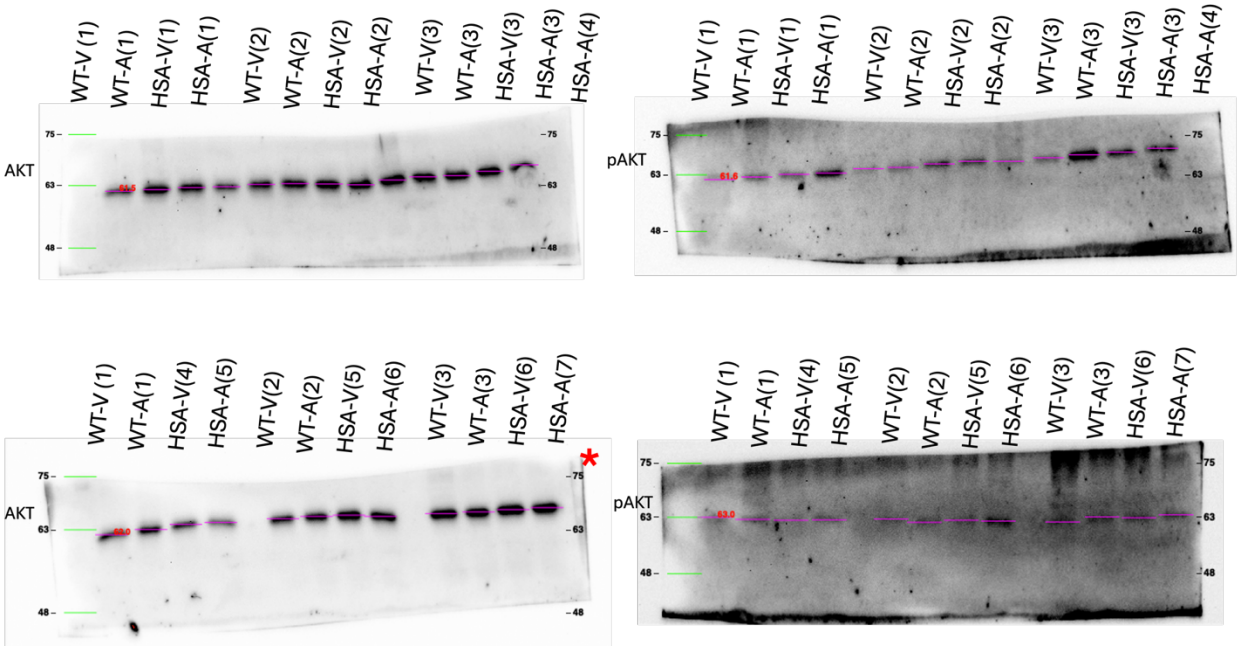

Supplemental Figure 8. Uncropped total and phosphorylated (Serine 473) AKT mouse western blots used for Figure 3A. Expected banding at 60 kDa. Western blot banding found between ~61-64 kDa (Pink lines). Red asterisks indicates the blot used for representative blot. "WT" represents wildtype mice and "HAS" represents human skeletal actin long repeat mice. "V" represents vehicle treatment and "A" represents AICAR treatment.

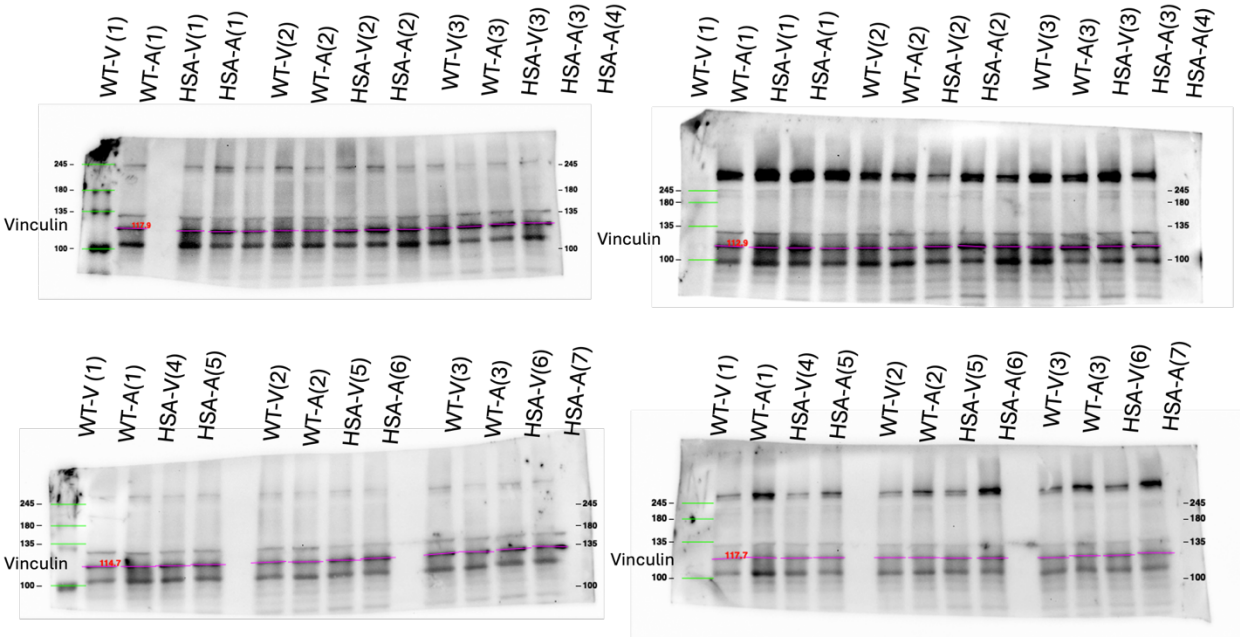

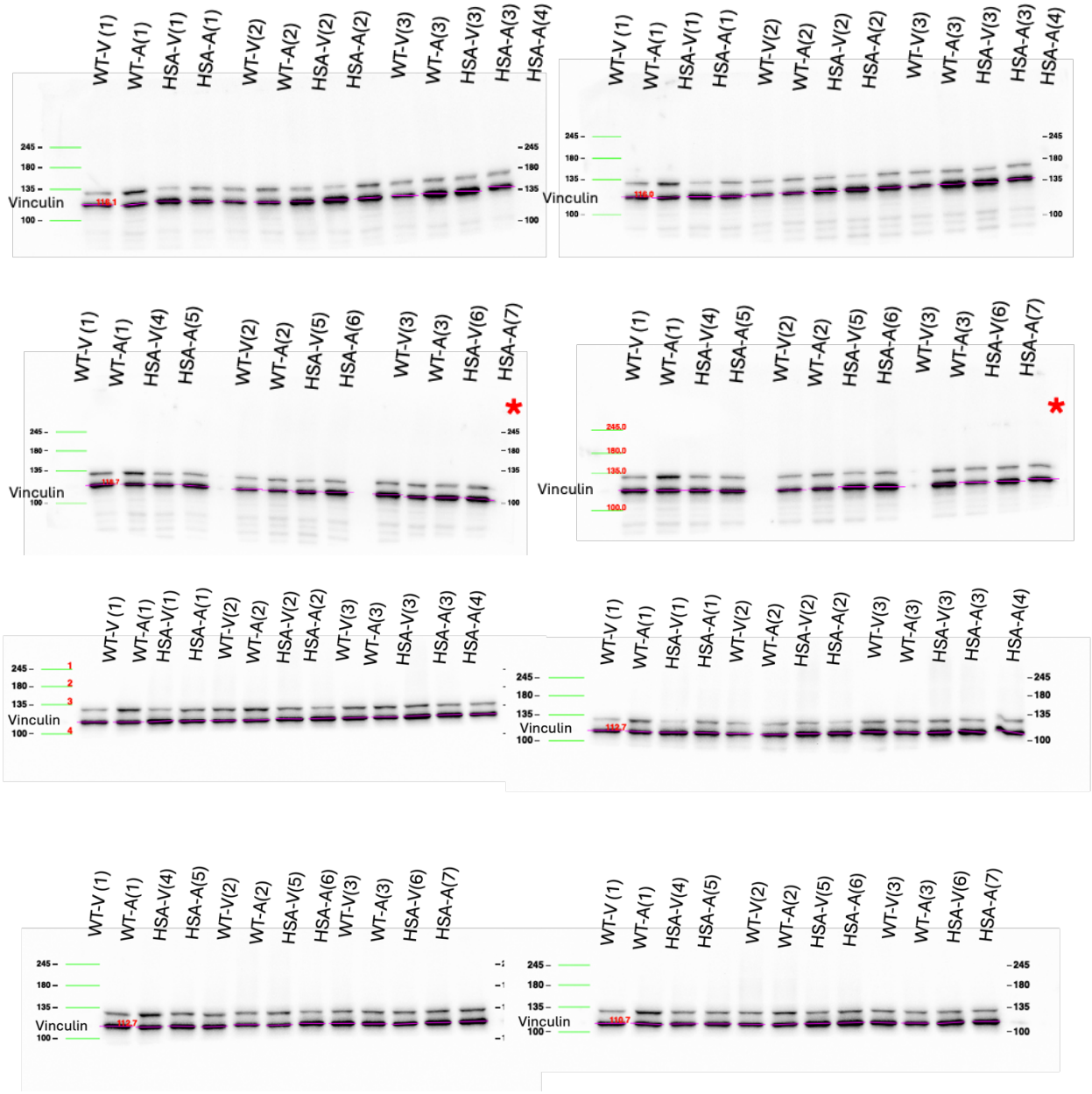

Supplemental Figure 9. Uncropped total vinculin mouse western blots used for Figure 2A and 3A. Expected banding at ~124 kDa. Western blot banding found at ~110-120 kDa (Pink lines). Red asterisks indicates the blot used for representative blot. “WT” represents wildtype mice and “HSA” represents human skeletal actin long repeat mice. “V” represents vehicle treatment and “A” represents AICAR treatment.

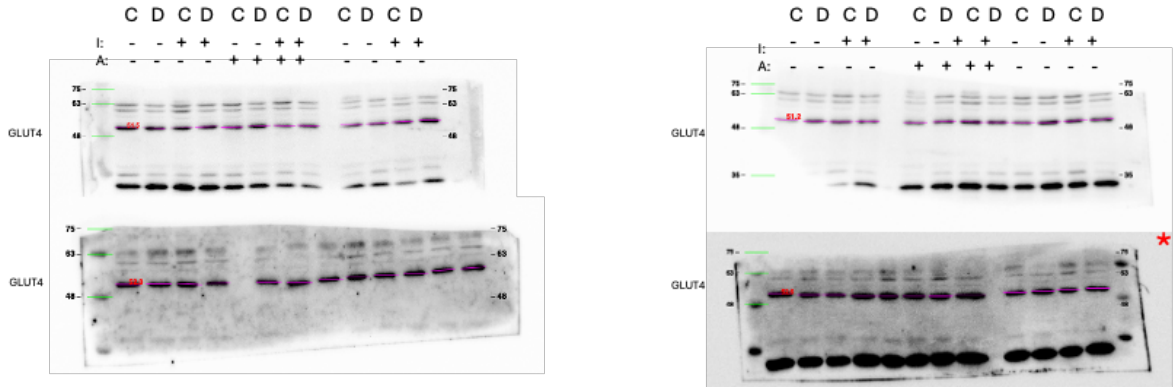

Supplemental Figure 10. Uncropped total GLUT4 myotube western blots used for Figure 5A. Expected banding at 50-55 kDa. Western blot banding found between ~50-55 kDa (Pink lines). Red asterisks indicates the blot used for representative blot. “C” represents Control myotubes and “D” represents DM1 myotubes. “I” represents insulin treatment and “A” represents AICAR treatment. ”nc” represents normalizing control.

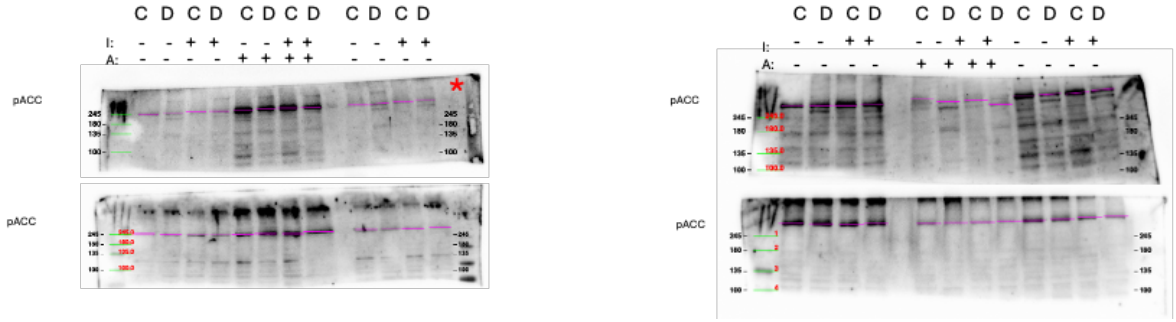

Supplemental Figure 11. Uncropped phosphorylated (Serine 79) ACC myotube western blots for Figure 5A. Expected banding at ~285 kDa. Western blot banding above ~245 kDa (Pink lines). Red asterisks indicates the blot used for representative blot. “C” represents Control myotubes and “D” represents DM1 myotubes. “I” represents insulin treatment and “A” represents AICAR treatment. ”nc” represents normalizing control.

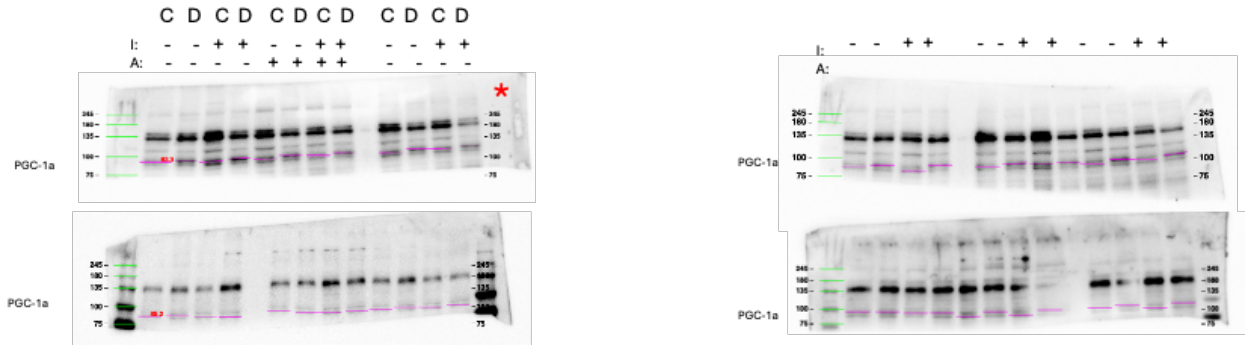

Supplemental Figure 12. Uncropped total PGC-1a myotube western blots for Figure 5A. Expected banding at 90-100 kDa. Western blot banding found between ~85-95 kDa (Pink lines). Red asterisks indicates the blot used for representative blot. “C” represents Control myotubes and “D” represents DM1 myotubes. “I” represents insulin treatment and “A” represents AICAR treatment. ”nc” represents normalizing control.

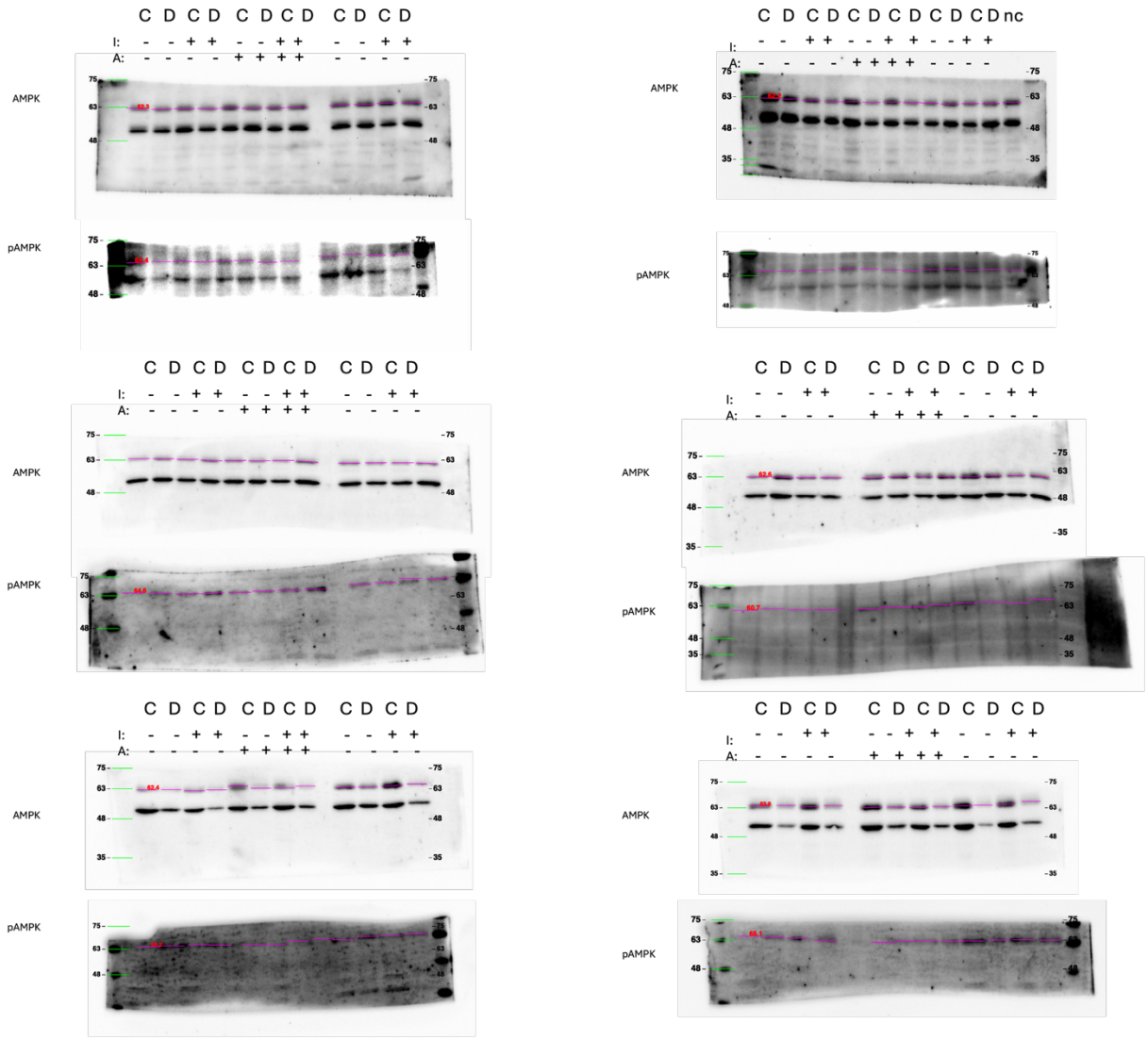

Supplemental Figure 13. Uncropped total and phosphorylated (Threonine 172) AMPK myotube western blots used for Figure 5A. Expected banding at 62 kDa. Western blot banding found between ~60-65 kDa (Pink lines). Red asterisks indicates the blot used for representative blot. "C" represents Control myotubes and "D" represents DM1 myotubes. "I" represents insulin treatment and "A" represents AICAR treatment. "nc" represents normalizing control.

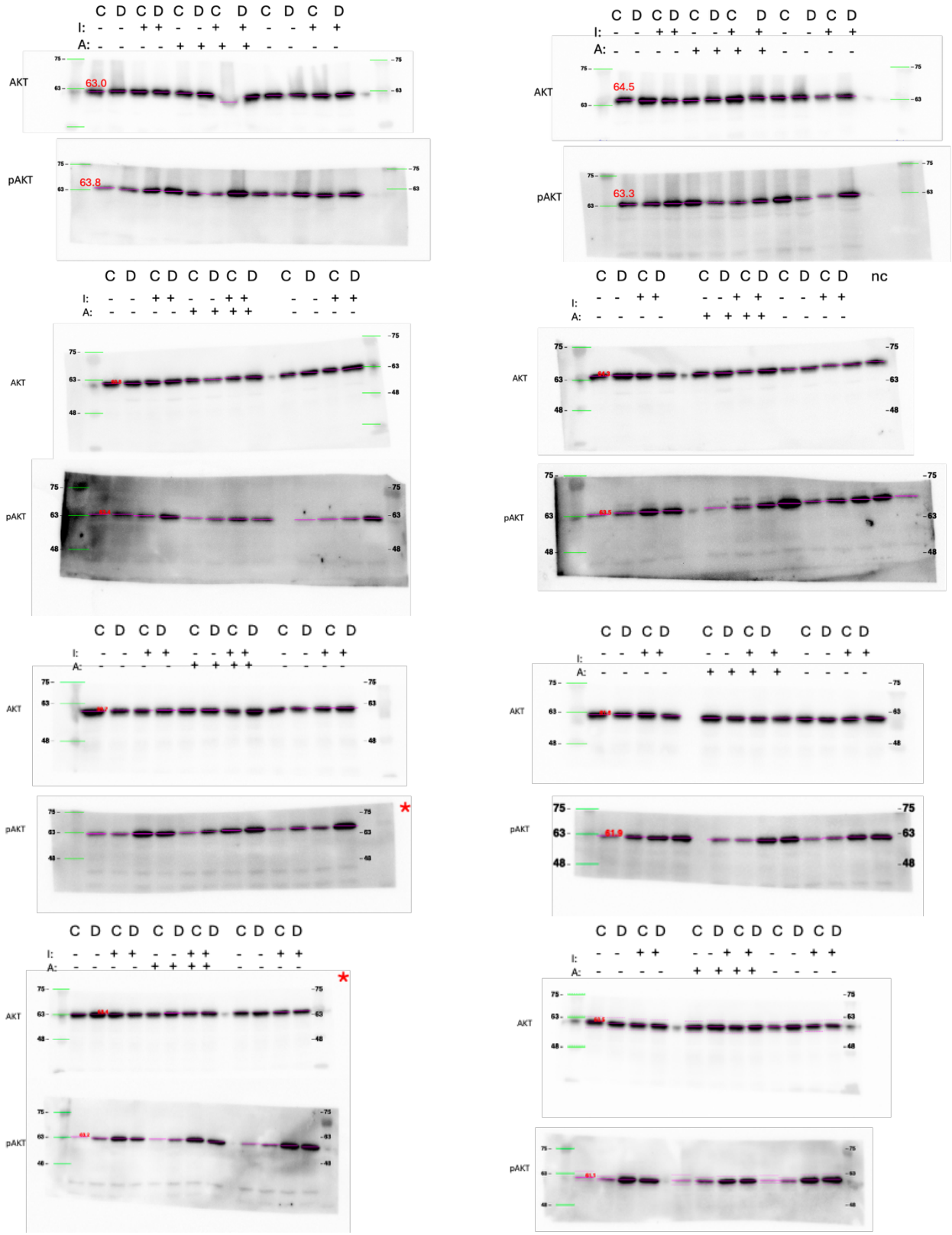

Supplemental Figure 14. Uncropped total and phosphorylated (Serine 473) AKT myotube western blots used for Figure 6A. Expected banding at 60 kDa. Western blot banding found between ~60-65 kDa (Pink lines). Red asterisks indicates the blot used for representative blot.

“C” represents Control myotubes and “D” represents DM1 myotubes. “I” represents insulin treatment and “A” represents AICAR treatment. ”nc” represents normalizing control.

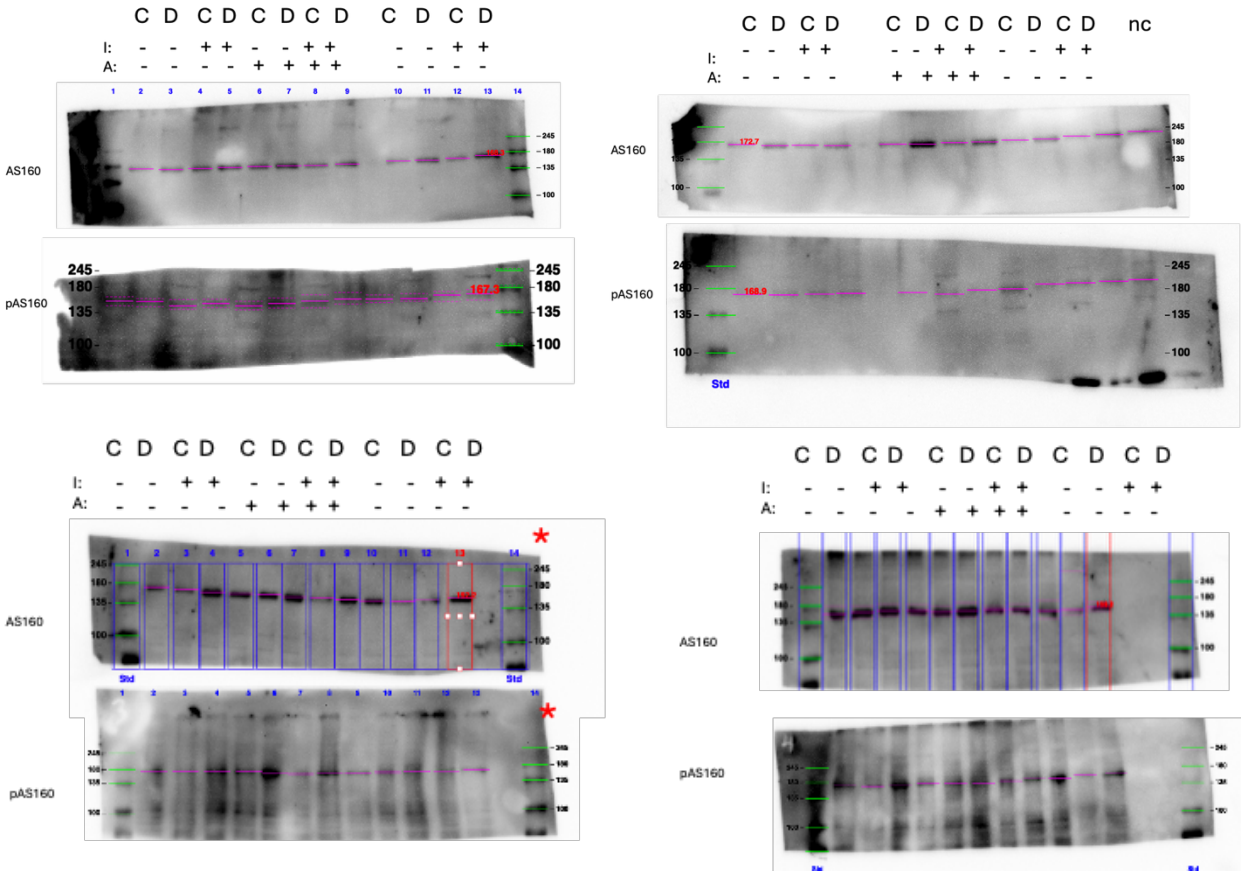

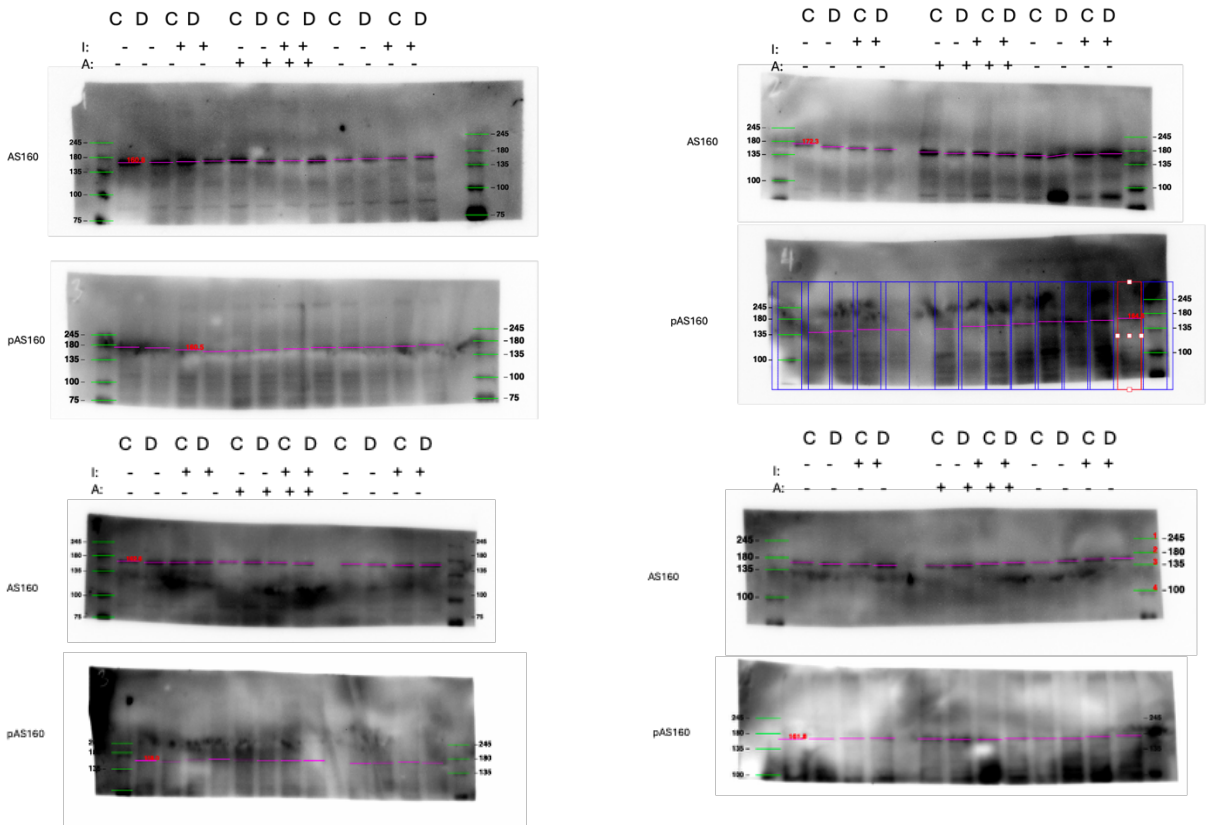

Supplemental Figure 15. Uncropped total and phosphorylated (Threonine 642) AS160 myotube western blots used for Figure 7A. Expected banding at 160 kDa. Western blot banding found between ~160-175 kDa (Pink lines). Red asterisks indicates the blot used for representative blot. “C” represents Control myotubes and “D” represents DM1 myotubes. “I” represents insulin treatment and “A” represents AICAR treatment. ”nc” represents normalizing control.

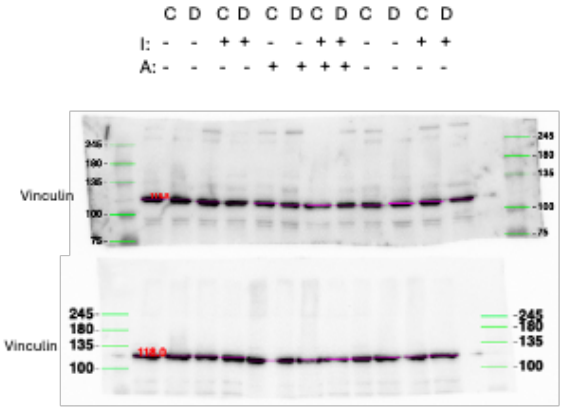
C D C D C D C D C D C D
I: - - + + - - + + - - + +
A: - - - - + + + + - - - -
Vinculin
245
180
135
100
Vinculin
245
180
135
100

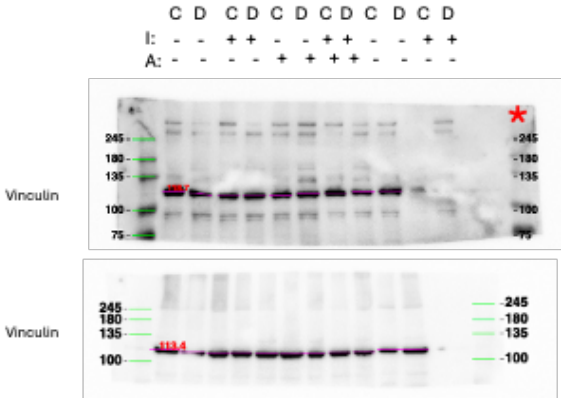
C D C D C D C D C D C D
I: - - + + - - + + - - + +
A: - - - - + + + + - - - -
Vinculin
*
Vinculin
245
180
135
100

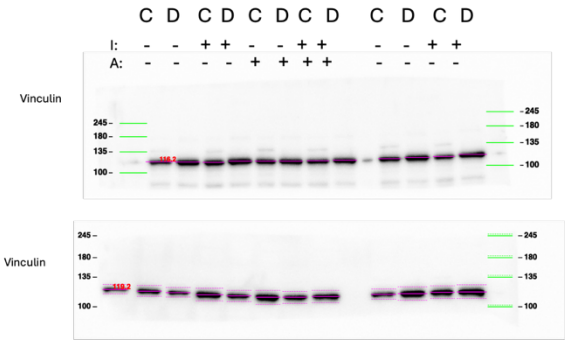
C D C D C D C D C D C D
I: - - + + - - + + - - + +
A: - - - - + + + + - - - -
Vinculin
Vinculin
245
180
135
100

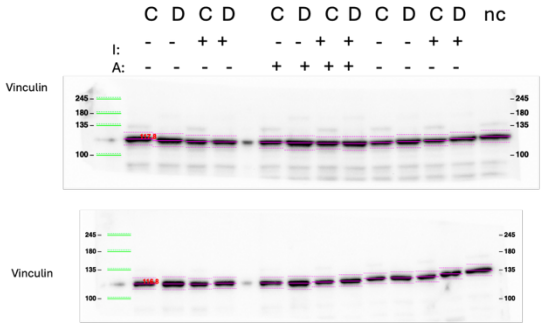
C D C D C D C D C D C D nc
I: - - + + - - + + - - + +
A: - - - - + + + + - - - -
Vinculin
Vinculin
245
180
135
100

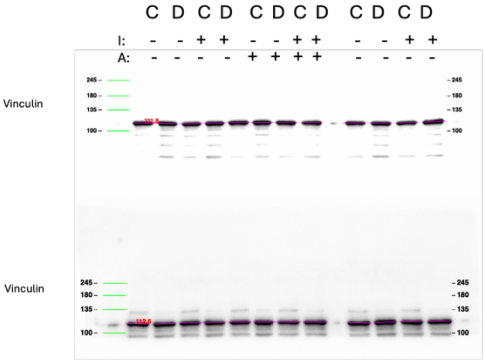
C D C D C D C D C D C D
I: - - + + - - + + - - + +
A: - - - - + + + + - - - -
Vinculin
Vinculin
245
180
135
100

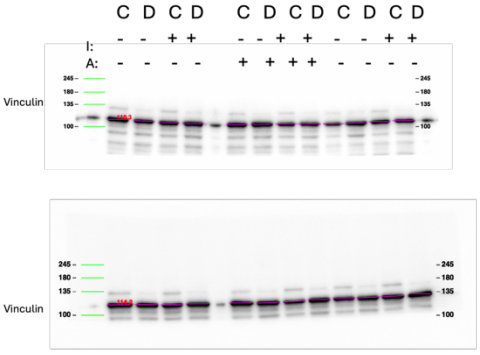
C D C D C D C D C D C D
I: - - + + - - + + - - + +
A: - - - - + + + + - - - -
Vinculin
Vinculin
245
180
135
100

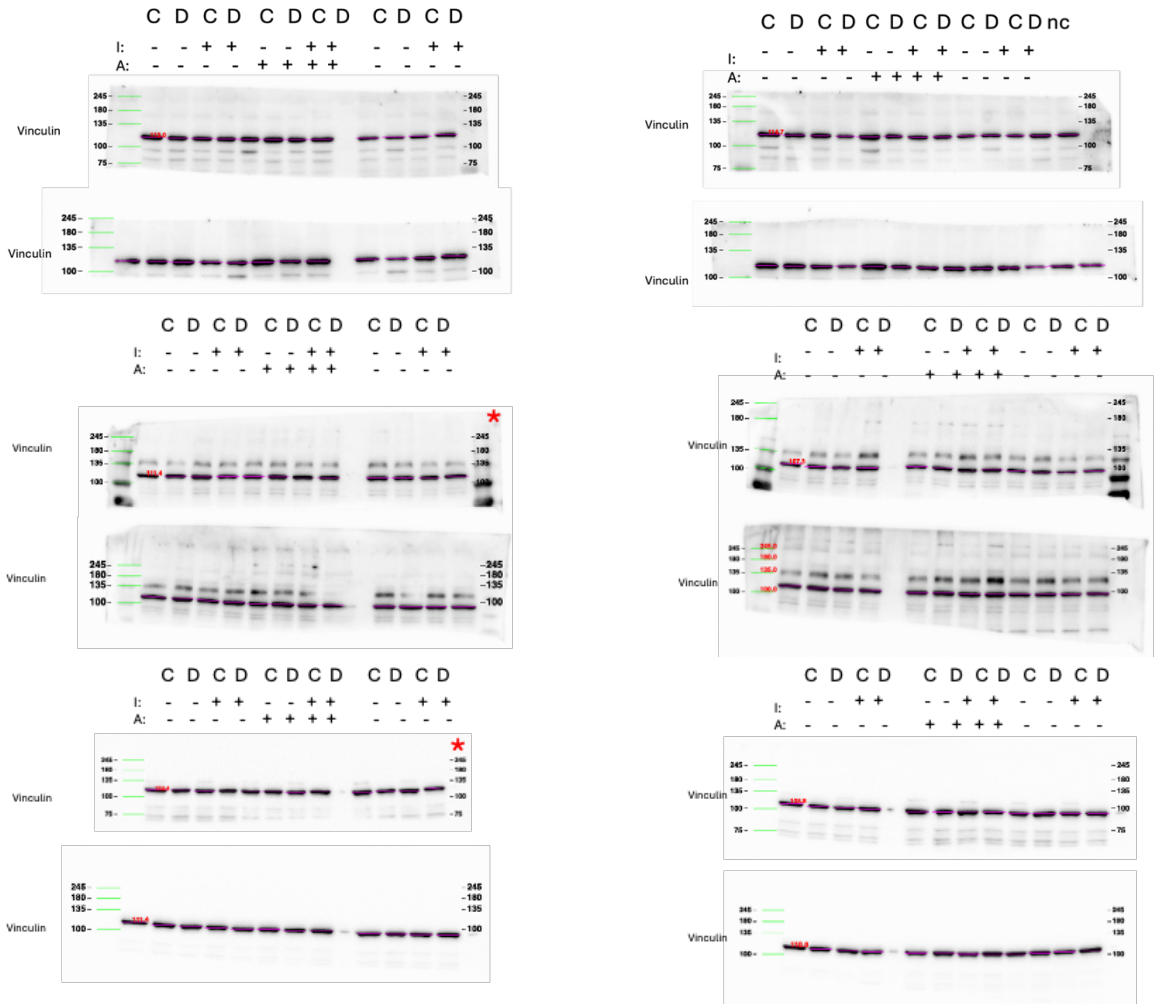

Supplemental Figure 16. Uncropped total vinculin myotube western blots for Figure 5A, 6A, 7A. Expected banding at ~124 kDa. Western blot banding found between ~110-120 kDa (Pink lines). Red asterisks indicate the blot used for representative blot. “C” represents Control myotubes and “D” represents DM1 myotubes. “I” represents insulin treatment and “A” represents AICAR treatment. ”nc” represents normalizing control.

Supplemental Table 1. List of Antibodies Used in Western Blotting.

Primary Antibody	**Company, Catalogue Number, RRID**	**Dilution**	**Secondary Antibody**	**Company, Catalogue Number, RRID**	**Dilution**
Mouse anti-Vinculin	Santa Cruz, 73614, RRID:AB_2941767	1:2000	Goat anti-mouse horse radish peroxidase (HRP)	Thermo Fisher Scientific, 31430, RRID:AB_228307	1:5000
Rabbit anti-ACC	Cell Signaling, 3662S, RRID:AB_2219400	1:1000	Goat anti-rabbit HRP	Thermo Fisher Scientific, 31460, RRID:AB_228341	1:5000
Rabbit anti-pACC (Ser79)	Cell Signaling, 3661, RRID:AB_330337	1:500			
Rabbit anti-AS160	Cell Signaling, 2447S, RRID:AB_2199376	1:1000			
Rabbit anti-	Cell Signaling, 4288S, RRID:AB_10545274	1:1000			

pAS160 (Thr642)					
Rabbit anti-PGC-1α	Thermo Fisher Scientific, PA5-72948, RRID:AB_2718802	1:500			
Rabbit anti-AKT	Cell Signaling, 9272, RRID:AB_329827	1:1000			
Rabbit anti-pAKT (Ser473)	Cell Signaling, 9271S, RRID:AB_329825	1:1000			
Rabbit anti-AMPK	Cell Signaling, 2532S, RRID:AB_330331	1:1000			
Rabbit anti-pAMPK (Thr172)	Cell Signaling, 2531S, RRID:AB_330330	1:500			
Rabbit anti-GLUT4	Abcam, ab33780, RRID:AB_2191441	1:1000			

Supplemental table 2. List of molecular targets identified in sedentary HSA-LR versus sedentary WT condition
See excel file *Molecular Targets sed vs wt*

Supplemental table 3. List of molecular targets identified in exercised HSA-LR versus sedentary HSA-LR condition
See excel file *Molecular Targets ex vs sed*

Supplemental table 4. List of all canonical pathways identified in sedentary HSA-LR versus sedentary WT condition
See excel file *canonical pathways sed vs wt*

Supplemental table 5. List of all canonical pathways identified in exercised HSA-LR versus sedentary HSA-LR condition
See excel file *canonical pathways ex vs sed*

Supplemental table 6. List of molecular targets identified in PI3K-AKT canonical pathway in HSA-LR versus sedentary WT condition
See excel file *pi3k akt sed vs wt*

Supplemental table 7. List of molecular targets identified in PI3K-AKT canonical pathway in exercised HSA-LR versus sedentary HSA-LR condition
See excel file *pi3k akt ex vs sed*

Supplemental table 8. List of molecular targets identified in SLC2A4 (GLUT4) translocation canonical pathway in HSA-LR versus sedentary WT condition
See excel file *glut4 translocation sed vs wt*

Supplemental table 9. List of molecular targets identified in SLC2A4 (GLUT4) translocation in exercised HSA-LR versus sedentary HSA-LR condition
See excel file *pi3k glut4 translocation ex vs sed*

Supplemental table 10. List of upstream regulators identified in HSA-LR versus sedentary WT condition
See excel file *upstream regulators sed vs wt*

Supplemental table 11. List of upstream regulators identified in exercised HSA-LR versus sedentary HSA-LR condition
See excel file *upstream regulators ex vs sed*